

University of Nevada Reno

An Exploratory Experimental Evaluation of ε_{50} in c- ϕ soils

A thesis submitted in partial fulfillment of
the requirements for the degree of Master of Science
in Civil and Environmental Engineering

by

Maryam Ostovar

Dr. Ramin Motamed/ Thesis Advisor

August, 2016



University of Nevada, Reno

THE GRADUATE SCHOOL

We recommend that the thesis
prepared under our supervision by

Maryam Ostovar

Entitled

An Exploratory Experimental Evaluation of ε_{50} in c- ϕ soils

be accepted in partial fulfillment of the
requirements for the degree of

MASTER OF SCIENCE

Ramin Motamed, Ph.D., Advisor

Raj Siddharthan, Ph.D., Committee Member

Rajagopala Kallu, Ph.D., Graduate School Representative

David W Zeh, Ph.D., Graduate Dean, Graduate School

August, 2016

Abstract

In this research, we explored the influence of several factors on the strain at 50% of maximum deviatoric principle stress, ϵ_{50} , of c- ϕ (cohesive granular) soils. C- ϕ materials are described as Mixed Soils behaving like granular and cohesive soils with properties defined as containing 15%-35% of plastic clay/silt with $PI > 7$. These soils are often encountered in the design of deep foundations and the common practice is to treat them either as cohesionless or cohesive soils (i.e. assuming one behavior or another). ϵ_{50} is one of the key parameters in the design of deep foundations under axial and lateral loading. Evans and Duncan (1980) provided correlations with S_u (undrained shear strength) for cohesive soils and Norris (1977) suggested correlations with void ratio for various coefficients of uniformity (C_U) for cohesionless soils. However, available literature does not provide any recommendations for c- ϕ materials. In this study, we investigated the effects of several parameters such as relative density, confining stress, PI , fines content, friction angle, cohesion, etc. on ϵ_{50} through a series of consolidated undrained triaxial tests on c- ϕ soil samples. Ultimately, this research attempted to establish correlations with key characteristics of c- ϕ soils.

Furthermore, we collected and documented all available literature on recommended ϵ_{50} values for different soil types and summarized the recommendations in tables to be used in practice. In the end, we demonstrated the significance of ϵ_{50} selection through a field load test conducted on an axially loaded drilled shaft.

Keywords: ϵ_{50} , c- ϕ soil, undrained triaxial tests, soil properties.

DEDICATION

I dedicate this work to my lovely parents and siblings for all their boundless and unconditioned kindness and my husband, my world, for all his endless love, support and encouragement.

Table of Contents

1	Introduction.....	1
1.1	General Introduction	1
1.2	Problem Description.....	2
1.3	Scope	2
2	Literature review	3
3	BenchMarking Testing Program.....	17
3.1	Introduction	17
3.2	Main types of Triaxial tests and their objectives.....	18
3.3	Apparatus and supplies.....	19
3.4	Description of soil samples	20
3.5	Sample preparation.....	23
3.6	Adjustment and Calibration to Devices	23
3.7	Test Procedure and Triaxial Software.....	23
3.8	Data Obtained, Results, and Discussion.....	24
3.9	Summary of Observed Results.....	29
4	Experimental Program	30
4.1	Description of soil samples	30
4.1.1	C- ϕ soil Definition	30
4.1.2	General Test Results	30
4.2	Sample preparation.....	32

4.3	Adjustment and Calibration to Devices	33
4.4	Test Procedure and Triaxial Software.....	33
4.5	Triaxial Test Results.....	35
4.5.1	C- ϕ Soil 1 (Granite Soil).....	35
4.5.2	C- ϕ Soil 2 (Black Eagles)	46
4.5.3	C- ϕ Soil 3 (Mixed Soil)	57
4.6	Data Obtained, Results, and Discussion.....	68
5	Case Study of Pile Axial Load Testing.....	89
5.1	Introduction	89
5.2	Experimental testing site	90
5.3	In Situ testing	90
5.4	CGI-DFSAP	90
5.5	Material Properties	91
5.5.1	CPT Data.....	92
5.5.2	Shear Wave Velocity Data.....	93
5.5.3	Standard Penetration Data.....	93
5.5.4	Finalized Soil Profile	94
5.5.5	Blind Prediction Results.	94
5.6	Sensitivity Analysis.....	96
5.7	Summary of Sensitivity Analysis.....	99
6	Conclusions and Recommendations	100

7 References..... 101

List of Tables

Table 2-1. Measured Variation of ε_{50} with some Soil properties (Ebrahimian et al., 2015).....	5
Table 2-2. Measured Variation of ε_{50} with some Soil properties (Dunnivant et al., 1989).....	5
Table 2-3. Measured Variation of ε_{50} with various Soil properties of Site 2 (Jeong et al., 2007; Kim et al., 2009)	6
Table 2-4. Skempton's suggested value of ε_{50} (soft clay) (Sullivan et al., 1979).....	6
Table 2-5. Skempton's recommended value of ε_{50} (stiff clay) (Sullivan et al., 1979).....	7
Table 2-6. Skempton's recommended value of ε_{50} (Sullivan et al., 1979).....	7
Table 2-7. ε_{50} for different type of soil (Zhang et al., 2013).....	8
Table 2-8. Calculated ε_{50} based on data shown in Fig. 1 and Fig. 2. (Javadi et al., 2009).....	9
Table 2-9. Calculated Comparison Predicted and Experimental ε_{50} for Dense Sand (Konder et al., 1963)	10
Table 2-10. Calculated Comparison Predicted and Experimental ε_{50} for Loose Sand (Konder et al., 1963)	11
Table 2-11. Calculated Variation of ε_{50} with undrained strength of Clays (Evans et al., 1982)...	13
Table 2-12. Calculated Variation of ε_{50} with Relative Density for sands (Evans et al., 1982).....	13
Table 2-13. Calculated ε_{50} based on Figures 8 to 12 (McClellan (2013)).....	16
Table 3-1. Summary of Triaxial test data for Nevada sand – 40% relative density (Arulmoli et al. 1992)	21
Table 3-2. Average unit weight of Nevada sand.....	22
Table 3-3. Required soil mass for sample preparation	22
Table 3-4. Sample measurements	23

Table 3-5 Test Inputs (Arulmoil 1992).....	24
Table 4-1. Standard used in laboratory testing	30
Table 4-2. Soil sample sources	31
Table 4-3. Summary of general test results for Soil 1 (Granite).....	31
Table 4-4. Summary of general test results for Soil 2 (Black Eagle)	31
Table 4-5. Summary of general test results for Soil 3 (Mixeded)	31
Table 4-6. Summary of Sieve Analysis for Soil 1 (Granite).....	31
Table 4-7. Summary of Sieve Analysis for Soil 2 (Black Eagle)	31
Table 4-8. Summary of Sieve Analysis for Soil 3 (Mixeded)	32
Table 4-9. Sample measurements (Granite soil).....	32
Table 4-10. Sample measurements (Black Eagle soil)	32
Table 4-11. Sample measurements (Mixed Soil).....	33
Table 4-12. Test Inputs (Granite soil).....	33
Table 4-13. Test Inputs (Black Eagle soil)	34
Table 4-14. Test Inputs (Mixed Soil).....	34
Table 4-15. Summary of Triaxial test data for C- ϕ Soil 1 (Granite)–40% relative density (Arulmoli et al., 1992)	35
Table 4-16. Required soil mass for sample preparation (Granite Soil)	35
Table 4-17. Summary of Triaxial test data for C- ϕ Soil 2 (Black Eagle).....	46
Table 4-18. Required soil mass for sample preparation (Black Eagle Soil).....	46
Table 4-19. Summary of Triaxial test data for C- ϕ Soil 2 (Black Eagles)	57
Table 4-20. Required soil mass for sample preparation (Mixed Soil).....	57

Table 4-21. The amount of ϵ_{50} for different relative density and confining pressure (Granite soil)
..... 83

Table 4-22. The amount of ϵ_{50} for different relative density and confining pressure (Black Eagle soil) 85

Table 4-23. The amount of ϵ_{50} for different relative density and confining pressure (Mixed Soil)
..... 86

Table 5-1. Assumed soil layering and properties for blind prediction 94

Table 5-2. Predicted loads at failure ($w/D=10\%$) 95

Table 5-3. Assumed soil layering and properties for sensitivity analysis..... 96

List of Figures

Figure 2 1. Variation of ϵ_{50} with undrained strength of Clays (Evans et al., 1982)	3
Figure 2 2. Relationship between ϵ_{50} , Uniformity Coefficient (C_u) and Void Ratio (e) (Norris 1977)	4
Figure 2-3. Results of using the EPR models (50 kPa, 200 kPa and 500 kPa Confining pressure) (Javadi et al., 2009).....	7
Figure 2-4. Results of using the EPR models (50 kPa, 200 kPa and 500 kPa Confining pressure) (Javadi et al., 2009).....	7
Figure 2-5. Results of using the EPR models (100 kPa and 400 kPa Confining pressure) (Javadi et al., 2009)	8
Figure 2-6. Comparison of Hyperbolic Prediction Eq. and measurement response: Dense Sand (Konder et al., 1963)	9
Figure 2-7. Comparison of Hyperbolic Prediction Eq. and measurement response: Loose Sand (Konder et al., 1963)	10
Figure 2-8. Variation of ϵ_{50} with undrained strength of Clays (Evans et al., 1982)	11
Figure 2-9. Variation of ϵ_{50} with Relative Density for Clays (Evans et al., 1982)	11
Figure 2-10. Variation of ϵ_{50} with Relative Density for Sands (Evans et al., 1982)	12
Figure 2-8. Deviatoric stress versus axial strain of 2.8 in. and 6 in. diameter triaxial compression tests for sample taken at a depth of 5 ft (Z. R. McClellan (2013))	13
Figure 2-11. Deviatoric stress versus axial strain of 2.8 in. and 6 in. diameter triaxial compression tests for sample taken at a depth of 14.5 ft (Z. R. McClellan (2013)).....	13

Figure 2-12. Deviatoric stress versus axial strain of 2.8 in. and 6 in. diameter triaxial compression tests for sample taken at a depth of 29 ft (Z. R. McClellan (2013))..... 14

Figure 2-13. Deviatoric stress versus axial strain of 2.8 in. and 6 in. diameter triaxial compression tests for sample taken at a depth of 42.8 ft (Z. R. McClellan (2013))..... 14

Figure 2-14. Deviatoric stress versus axial strain of 2.8 in. and 6 in. diameter triaxial compression tests for sample taken at a depth of 57.5 ft (Z. R. McClellan (2013))..... 15

Figure 3-1. Schematic diagram of triaxial test setup 17

Figure 3-2 Triaxial Test 18

Figure 3-3. Geocomp’s triaxial system..... 19

Figure 3-4 Deviatoric Stress vs. Axial Strain for 40 kPa Confining Pressure (Alumoli et al. study) 20

Figure 3-5. Deviatoric Stress vs. Axial Strain for 80 kPa Confining Pressure (Alumoli et al. study) 21

Figure 3-6. Deviatoric Stress vs. Axial Strain for 160 kPa Confining Pressure (Alumoli et al. study)..... 21

Figure 3-7. Deviatoric Stress vs. Axial Strain for 40 kPa Confining Pressure 25

Figure 3-8. Deviatoric Stress vs. Axial Strain for 80 kPa Confining Pressure 25

Figure 3-9. Deviatoric Stress vs. Axial Strain for 160 kPa Confining Pressure 26

Figure 3-10. Excess PWP vs. Axial Strain for 40 kPa Confining Pressure 27

Figure 3-11. Excess PWP vs. Axial Strain for 80 kPa Confining Pressure 27

Figure 3-12. Excess PWP vs. Axial Strain for 160 kPa Confining Pressure 28

Figure 3-13. Deviatoric Stress vs. P' for 80 kPa Confining Pressure..... 29

Figure 3-14. Deviatoric Stress vs. P' for 160 kPa Confining Pressure.....	29
Figure 4-1. The gradation curve of Soil 1 (Granite Soil).....	36
Figure 4-2. Atterberg Limit graph of Soil 1 (Granite Soil).....	36
Figure 4-3. Triaxial test results of Granite Soil 1	36
Figure 4-4. Triaxial test results of Granite Soil 2	36
Figure 4-5. Triaxial test results of Granite Soil 3	40
Figure 4-6. Triaxial test results of Granite Soil 4	41
Figure 4-7. Triaxial test results of Granite Soil 5	42
Figure 4-8. Triaxial test results of Granite Soil 6	43
Figure 4-9. Triaxial test results of Granite Soil 7	44
Figure 4-10. Triaxial test results of Granite Soil 8	45
Figure 4-11. Triaxial test results of Granite Soil 9	46
Figure 4-12. The gradation curve of Soil 2 (Black Eagle Soil)	48
Figure 4-13. Atterberg Limit graph of Soil 2 (Black Eagle Soil)	48
Figure 4-14. Triaxial test results of Black Eagle Soil 10.....	49
Figure 4-15. Triaxial test results of Black Eagle Soil 11	50
Figure 4-16. Triaxial test results of Black Eagle Soil 12.....	51
Figure 4-17. Triaxial test results of Black Eagle Soil 13.....	52
Figure 4-18. Triaxial test results of Black Eagle Soil 14.....	53
Figure 4-19. Triaxial test results of Black Eagle Soil 15.....	54
Figure 4-20. Triaxial test results of Black Eagle Soil 16.....	55
Figure 4-21. Triaxial test results of Black Eagle Soil 17	56

Figure 4-22. Triaxial test results of Black Eagle Soil 18.....	57
Figure 4-23. The gradation curve of Soil 3 (Mixed Soil)	59
Figure 4-24 . Atterberg Limit graph of Soil 3 (Mixed Soil)	59
Figure 4-25. Triaxial test results of Mixed Soil 19.....	60
Figure 4-26. Triaxial test results of Mixed Soil 20.....	61
Figure 4-27. Triaxial test results of Mixed Soil 21	62
Figure 4-28. Triaxial test results of Mixed Soil 22.....	63
Figure 4-29. Triaxial test results of Mixed Soil 23.....	64
Figure 4-30. Triaxial test results of Mixed Soil 24.....	65
Figure 4-31. Triaxial test results of Mixed Soil 25.....	66
Figure 4-32. Triaxial test results of Mixed Soil 26.....	67
Figure 4-33. Triaxial test results of Mixed Soil 27.....	68
Figure 4-34. Triaxial test results of Granite Soil (40% relative density).....	70
Figure 4-35. Triaxial test results of Granite Soil (60% relative density).....	71
Figure 4-36. Triaxial test results of Granite Soil (80% relative density).....	72
Figure 4-37. Triaxial test results of Granite Soil (Mohr Circle).....	73
Figure 4-38. Triaxial test results of Black Eagle Soil (40% relative density)	75
Figure 4-39. Triaxial test results of Black Eagle Soil (60% relative density)	76
Figure 4-40. Triaxial test results of Black Eagle Soil (80% relative density)	77
Figure 4-41. Triaxial test results of Black Eagle Soil (Mohr Circle).....	78
Figure 4-42. Triaxial test results of Mixed Soil (40% relative density)	80
Figure 4-43. Triaxial test results of Mixed Soil (60% relative density)	81

Figure 4-44. Triaxial test results of Mixed Soil (80% relative density)	82
Figure 4-45. Triaxial test results of Mixed Soil (Mohr Circle).....	83
Figure 4-46. The amount of ϵ_{50} versus relative density (Granite Soil)	84
Figure 4-47. The amount of ϵ_{50} versus confining pressure (Granite Soil)	84
Figure 4-48. The amount of ϵ_{50} versus relative density (Black Eagles Soil)	85
Figure 4-49. The amount of ϵ_{50} versus confining pressure (Black Eagle Soil).....	85
Figure 4-50. The amount of ϵ_{50} versus relative density (Mixed Soil).....	86
Figure 4-51. The amount of ϵ_{50} versus confining pressure (Mixed Soil).....	86
Figure 5-1. Comparison of soil properties estimated using CPT, SPT and V_s data.	90
Figure 5-2. Comparison of soil behavior types suggested by Robertson (1986) (right) and Robertson (2009) (left) for CPT-03.	91
Figure 5-3 Predicted axial shaft head load-settlement response	94
Figure 5-4. Load distribution for a settlement equal to 10% of the shaft diameter	94
Figure 5-5. Comparison chart for predicted axial shaft head load-settlement response	96
Figure 5-6. Comparison chart for predicted load distribution for a settlement equal to 10% of the shaft diameter	96
Figure 5-7. Average root mean square error (RMSE) between the predicted and measured results for axial shaft head load-settlement response	97
Figure 5-8 Average root mean square error (RMSE) between the predicted and measured results for a settlement equal to 10% of the shaft diameter.....	97

1 Introduction

1.1 General Introduction

C- ϕ materials are described as Mixed Soils behaving like granular and cohesive soils with properties defined as containing 15%-35% of plastic clay/silt with $PI > 7$. These soils are often encountered in the design of deep foundations, and the common practice is to treat them either as cohesionless or cohesive soils (i.e. assuming one behavior or another).

ϵ_{50} , which is intended to represent the strain at an axial compressive stress equal to 50% of the yield stress in the UU triaxial test, is one of the key parameters in the design of deep foundations under axial and lateral loading. Evans and Duncan (1982) provided correlations with S_u (undrained shear strength) for cohesive soils, and Norris (1977) suggested correlations with the void ratio for various coefficients of uniformity (CU) for cohesionless soils. Moreover, typical values of ϵ_{50} are often simply related with a given range of S_u . The use of undrained shear strength has proven to provide a reliable correlation with load test results of short duration.

Furthermore, p-y (lateral load resistance) and t-z (axial load-transfer method) are the most important methods which need the amount of ϵ_{50} in their analysis. For instance, Engineers using p-y criteria to design a drilled shaft for lateral loading should perform analyses using a range of values of S_u and ϵ_{50} in order to estimate the sensitivity of the analysis to these parameters (p-y method). In addition, in chapter 5, a t-z style analysis was employed to obtain the load-settlement response and axial load distribution of a drilled shaft. It is observed that prediction quality of the response of the drilled shaft is significantly dependent on the assumed material parameters for the soil layers, especially within the range of estimated values for ϵ_{50} .

Additionally, Sensitivity studies can provide the information needed to develop judgment regarding the reliability of the design and the relative importance of various input parameters. In chapter 5, the sensitivity of settlement prediction for an axially loaded drilled shaft to ϵ_{50} is studied. This sensitivity study further exhibited the need for careful selection of the parameter ϵ_{50} when predicting the axial response of drilled shafts. This highlights the need for proper sampling and testing of the soils, including carrying out laboratory tests such as triaxial compression on collected samples.

1.2 Problem Description

According to available papers regarding ϵ_{50} , these literature do not provide any recommendations for $c-\phi$ materials. Hence, several papers were reviewed and all of them talked about cohesive soil or cohesionless soil separately (chapter2). All available literature on recommended ϵ_{50} values for different soil types were collected and documented, and then the recommendations were summarized in tables to be used in practice. In addition, Benchmarking tests were conducted for proving the accuracy of the Triaxial test device and the testing method in chapter 3. In this chapter, several tests were conducted and their results were compared with VELASC report's (1992) results. All Experimental programs including the soil types, basic tests, testing program, and results and discussion come in chapter 4. Additionally, in chapter 5, the case study of pile axial testing can be seen, which investigates the sensitivity of settlement prediction for an axially loaded drilled shaft to ϵ_{50} .

1.3 Scope

In this research, we have explored the influence of several factors on the strain at 50% of maximum deviatoric principle stress, ϵ_{50} , of $c-\phi$ (cohesive granular) soils. The effects of several parameters are investigated, such as relative density, confining stress, PI, fines content, friction angle, cohesion, etc. on ϵ_{50} through a series of consolidated undrained triaxial tests on $c-\phi$ soil samples. Ultimately, this research will attempt to establish correlations with key characteristics of $c-\phi$ soils.

Furthermore, we have collected and documented all available literature on recommended ϵ_{50} values for different soil types and summarized the recommendations in tables to be used in practice. In the end, we have demonstrated the significance of ϵ_{50} selection through a field load test conducted on an axially loaded drilled shaft.

2 Literature review

In this research, the influence of several factors on the strain at 50% of maximum deviatoric principle stress, ϵ_{50} , of c- ϕ (cohesive granular) soils was explored. ϵ_{50} is one of the key parameters in the design of deep foundations under axial and lateral loading. Evans and Duncan (1982) provided correlations with undrained shear strength (S_u) for cohesive soils (Figure 2-1) and Norris (1977) suggested correlations with void ratio for various coefficients of uniformity (C_U) for cohesionless soils (Figure 2-2).

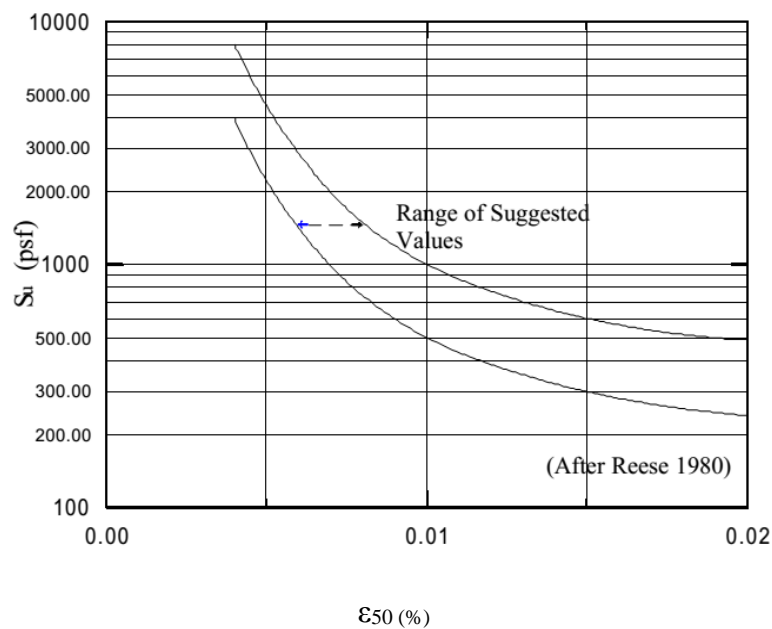


Figure 2-1. Variation of ϵ_{50} with undrained strength of Clays (Evans et al., 1982)

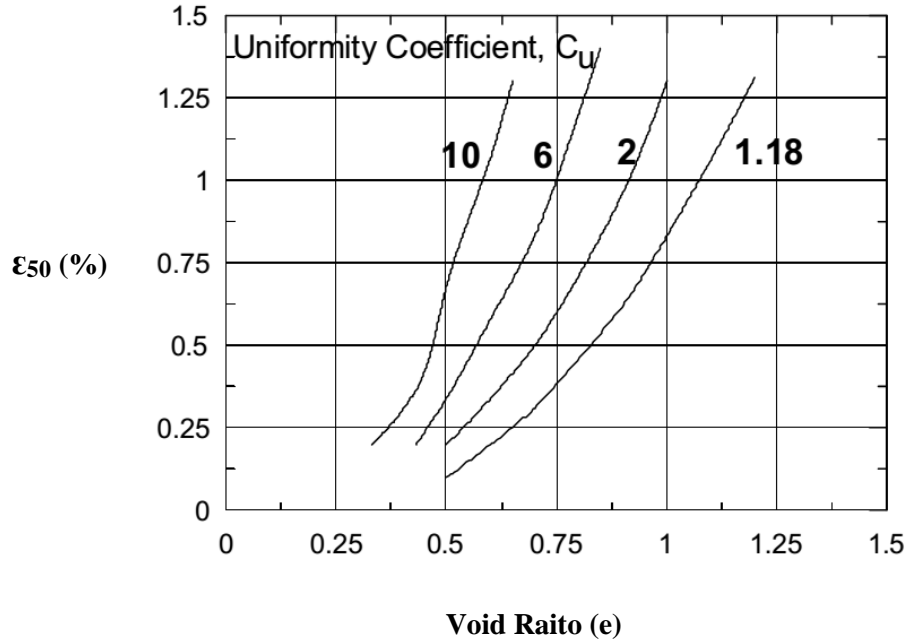


Figure 2-2. Relationship between ϵ_{50} , Uniformity Coefficient (C_u) and Void Ratio (e) (Norris 1977)

However, available literature does not provide any recommendations for c - ϕ materials. In this study, several available literature on recommended ϵ_{50} values were collected and documented for different soil types and the recommendations were summarized in tables.

The goal of Ebrahimian et al. (2015) was predicting ϵ_{50} amounts investigating the lateral behavior of very long pile foundations of offshore oil and gas platforms in the South Pars field in the Persian Gulf, Iran (Table 2-1). From this research, several models were proposed based on the strength and deformation properties of soil. For obtaining ϵ_{50} from extensive soil data of marine clays which include laboratory and in-situ test results, evolutionary polynomial regression (EPR) was used. The values of ϵ_{50} obtained from cone tip resistance of CPT are more realistic in comparison with laboratory test results (undrained shear strength parameter).

South Pars field with the largest gas resources of the world has many gas extraction facilities supported on long pile foundations. For evaluating ϵ_{50} as an influential parameter in analysis and

design of piles against lateral loads several models were proposed, based on EPR method. In this regard, some parameters which were evaluated and discussed on ϵ_{50} are the effects of cone tip and normalized cone tip resistances, initial tangent elastic modulus, over-consolidation ratio and undrained shear strength. As seen in Table 2-1, soil properties have been identified by extensive field and laboratory tests.

Table 2-1. Measured Variation of ϵ_{50} with some Soil properties (Ebrahimian et al., 2015)

Soil Type	Depth (m)	Unit Weight (kN/m ³)	Su (kPa)	ϵ_{50} (%)
Very Soft Clay	0-18.6	16.5	10	3
Very Stiff Clay	18.6-43	19-20	250-550	1.1-2.5
Very Stiff Clay	43-70	19-21	70-300	1.5-6.5
Very Stiff Clay	70-110	18.5-21.5	50-600	1.5-7

Based on the study by Dunnavant et al. in 1989, several full scale cyclic lateral load tests on varying diameter piles were conducted on overconsolidated clay. A P-Y model used in this research was meaningful for large-diameter piles (driven as well as bored).

The site soils were natural, saturated, overconsolidated clays. Moreover, the soils were borderline CL to CH clays which are jointed with small, discontinuous slickensides and some isolated sands. Table 2-2 illustrates the profile of ϵ_{50} in terms of depth as well as some other soil properties below pit, which included the axial strain at one-half of the peak principal stress difference in a monotonic, undrained triaxial compression test.

Table 2-2. Measured Variation of ϵ_{50} with some Soil properties (Dunnavant et al., 1989)

Soil Type	Depth (m)	Unit Weight (kN/m ³)	Su (kPa)	ϵ_{50} (%)
Heavily OC Clay	0-0.5	19.6	50-70	1.75
	0.5-2	19.6	70-90	0.75
	2-5	21	70-125	1.1
	5-7	20.1	130	0.5
	7-10	21	90	1.7

As presented by Jeong et al. in 2011, fundamental research was carried out on a lateral load of pile-soil systems in marine clay of offshore deposits. Both field and laboratory tests were conducted for determining the p-y curve as well as rigid and flexible analysis for comparison. For determining some of the soil properties such as particle size distribution, shear strength and consolidation characteristics, laboratory tests were conducted. Table 2-3 shows the summary of the subsoil profile and the material properties of this study. As seen, ϵ_{50} amounts for soft marine clay and medium marine clay are equal to 0.02 and 0.01, respectively.

This study demonstrates that the rigid pile is not influenced by the features of various p-y curves.

Table 2-3. Measured Variation of ϵ_{50} with various Soil properties of Site 2 (Jeong et al., 2007; Kim et al., 2009)

Soil Type	Depth (m)	Unit Weight (kN/m ³)	S_u (kPa)	q_c (kPa)	OCR	Recommended ϵ_{50}
Soft Clay	0-6.3	14.4	15-30	375-850	3-5	0.02
Medium Clay	6.3-16.5	16.3	30-50	850-1440	2-3	0.01
Silty Clay	16.5-22	15.8	-	-	1-2	0.005

In 1979, Sullivan et al. studied the influence of lateral loading on a pile by using computers for solving equations. P-Y curves gave the soil response and two experimental programs were performed on a full sized pile in submerged clay. Stiff and soft clay were used for reanalyzing and predicting P-Y curves for clay. In addition, the Unified method as well as experiments were used to predict the pile behavior. Based on Matlock's recommendation, obtaining the best possible estimates of undrained shear strength, effective unit weight, and the values of ϵ_{50} , used as the parameters of the P-Y curve procedure for soft clay. Table 2-4 shows Skempton's ϵ_{50} value suggestion for soft clay if no values are available for ϵ_{50} .

Table 2-4. Skempton's suggested value of ϵ_{50} (soft clay) (Sullivan et al., 1979)

Consistency of Clay	ϵ_{50}
Soft	0.020
Medium	0.010
Stiff	0.005

Furthermore, the following equation computes Y_{50} (the deflection) at one half the ultimate soil resistance.

$$Y_{50} = 2.5 \epsilon_{50} b$$

Reese et al. (1980) conducted lateral load tests on pipe piles driven into stiff clay. The experimental and analytical steps were very close to Matlock's procedure. Table 2-5 shows Skempton's ϵ_{50} value recommendation for stiff soil if no values are available for ϵ_{50} . In addition, Table 2-6 shows Skempton's ϵ_{50} value recommendation for stiff, medium and soft clays. Moreover, the following correlation is derived for computing ϵ_{50} in stiff clay.

$$Y_{50} = \epsilon_{50} b$$

Table 2-5. Skempton's recommended value of ϵ_{50} (stiff clay) (Sullivan et al., 1979)

	Average undrained shear strength (kPa)		
	50-100	100-200	200-400
ϵ_{50}	0.007	0.005	0.004

Table 2-6. Skempton's recommended value of ϵ_{50} (Sullivan et al., 1979)

Consistency of Clay	Unit Weight (kN/m ³)	Average Undrained shear strength (kPa)	ϵ_{50} (%)
Soft	7.85	12-25	2
Medium	7.85	25-50	1
Stiff	7.85	50-100	0.7
Stiff	7.85	100-200	0.5
Stiff	7.85	200-400	0.4

Regarding Zhang et al. (2013), a method of laterally loaded rigid pile in cohesive clay for nonlinear analysis was presented. The force and moment equilibrium, the nonlinear change of lateral load resistance versus depth, the horizontal shear resistance at the pile base, and the relationship between the shear resistance and displacement was considered for this method. The developed method was checked for validation in comparison with its results using 3D finite element analysis. This method was also applied to analysis of five field test piles and agreeable results were acquired. Table 2-7 represents calculated epsilon 50 based on several tables in the paper.

Table 2-7. ϵ_{50} for different type of soil (Zhang et al., 2013)

Clay Consistency	C_u (kPa)	E_s (MPa)	ϵ_{50} (%) for
very soft clay	2-25	0.5-5	3-3.5
Soft clay	25-50	5-20	1.9-3.5
Medium	50-100	20-50	1.5-1.9
stiff	100-200	50-100	1.5

Javadi et al. (2009), presented a new approach in finite element analysis for constitutive modeling of materials which prepares a framework using the evolutionary polynomial regression-based constitutive model (EPRCM). The most remarkable benefit of EPRCM was providing the optimum structure for the material constitutive model representation and its parameters from experimental or field data.

Fig. 1 and Fig. 2 illustrate the stress–strain curves predicted by EPR process versus those expected as experimental data. A significant agreement can be seen between the EPR predicted values and the experimentally determined values. In addition, Table 2-8 shows the measured ϵ_{50} regarding Figure 2-3 and Figure 2-4.

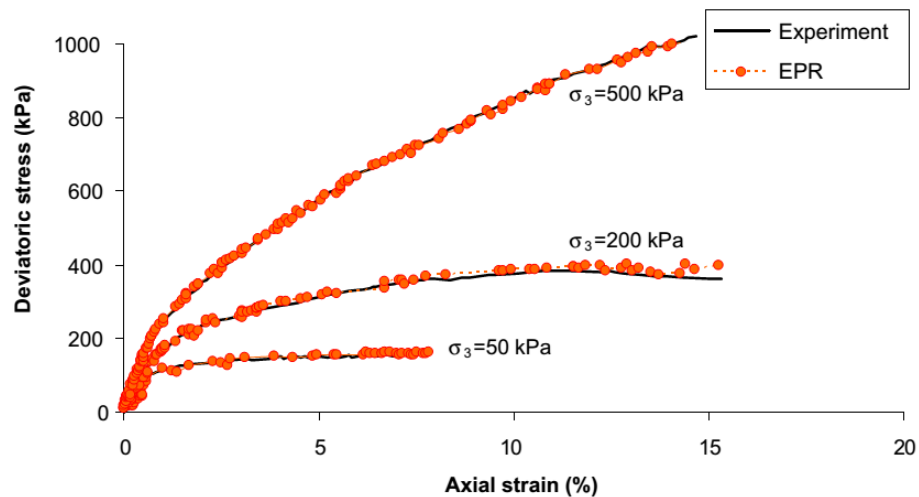


Figure 2-3. Results of using the EPR models (50 kPa, 200 kPa and 500 kPa Confining pressure) (Javadi et al., 2009)

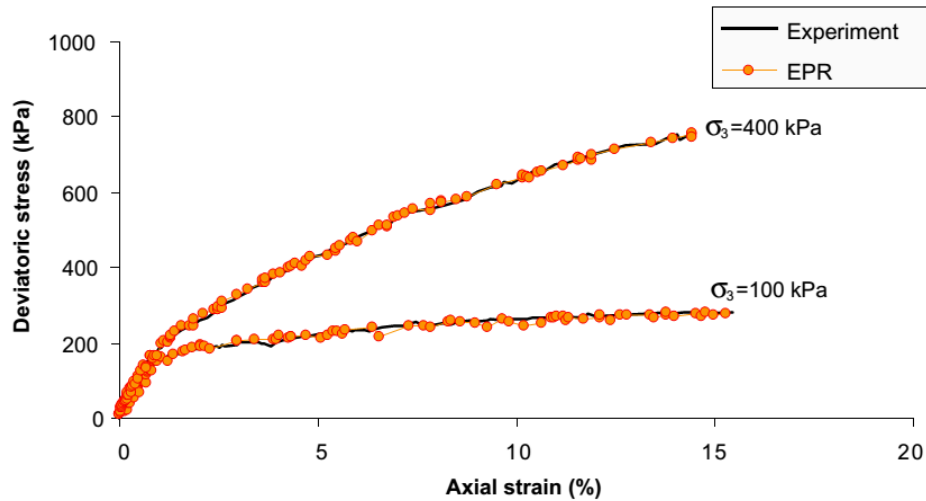


Figure 2-4. Results of using the EPR models (100 kPa and 400 kPa Confining pressure) (Javadi et al., 2009)

In addition, Table 8 illustrates the calculated epsilon 50 based on figure 1 and 2.

Table 2-8. Calculated ϵ_{50} based on data shown in Fig. 1 and Fig. 2. (Javadi et al., 2009)

Soil Type	Unit Weight (kN/m ³)	Friction Angle (°)	Confining Pressure (kPa)	ϵ_{50}^* (%) (EPR)	ϵ_{50} (%) (Experimental)
Sand	17	30	50	0.9	0.85
Sand	17	30	100	1.1	1.15
Sand	17	30	200	1.3	1.2
Sand	17	30	400	4.55	4.6
Sand	17	30	500	4.75	4.7

ϵ_{50}^* : This parameter is calculated based on mentioned figures.

Konder et al. (1963) compared constant hyperbolic stress-strain equations and Triaxial compression tests on dense and loose sand. The general stress-strain formulation was well-matched with the results of experimental Triaxial test data. Figure 2-5 and Figure 2-6 illustrate the stress-strain curves predicted by the hyperbolic equation versus those expected as Triaxial experimental data. A clear agreement can be observed between the Hyperbolic predicted values

and the experimentally determined ones. Furthermore, Table 2-9 and Table 2-10 show the measured ϵ_{50} regarding the figures.

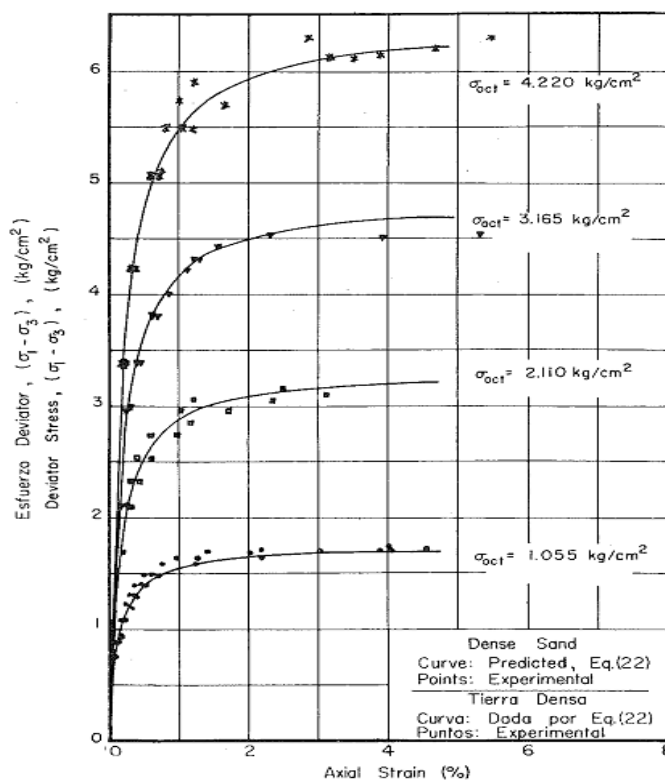


Figure 2-5. Comparison of Hyperbolic Prediction Eq. and measurement response: Dense Sand (Konder et al., 1963)

Table 2-9. Calculated Comparison Predicted and Experimental ϵ_{50} for Dense Sand (Konder et al., 1963)

Soil Type	Unit Weight (kN/m ³)	Friction Angle (°)	Confining Pressure (kPa)	Predicted ϵ_{50}^* (%)	Experimental ϵ_{50}^* (%)
Loose Sand	14	22-35	100	0.1	0.1
Loose Sand	14	22-35	200	0.16	0.15
Loose Sand	14	22-35	300	0.21	0.19
Loose Sand	14	22-35	400	0.29	0.3

ϵ_{50}^* : This parameter is calculated based on mentioned figures.

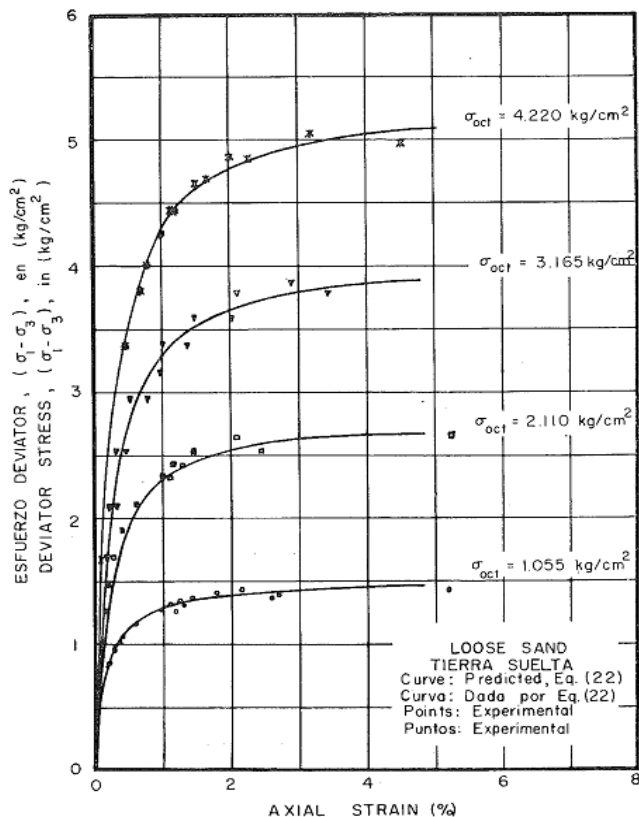


Figure 2-6. Comparison of Hyperbolic Prediction Eq. and measurement response: Loose Sand (Konder et al., 1963)

Table 2-10. Calculated Comparison Predicted and Experimental ϵ_{50} for Loose Sand (Konder et al., 1963)

Soil Type	Unit Weight (kN/m^3)	Friction Angle ($^\circ$)	Confining Pressure (kPa)	Predicted ϵ_{50}^* (%)	Experimental ϵ_{50}^* (%)
Dense Sand	17	29-46	100	0.07	0.07
Dense Sand	17	29-46	200	0.1	0.1
Dense Sand	17	29-46	300	0.15	0.13
Dense Sand	17	29-46	400	0.18	0.16

ϵ_{50}^* : This parameter is calculated based on mentioned figures.

In research by Evans et al. (1982), included Figure 2-7, Figure 2-8, Figure 2-9 and Table 2-11 and Table 2-12 which show ϵ_{50} versus undrained shear stress and relative density.

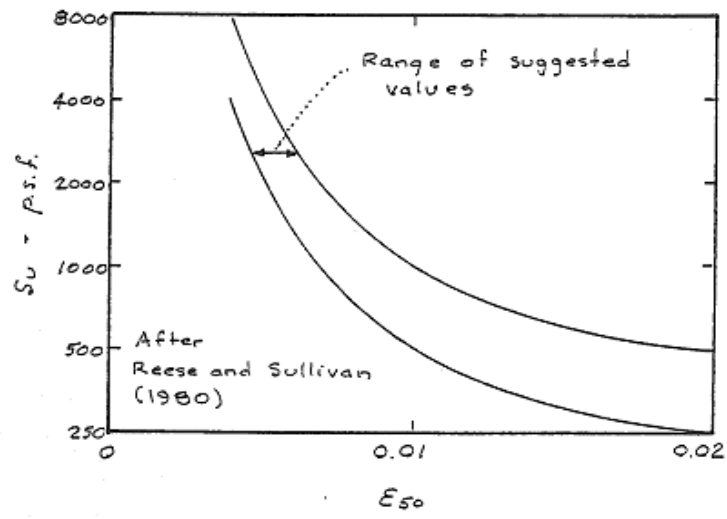


Figure 2-7. Variation of ϵ_{50} with undrained strength of Clays (Evans et al., 1982)

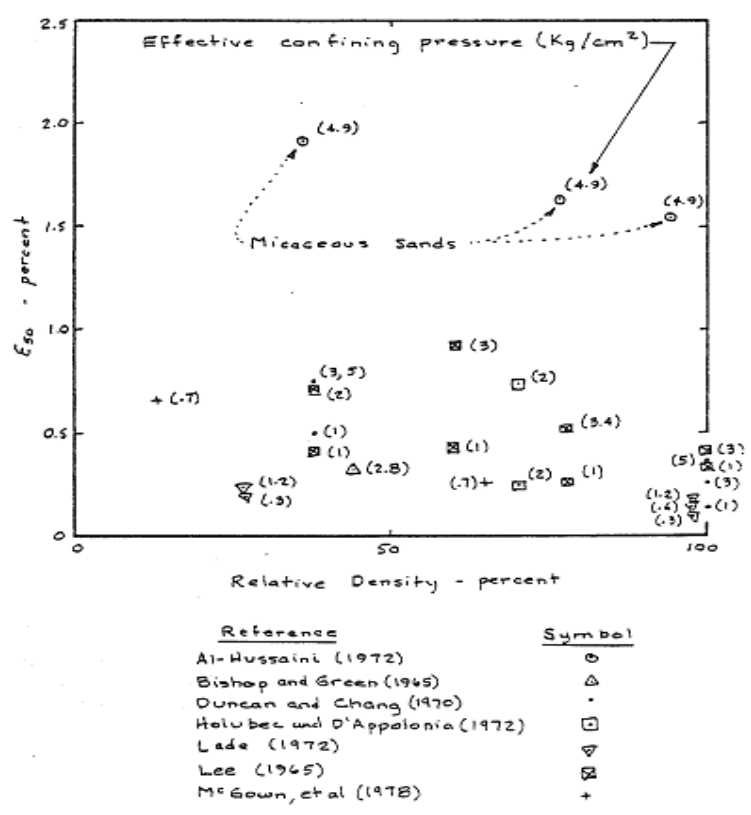
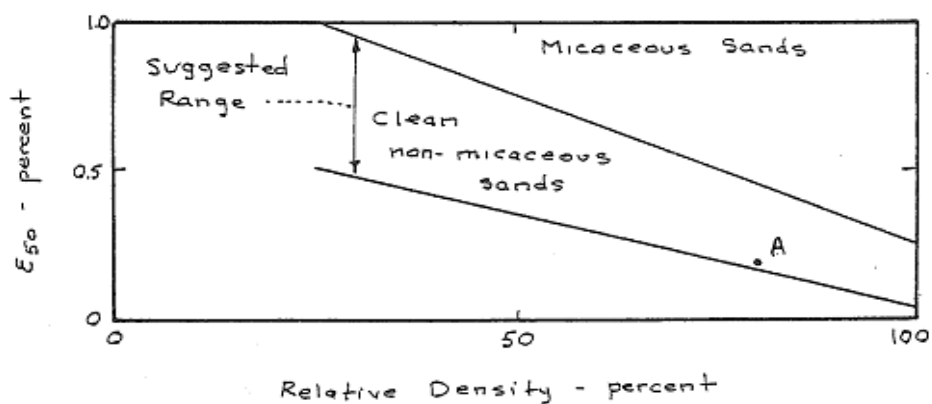


Figure 2-8. Variation of ϵ_{50} with Relative Density for Clays (Evans et al., 1982)

Table 2-11. Calculated Variation of ϵ_{50} with undrained strength of Clays (Evans et al., 1982)

Type of Soil	Su (kPa)	ϵ_{50}^* (%)
Clay	12-24	1.4-2
	24-48	0.9-1.4
	48-96	0.7-0.9
	96-192	0.5-.0.7
	192-383	0.5

ϵ_{50}^* : This parameter is calculated based on mentioned figures.

Figure 2-9. Variation of ϵ_{50} with Relative Density for Sands (Evans et al., 1982)Table 2-12. Calculated Variation of ϵ_{50} with Relative Density for sands (Evans et al., 1982)

Type of Soil	Friction Angle	Relative Density	ϵ_{50}^* (%) (Lee1965)
Sand	30-40	30	0.6
	30-40	40	0.5-1.9
	30-40	50	0.5
	30-40	60	0.6
	30-40	80	0.4-1.6
	30-40	90	1.5

ϵ_{50}^* : This parameter is calculated based on mentioned figures.

In a thesis by McClellan (2013), Figure 2-10, Figure 2-11, Figure 2-12, Figure 2-13, and Figure 2-14 showed the smaller diameter triaxial tests resulted in higher deviatoric stress.

Moreover, Table 2-13 illustrates the internal friction angle, undrained shear strength and depth of smaller diameter sample. Additionally, ϵ_{50} is measured based on these figures.

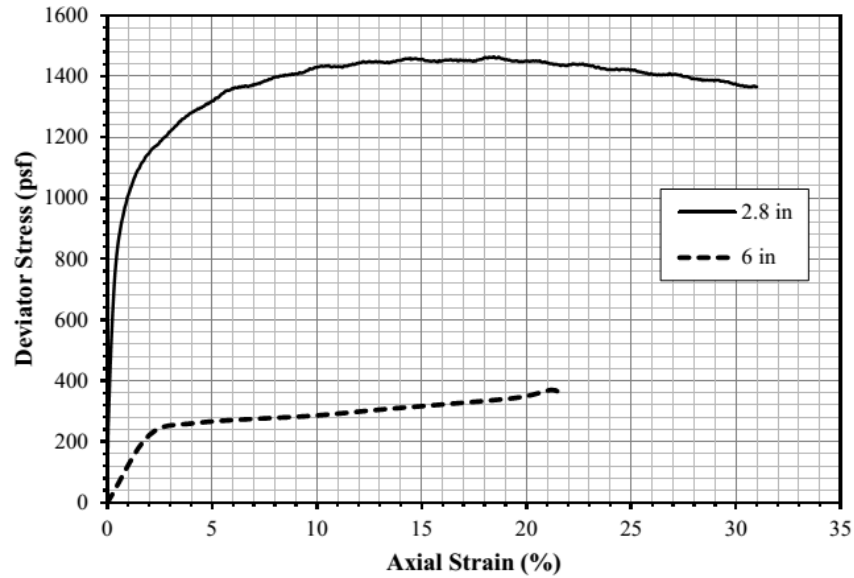


Figure 2-10. Deviatoric stress versus axial strain of 2.8 in. and 6 in. diameter triaxial compression tests for sample taken at a depth of 5 ft (McClellan (2013))

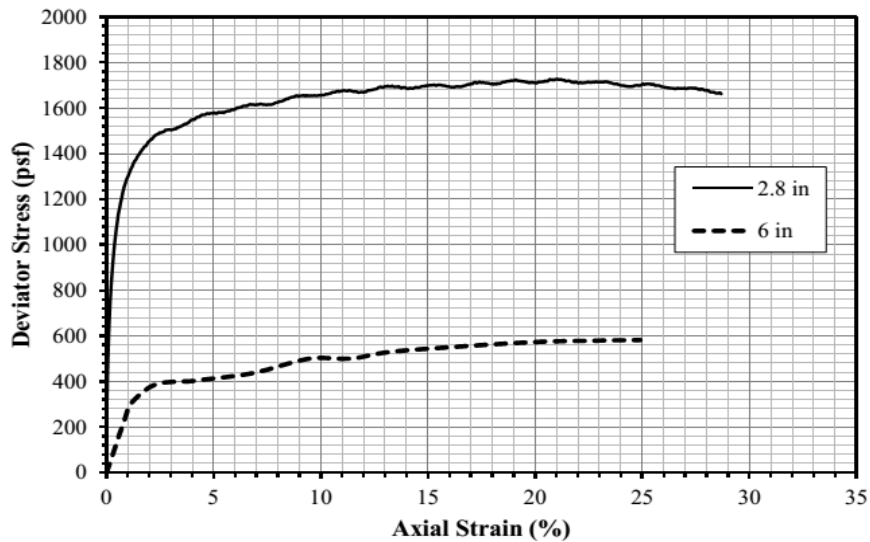


Figure 2-11. Deviatoric stress versus axial strain of 2.8 in. and 6 in. diameter triaxial compression tests for sample taken at a depth of 14.5 ft (McClellan (2013))

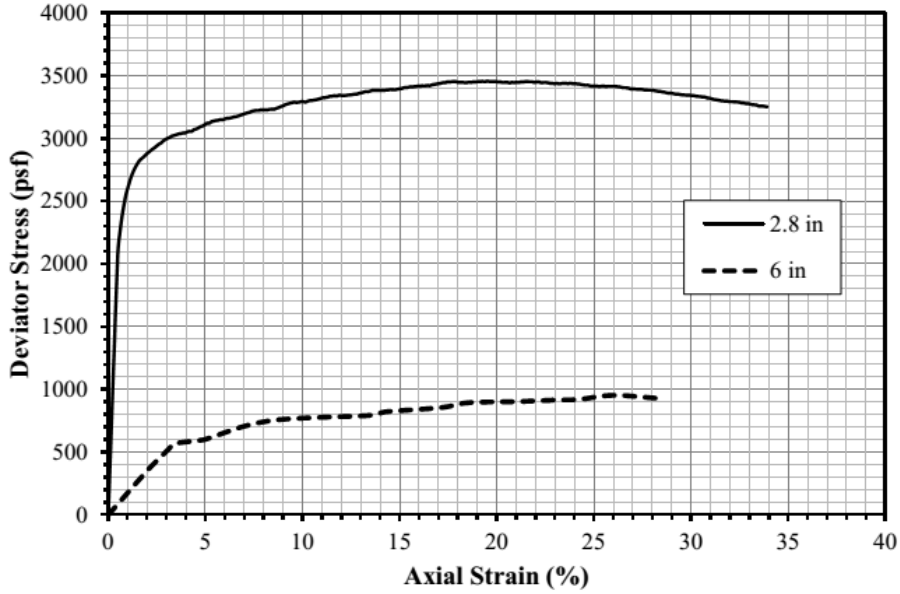


Figure 2-12. Deviatoric stress versus axial strain of 2.8 in. and 6 in. diameter triaxial compression tests for sample taken at a depth of 29 ft (McClellan (2013))

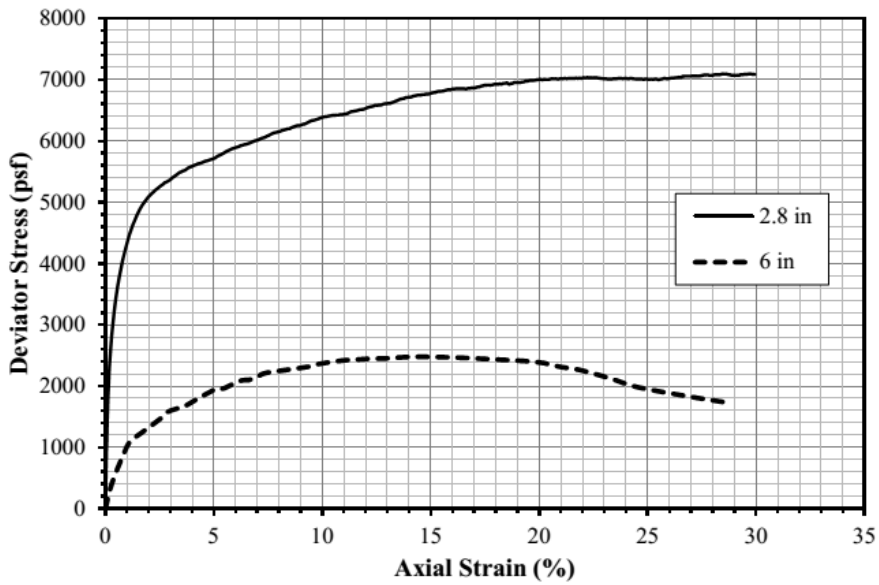


Figure 2-13. Deviatoric stress versus axial strain of 2.8 in. and 6 in. diameter triaxial compression tests for sample taken at a depth of 42.8 ft (McClellan (2013))

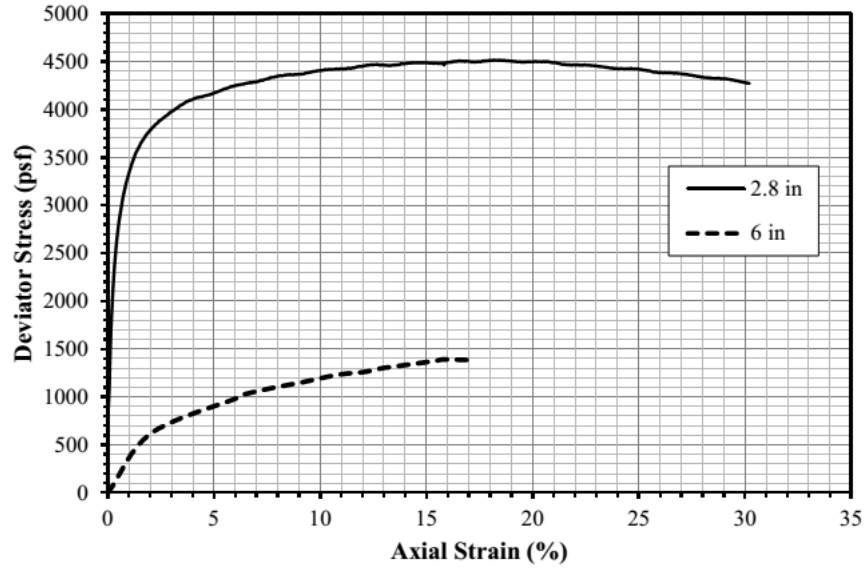


Figure 2-14. Deviatoric stress versus axial strain of 2.8 in. and 6 in. diameter triaxial compression tests for sample taken at a depth of 57.5 ft (McClellan (2013))

Table 2-13. Calculated ϵ_{50} based on Figures 8 to 12 (McClellan (2013))

Soil type	Depth (m)	ϵ_{50}^* (%)	$(\phi)_p$ (Degree)	S_u (kPa)
Sand	0.13	0.4	66	34.5
Sand	0.37	0.3	60	41.4
Sand	0.74	0.45	36	82.7
Sand	1.1	0.5	42	172.4
Sand	1.5	0.3	28	110.3

ϵ_{50}^* : This parameter is calculated based on mentioned figures.

3 BenchMarking Testing Program

3.1 Introduction

One of the most extensively performed geotechnical laboratory tests is Triaxial Test which is allowing the shear strength and stiffness of soil as well as rock to be determined for use in geotechnical design. The ability to control specimen drainage (CD Test) and take measurements of pore water pressures are several advantages of triaxial test. The angle of shearing resistance ϕ , cohesion c , and undrained shear strength C_u are some of primary parameters gained from the test. The shear strength which is a function of normal stress on the failure plane, can be conveyed by Equation 3-1.

$$\tau_f = C + \sigma \cdot \tan\phi$$

Equation 3-1. Mohr-Coulomb failure criterion

C = cohesion

ϕ = angle of internal friction

τ_f = shear strength

σ = normal stress on the failure plane

Figure 3-1 shows the schematic diagram of triaxial test setup.

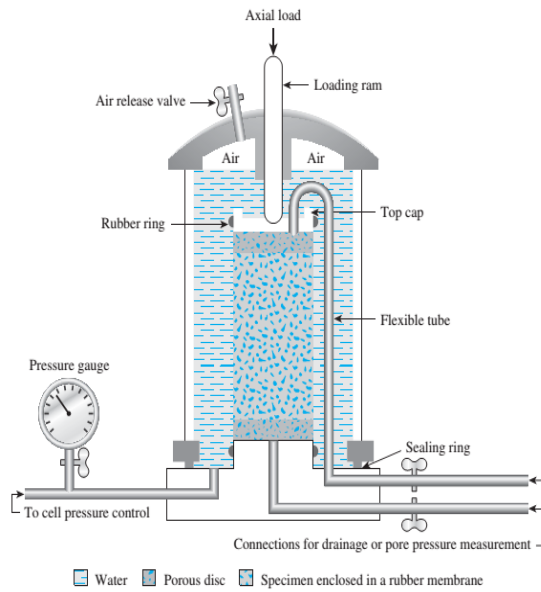


Figure 3-1. Schematic diagram of triaxial test setup

Bench Marking Triaxial tests were conducted to prove the currency and validation of the device and method of testing. These tests were conducted on seven samples in comparison with “VELACS Verification Analyses by centrifuge studies laboratory testing program soil data report” by Arulmoli et al (1992).

3.2 Main types of Triaxial tests and their objectives

There are three main types of triaxial tests that depend on the loading and drainage condition:

- Consolidated – Drained (CD)
- Consolidated – Undrained (CU)
- Unconsolidated - Undrained (UU)

Figure 3-2 illustrates the two main steps in a triaxial test. Furthermore, in the CD test, since the drainage valve is closed during the consolidation and shear phase, pore water pressure is generated. Hence, the volume is constant in a CU test.

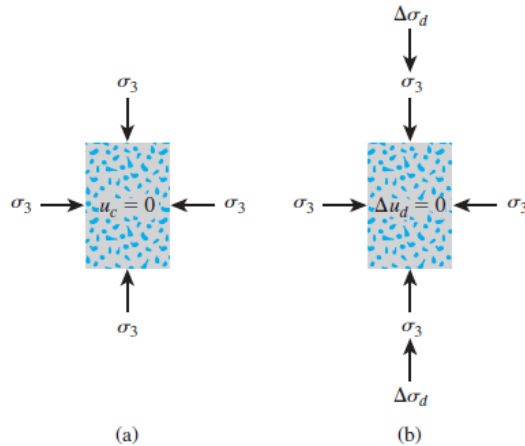


Figure 3-2 Triaxial Test

Several tests were performed on Navada sand at 40 % relative density. These tests include Triaxial tests with the 40, 80 and 160 kPa confining pressure. The results of these tests are presented in the following section.

3.3 Apparatus and supplies

Geocomp's fully automated triaxial system runs CU tests from start to finish. This system is operated by the software which includes the initialization, saturation, consolidation and shear phase. Figure 3-3 shows triaxial main part devices:



Figure 3-3. Geocomp's triaxial system

- **LoadTrac-II:** The unit that applies and controls the load during the shear phase.
- **Load Cell:** This unit measures the applied load during shear phase.
- **FlowTrac-II:** There are two FlowTrac-II units. One of them is controls and measures the water pressure inside the sample as well as volume change in it. The second one applies the cell pressure and measures the cell volume changes.
- **Triaxial Test Cell:** Chamber that confines the specimen to be tested using the load frame and two FlowTrac-II units.

-

3.4 Description of soil samples

Seven samples with 40 % relative density on Nevada sand was prepared for CU test.

Table 3-1 and Figure 3-4, Figure 3-5 and Figure 3-6 show the summary of Triaxial test data for Nevada sand as well as some examples of stress strain figures for 40 kPa, 80 kPa and 160 kPa Arulmoli et al. study.

Table 3-1. Summary of Triaxial test data for Nevada sand – 40% relative density (Arulmoli et al. 1992)

Test Type (1)	Test No.	AFTER SAMPLE PREPARATION				DURING SATURATION			CONSOLIDATION		AFTER CONSOLIDATION				
		Height H (m)	Density(2) (kN/m ³)	Void Ratio(3) e	Dr (4) (%)	Eff. Conf. Pressure (kPa)	Back Pressure (kPa)	B Value	Eff. Cons. Pressure (kPa)	q/p' during Consol.	Height H (m)	Diameter D (m)	Density (kN/m ³)	Void Ratio e	Dr (%)
CIUC	40-06	0.1533	15.05	0.740	39.2	13.8	694	0.98	40.0	0.00	0.1532	0.0637	15.08	0.736	40.2
CIUC	40-51	0.1544	15.06	0.739	39.4	13.8	691	1.00	40.0	0.00	0.1542	0.0637	15.11	0.733	41.1
CIUC	40-04	0.1532	15.09	0.735	40.4	13.8	695	0.98	80.0	0.00	0.1530	0.0637	15.14	0.729	42.2
CIUC	40-34	0.1545	15.08	0.736	40.1	13.8	695	0.98	80.0	0.00	0.1545	0.0637	15.12	0.732	41.4
CIUC	40-05	0.1549	15.03	0.742	38.6	13.8	696	0.98	160.0	0.00	0.1548	0.0636	15.12	0.732	41.5
CIUC	40-35	0.1525	15.12	0.732	41.3	13.8	701	1.00	160.0	0.00	0.1523	0.0636	15.18	0.725	43.1
CIUC	40-54	0.1527	15.07	0.738	39.8	13.8	695	1.00	160.0	0.00	0.1526	0.0635	15.17	0.726	42.9

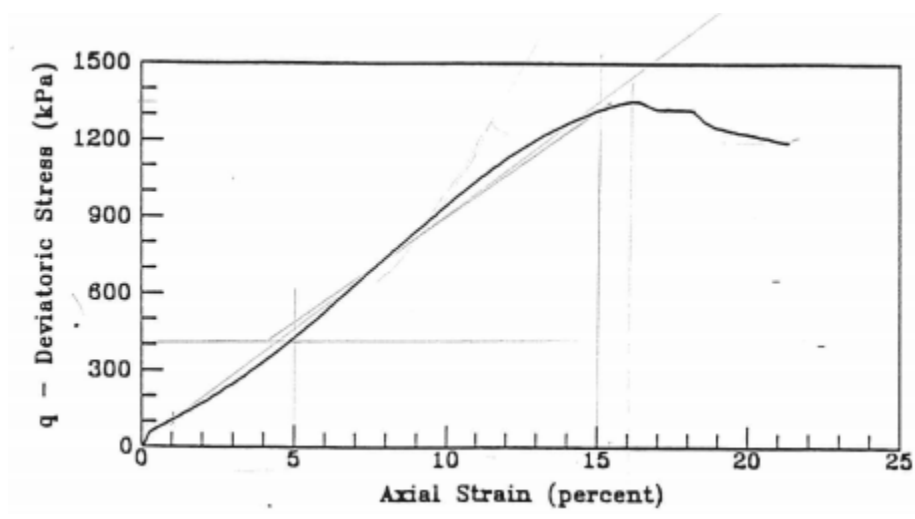


Figure 3-4 Deviatoric Stress vs. Axial Strain for 40 kPa Confining Pressure (Arulmoli et al. 1992)

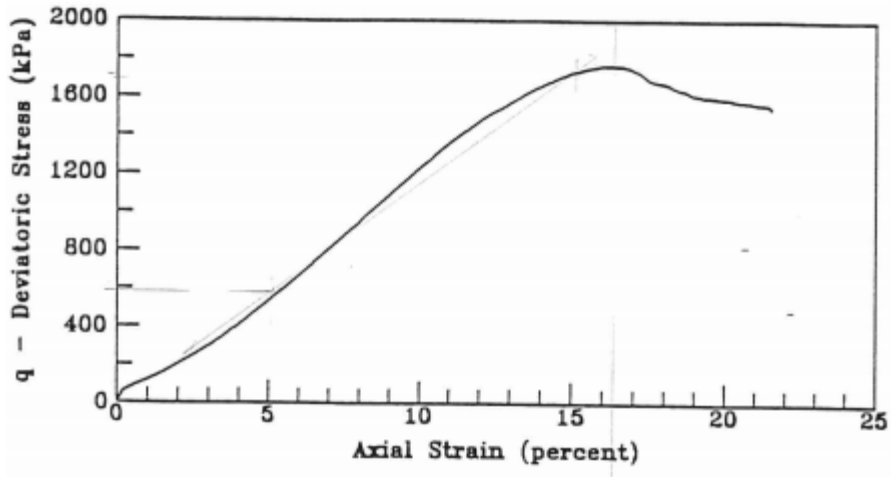


Figure 3-5. Deviatoric Stress vs. Axial Strain for 80 kPa Confining Pressure (Arulmoli et al. 1992)

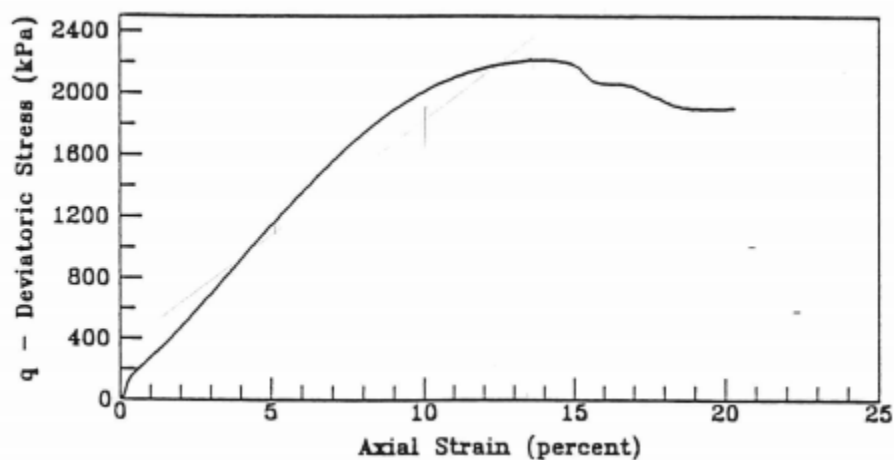


Figure 3-6. Deviatoric Stress vs. Axial Strain for 160 kPa Confining Pressure (Arulmoli et al. 1992)

Based on Arulmoli et al. 1992 report on Nevada sand the maximum dry unit weight ($\gamma_{d,max}$) and minimum dry unit weight ($\gamma_{d,min}$) was specified (Table 3-2, the first row). Hence, regarding equation 3-2 and with measuring the volume of samples, their weights were calculated (Table 3-3).

Table 3-2. Average unit weight of Nevada sand

Source	G _s	e _{min}	e _{max}	$\gamma_{d, min}$ (kN/m ³)	$\gamma_{d, max}$ (kN/m ³)
Arulmoli et al. (1991)	2.67	0.51	0.887	13.87	17.33
Balakrishnan (1997)	-	0.55	0.84	14.21	16.92
Woodward Clyde (1997)	-	-	-	13.97	16.75
Kammerer et al. (2000)	2.67	0.533	0.887	13.87	17.09
UC Davis - Seiji Kano (2007)	2.65	0.486	0.793	14.50	17.49
Cooper Lab (2007)	-	0.52	0.78	14.57	17.05
Cooper Lab (2008)	2.65	0.510	0.748	14.86	17.20

Table 3-3. Required soil mass for sample preparation

$\gamma_{d,max}$ (kN/m ³)	$\gamma_{d,min}$ (kN/m ³)	Dr (%)	γ_d (kN/m ³)	Average Sample Volume (ml.)	Soil Mass (gr)
17.33	13.87	40	15.078	612.79	924

$$D_r = \frac{\gamma_d - \gamma_{d,min}}{\gamma_{d,max} - \gamma_{d,min}} \times \frac{\gamma_{d,max}}{\gamma_d}$$

Equation 3-2. Mohr-Coulomb failure criterion

3.5 Sample preparation

Dry pluviation method was used based on ASTM D4767 for sample preparation. This test was conducted with 40% target relative density. A membrane-lined split mold was used for it. Then, the porous stone and paper filter was put at the bottom of the mold. After tamping, second paper filter was placed on the soil on the bottom of porous stone. The final step for preparing sample was measuring height and diameter at least 3 times for calculating real volume. Table 3-4 indicates these measurements.

Table 3-4. Sample measurements

Sample Number	Target Dr (%)	Average Diameter (in.)	Average Height (in.)	Weigh (gr)
CIUC	40	2.817	6	924

3.6 Adjustment and Calibration to Devices

Before running the test, the devices (FlowTrack, LoadTrack, Displacement and Load) should be calibrated. It means that all the pressures (Cell, Sample, and Deviator) as well as displacements are zeros.

3.7 Test Procedure and Triaxial Software

There are four phases in Geocomp's Triaxial software:

- **Initialization:** Applies and maintains a small vertical and horizontal stress to achieve a pressure differential within the triaxial cell chamber so that the user can check for possible leaks.
- **Consolidation/A:** Consolidates specimen in steps to specified horizontal and vertical stresses before saturation.
- **Saturation:** Saturates specimen to a specified minimum saturation ratio by incrementally increasing the cell pressure and pore pressure.

- **Consolidation/B:** Consolidates specimen in steps to specified horizontal and vertical stresses after saturation.
- **Shear:** Shears specimen, either drained or undrained, with absolute or relative stress type and under stress or strain control.

Some inputs was used in the software:

Effective confining pressure was equal to 40, 80 and 160 kPa in consolidation phase while in shear phase their amounts were 1000 and 0 psi, respectively. Additionally, stress rate was 15 psi/min for 40 kPa confining pressure and 20 psi/min for 80 and 160 kPa as well as strain rate was 0.02 per minute for all of them. Table 3-5 shows these inputs.

Table 3-5 Test Inputs (Arulmoil 1992)

Test No.	Eff. Confining Pressure (Kpa)	Eff. Consolidation Pressure (Kpa)	Back Pressure (Kpa)	Initial Dry Density (kN/m ³)	Initial Void Ratio	Initial Relative Density (%)
CIUC4006-4	13.8	40	700	15.078	0.773	40.1
CIUC4051-2	13.8	40	700	15.1	0.769	40.8
CIUC4004	13.8	80	700	15.1	0.77	40.8
CIUC4034	13.8	80	700	15.078	0.773	40.1
CIUC4005	13.8	160	700	15.1	0.764	40.8
CIUC4035	13.8	160	700	15.078	0.771	40.1
CIUC4054	13.8	160	700	15.074	0.773	40.02

3.8 Data Obtained, Results, and Discussion

Some important results of triaxial test are shown in the following figures.

Figure 3-7, Figure 3-8 and Figure 3-9 show deviatoric stress changes vs. axial strain for Arulmoli et al samples (yellow, red and green) as well as our samples(black, blue and orange) for 40, 80 and 160 kPa confining pressure, respectively. As it can be observed, Arulmoli et al samples reach their peak at the greater amount vs. ours. Interestingly, both groups are approximately similar in axial strain at this time, with a slight difference of nearly 2% for all of confining

pressure. Furthermore, 160 kPa confining pressure for both groups have the maximum value of the deviatoric stress at the smaller axial strain.

Moreover, for 80 kPa confining pressure, while the peak value is gained around 13% axial strain for blue and black graphs, yellow and red graphs summits in 15% axial strain.

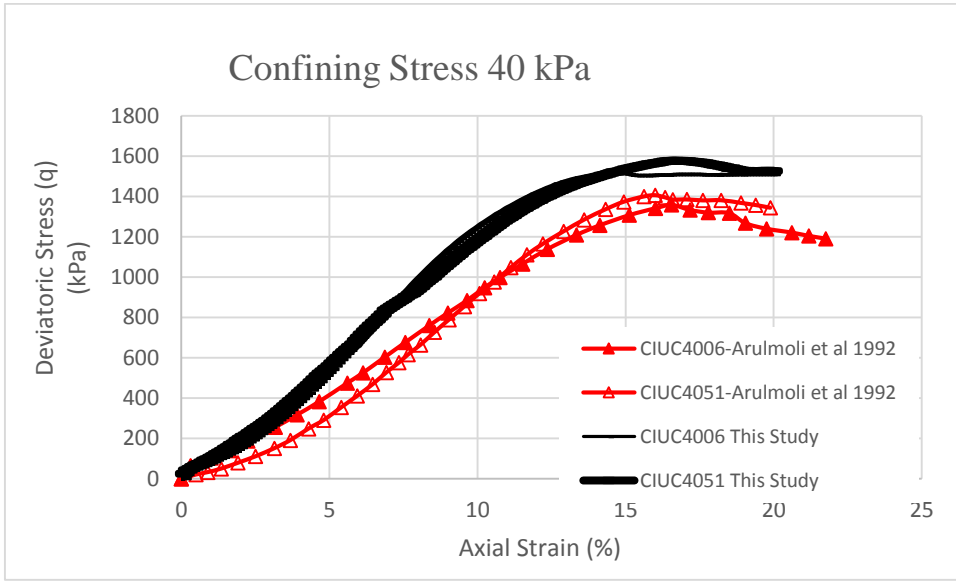


Figure 3-7. Deviatoric Stress vs. Axial Strain for 40 kPa Confining Pressure

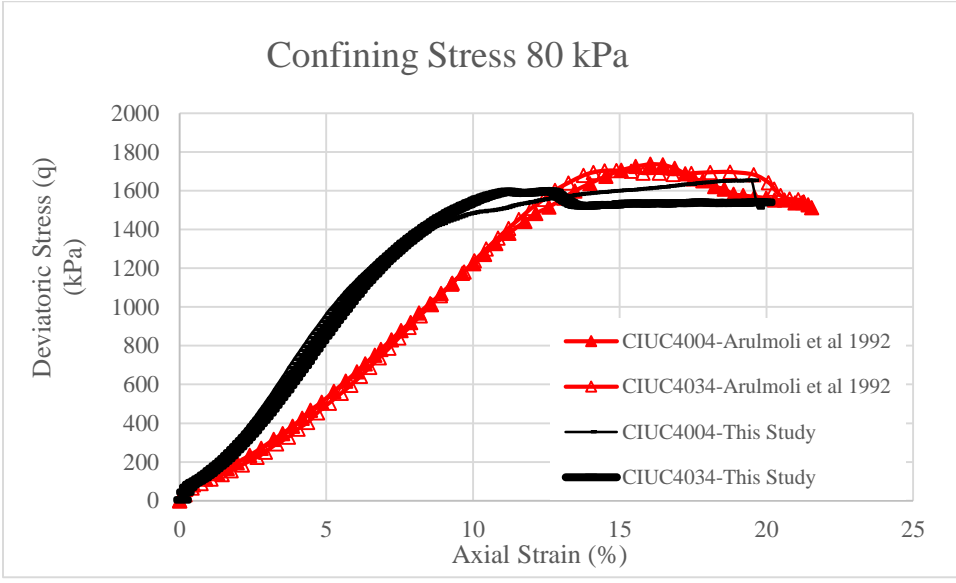


Figure 3-8. Deviatoric Stress vs. Axial Strain for 80 kPa Confining Pressure

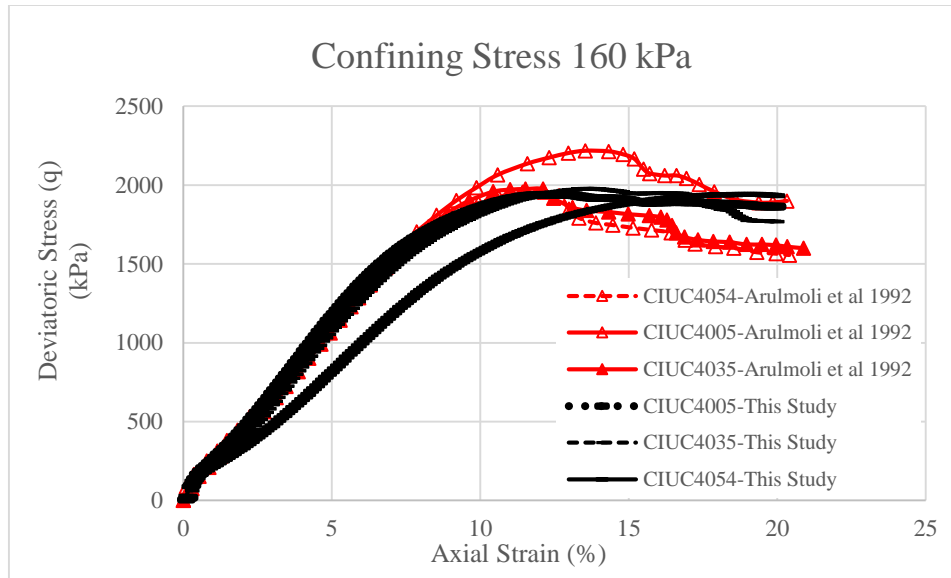


Figure 3-9. Deviatoric Stress vs. Axial Strain for 160 kPa Confining Pressure

In CU test, the excess pore water pressure is generated because the drainage valve is close. Figure 3-10, Figure 3-11 and Figure 3-12 illustrate the generated pore water pressure vs. axial strain in shear phase. For all these three graphs, following a quick rise, they dive. It should be noted that overall there is a rough similarity between Arulmoli et al graphs and ours. Besides, 160 kPa confining pressure for both groups have the minimum amount of the pore water pressure.

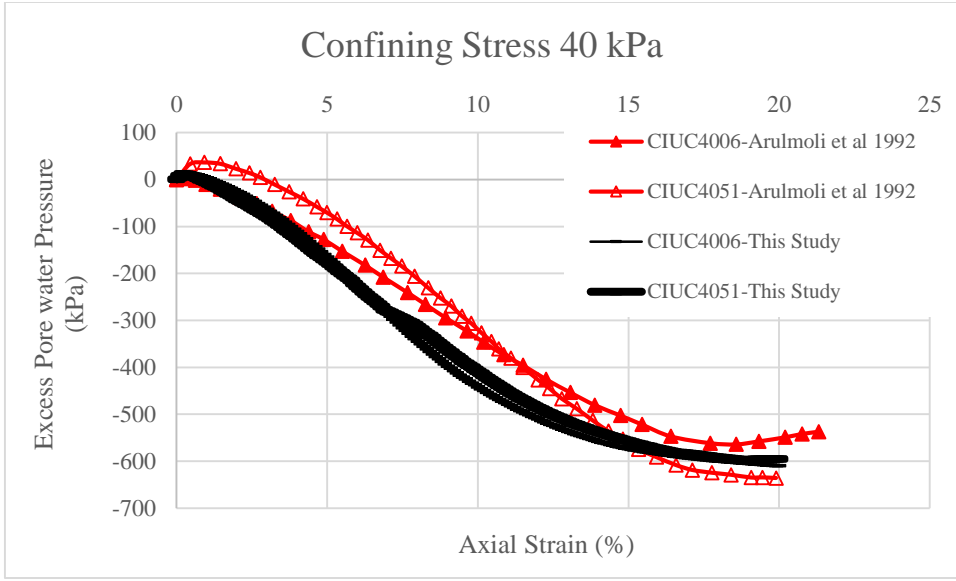


Figure 3-10. Excess PWP vs. Axial Strain for 40 kPa Confining Pressure

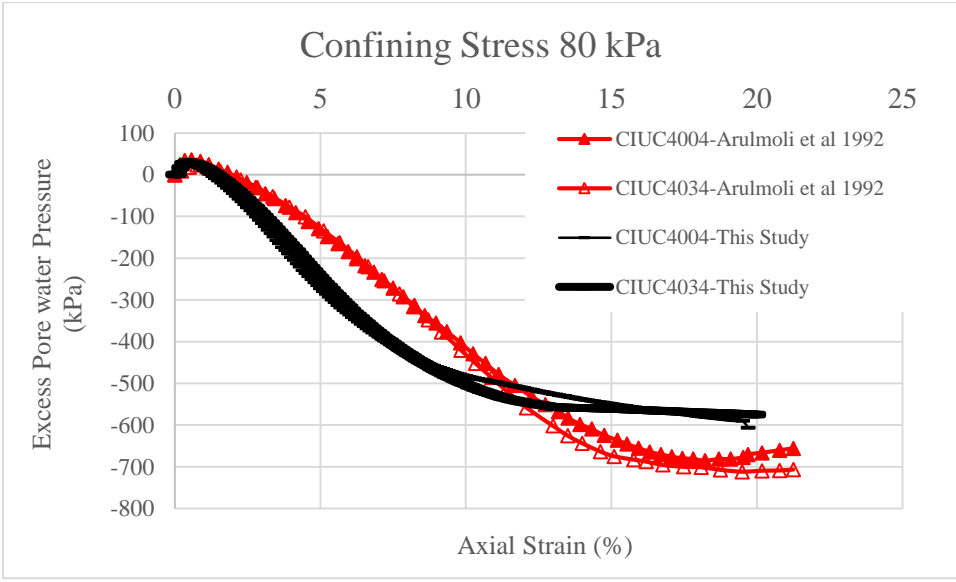


Figure 3-11. Excess PWP vs. Axial Strain for 80 kPa Confining Pressure

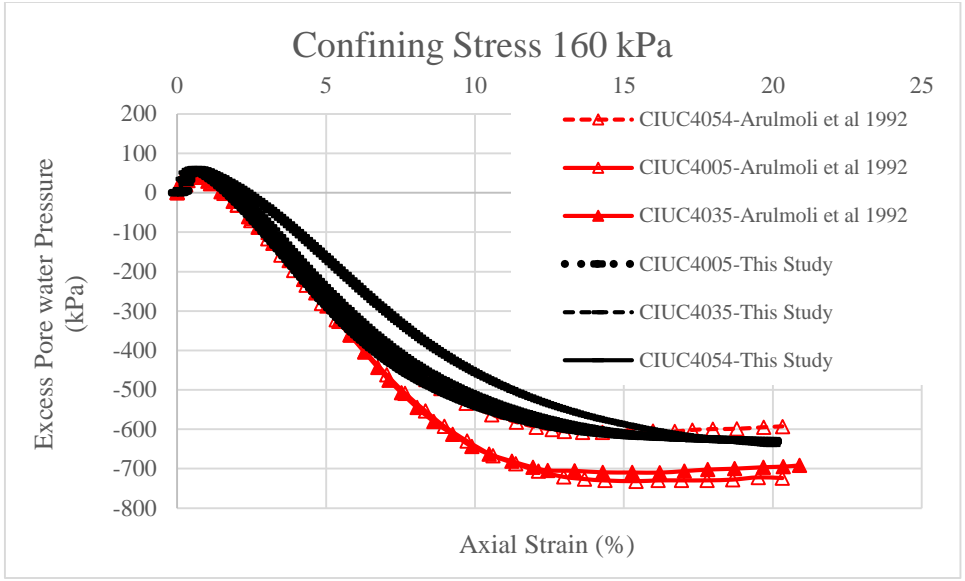


Figure 3-12. Excess PWP vs. Axial Strain for 160 kPa Confining Pressure

Figure 3-14, Figure 3-15 and Figure 3-15 deals with deviatoric stress vs. effective P [$P' = (\sigma_1 + \sigma_3)/2$]. All samples' graphs mount moderately. However, Arulmoli et al graph have sharper slope in compare with ours.

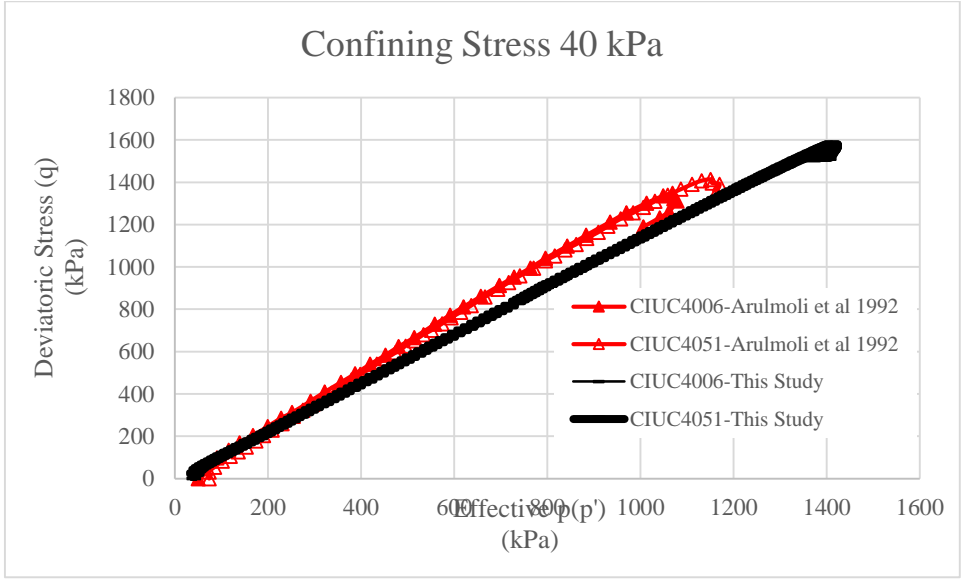


Figure 3-13. Deviatoric Stress vs. P' for 40 kPa Confining Pressure

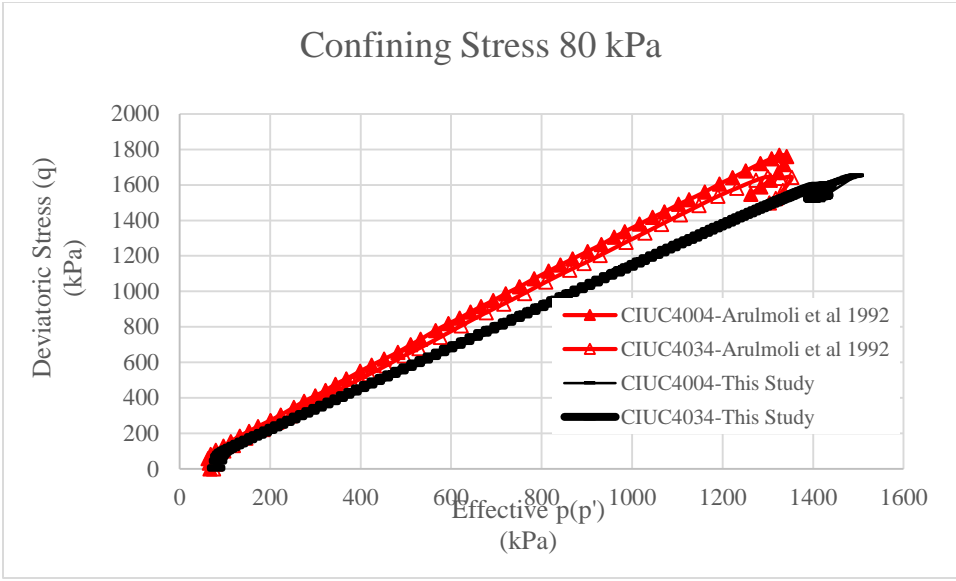


Figure 3-14. Deviatoric Stress vs. P' for 80 kPa Confining Pressure

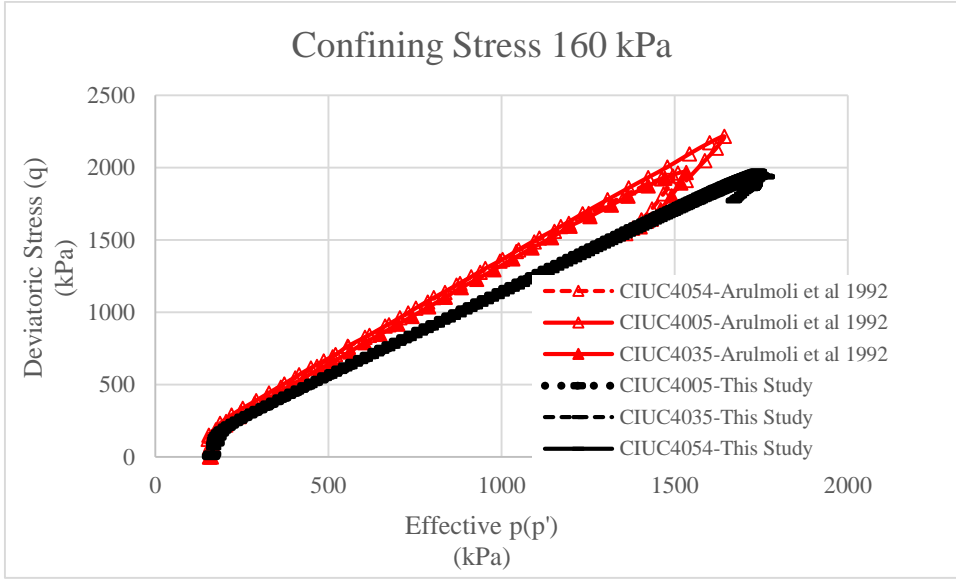


Figure 3-15. Deviatoric Stress vs. P' for 160 kPa Confining Pressure

3.9 Summary of Observed Results

This report shows triaxial tests and their results for seven different samples which prove the accuracy and validation of the devise and someone conduct the tests.

4 Experimental Program

4.1 Description of soil samples

4.1.1 C- ϕ soil Definition

C- ϕ materials are described as Mixed Soils behaving like granular and cohesive soils with properties defined as containing 15%-35% of plastic clay/silt with $PI > 7$. These soils are often encountered in the design of deep foundations and the common practice is to treat them either as cohesionless or cohesive soils (i.e. assuming one behavior or another).

Three different soil types were used in this research. The first one is called Granite soil, second one is called Black Eagles and the third one is called Mixed Soil.

4.1.2 General Test Results

There are several general laboratory tests including sieve analysis, specific gravity tests, minimum and maximum density tests, Specific Gravity test, Atterberg limits tests, and sieve analysis. They listed in Table 4-1. Standard used in laboratory testing Table 4-1, Table 4-2, Table 4-3, Table 4-4, Table 4-5, Table 4-6, Table 4-7, and

Table 4-8.

Table 4-1. Standard used in laboratory testing

Test Performed	Standard Used
Particle-Size Analysis	D422
Maximum Density	D4253
Minimum Density	D4254
Specific Gravity	D854
Atterberg Limits	D4318
Consolidated-Undrained Triaxial Compression	D4767

Table 4-2. Soil sample sources

Soil Number	Source
Soil 1	Granite
Soil 2	Black Eagle
Soil 3	Mixed of Black Eagle and Concrete Sand

Table 4-3. Summary of general test results for Soil 1 (Granite)

Specific Gravity	2.7
Maximum Dry Density	17.75
Minimum Dry Density	14.85

Table 4-4. Summary of general test results for Soil 2 (Black Eagle)

Specific Gravity	2.7
Maximum Dry Density	15.017
Minimum Dry Density	12.814

Table 4-5. Summary of general test results for Soil 3 (Mixed)

Specific Gravity	2.7
Maximum Dry Density	16.834
Minimum Dry Density	13.777

Table 4-6. Summary of Sieve Analysis for Soil 1 (Granite)

Sieve Number	3/8"	#4	#8	#10	#16	#30	#40	#50	#100	#200	Pan
Sieve Size (mm)	9.5	4.75	2.36	2	1.18	0.6	0.425	0.3	0.15	0.075	
Percent Passing	100.0	84.3	67.1	63.5	52.6	42.3	38.3	34.6	30.0	24.9	0.0

Table 4-7. Summary of Sieve Analysis for Soil 2 (Black Eagle)

Sieve Number	#4	#10	#20	#40	#60	#100	#200	Pan
Sieve Size (mm)	4.75	2	0.85	0.425	0.25	0.15	0.075	
Percent Passing	100	95.27	86.82	72.02	64.94	53.42	38.77	0.0

Table 4-8. Summary of Sieve Analysis for Soil 3 (Mixeded)

Sieve Number	#3/8"	#4	#10	#20	#40	#60	#100	#200	Pan
Sieve Size (mm)	9.5	4.75	2	0.85	0.425	0.25	0.15	0.075	
Percent Passing	100	98.3	84.08	61.41	46.99	35.82	27.11	19.385	0.0

4.2 Sample preparation

Dry pluviation method was used based on ASTM D4767 for sample preparation. Three tests with 40%, three tests with 60% and three tests with 80% target relative density were conducted. A membrane-lined split mold was used for this method. Then, the porous stone and paper filter was put at the bottom of the mold. After tamping, second paper filter was placed on the soil on the bottom of porous stone. The final step for preparing samples was measuring height and diameter at least 3 times for calculating real volume. Table 4-9,

Table 4-10, and Table 4-11 indicate these measurements for Granite soil, Black Eagle soil and Mixed soil, respectively.

Table 4-9. Sample measurements (Granite soil)

Sample Number	Target Dr (%)	Average Diameter (in.)	Average Height (in.)	Weight (gr)
Granit soil 1	40	2.817	6	973
Granit soil 4	60	2.817	6	1008
Granit soil 7	80	2.817	6	1046

Table 4-10. Sample measurements (Black Eagle soil)

Sample Number	Target Dr (%)	Average Diameter (in.)	Average Height (in.)	Weight (gr)
Black Eagle soil 10	40	2.817	6	835
Black Eagle soil 13	60	2.817	6	863
Black Eagle soil 16	80	2.817	6	892

Table 4-11. Sample measurements (Mixed Soil)

Sample Number	Target Dr (%)	Average Diameter (in.)	Average Height (in.)	Weight (gr)
Mixed Soil 19	40	2.817	6	910
Mixed Soil 22	60	2.817	6	947
Mixed Soil 25	80	2.817	6	988

4.3 Adjustment and Calibration to Devices

Before running the test, the devices (FlowTrack, LoadTrack, Displacement and Load) should be calibrated. It means that all the pressures (Cell, Sample, and Deviator) as well as displacements should be zeros.

4.4 Test Procedure and Triaxial Software

Some inputs were used in the software including 40, 80 and 160 kPa effective confining pressure in consolidation phase while in shear phase their amounts were 1000 and 0 psi, respectively. Additionally, stress rate was 15 psi/min for 40 kPa confining pressure and 20 psi/min for 80 and 160 kPa as well as strain rate was 0.02 per minute for all of them. Table 4-12, Table 4-13, Table 4-14. show these inputs for Granite soil, Black Eagle soil, and Mixed Soil, respectively.

Table 4-12. Test Inputs (Granite soil)

Test No.	Eff. Confining Pressure (Kpa)	Eff. Consolidation Pressure (Kpa)	Back Pressure (Kpa)	Initial Dry Density (kN/m ³)	Initial Relative Density (%)
Granite Soil 1	13.8	40	700	15.89	40
Granite Soil 2	13.8	40	700	15.89	40
Granite Soil 3	13.8	40	700	15.89	40
Granite Soil 4	13.8	80	700	16.46	60
Granite Soil 5	13.8	80	700	16.46	60
Granite Soil 6	13.8	80	700	16.46	60
Granite Soil 7	13.8	160	700	17.08	80
Granite Soil 8	13.8	160	700	17.08	80
Granite Soil 9	13.8	160	700	17.08	80

Table 4-13. Test Inputs (Black Eagle soil)

Test No.	Eff. Confining. Pressure (Kpa)	Eff. Consolidation Pressure (Kpa)	Back Pressure (Kpa)	Initial Dry Density (kN/m ³)	Initial Relative Density (%)
Black Eagle Soil 10	13.8	40	700	13.63	40
Black Eagle Soil 11	13.8	40	700	13.63	40
Black Eagle Soil 12	13.8	40	700	13.63	40
Black Eagle Soil 13	13.8	80	700	14.083	60
Black Eagle Soil 14	13.8	80	700	14.083	60
Black Eagle Soil 15	13.8	80	700	14.083	60
Black Eagle Soil 16	13.8	160	700	14.564	80
Black Eagle Soil 17	13.8	160	700	14.564	80
Black Eagle Soil 18	13.8	160	700	14.564	80

Table 4-14. Test Inputs (Mixed Soil)

Test No.	Eff. Confining. Pressure (Kpa)	Eff. Consolidation Pressure (Kpa)	Back Pressure (Kpa)	Initial Dry Density (kN/m ³)	Initial Relative Density (%)
Mixed Soil 19	13.8	40	700	14.856	40
Mixed Soil 20	13.8	40	700	14.856	40
Mixed Soil 21	13.8	40	700	14.856	40
Mixed Soil 22	13.8	80	700	15.462	60
Mixed Soil 23	13.8	80	700	15.462	60
Mixed Soil 24	13.8	80	700	15.462	60
Mixed Soil 25	13.8	160	700	16.119	80
Mixed Soil 26	13.8	160	700	16.119	80
Mixed Soil 27	13.8	160	700	16.119	80

4.5 Triaxial Test Results

4.5.1 C- ϕ Soil 1 (Granite Soil)

Nine samples with 40%, 60% and 80% relative density on a C- ϕ soil 1 were prepared for CU tests. These tests were conducted on 40 kPa, 80 kPa and 160 kPa.

Table 4-15 shows the summary of Triaxial test data for this soil.

Table 4-15. Summary of Triaxial test data for C- ϕ Soil 1 (Granite)–40% relative density

Soil Type	Target Dr (%)	d (inch)	h (inch)	Target gamma (kN/m ³)	V (mm ³)	M (gr)	gamma, max (kN/ m ³)	gamma,min (kN/ m ³)	M (gr)	Final gamma (kN/ m ³)	Dr (%)
Granite C- ϕ soil 1	40	2.817	6	15.89	612485	973.239	17.75	14.85	973	15.88609	39.92
Granite C- ϕ soil 4	60	2.817	6	16.46	612485	1008.15	17.75	14.85	1008	16.45753	59.79
Granite C- ϕ soil 7	80	2.817	6	17.08	612485	1046.13	17.75	14.85	1046	17.07796	79.85

For determining the maximum dry unit weight ($\gamma_{d,max}$) and minimum dry unit weight ($\gamma_{d,min}$), ASTM 4253 and ASTM 4254 were used, respectively. Hence, regarding equation 4-1 and with measuring the volume of samples, their weights were calculated (Table 4-16).

Table 4-16. Required soil mass for sample preparation (Granite Soil)

$\gamma_{d,max}$ (kN/m ³)	$\gamma_{d,min}$ (kN/m ³)	Dr (%)	γ_d (kN/m ³)	Average Sample Volume (ml.)	Soil Mass (gr)
17.75	14.85	40	15.89	612.485	973.24
17.75	14.85	60	16.46	612.485	1008.15
17.75	14.85	80	17.08	612.485	1046.13

$$D_r = \frac{\gamma_d - \gamma_{d,min}}{\gamma_{d,max} - \gamma_{d,min}} \times \frac{\gamma_{d,max}}{\gamma_d}$$

Equation 5-1. Mohr-Coulomb failure criterion

The gradation curve and Atterberg limit are the other tests which are necessary for determining soil properties.

Figure 4-1 and Figure 4-2 show the results of these tests.

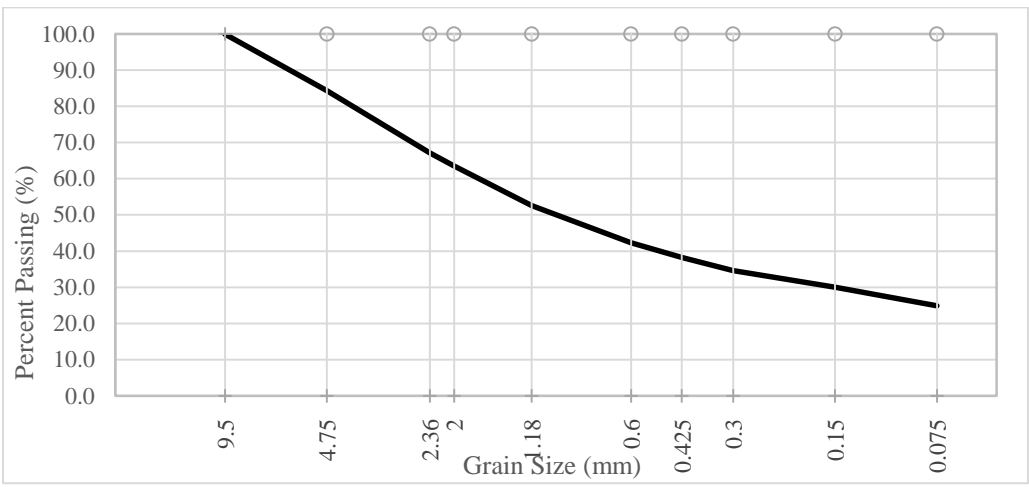


Figure 4-1. The gradation curve of Soil 1 (Granite Soil)

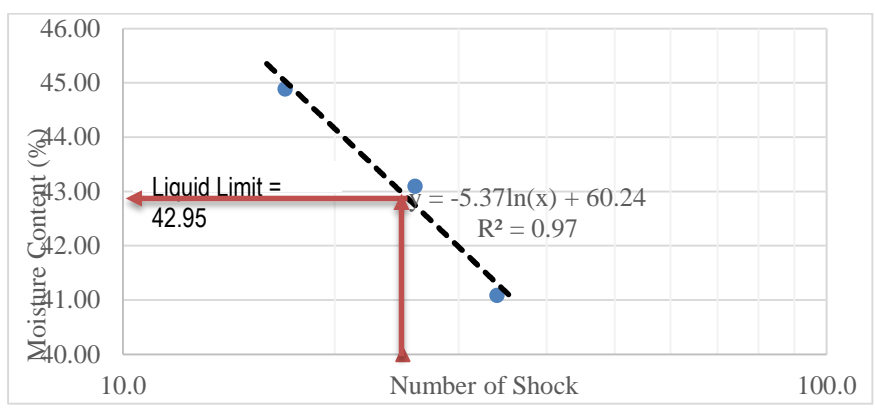
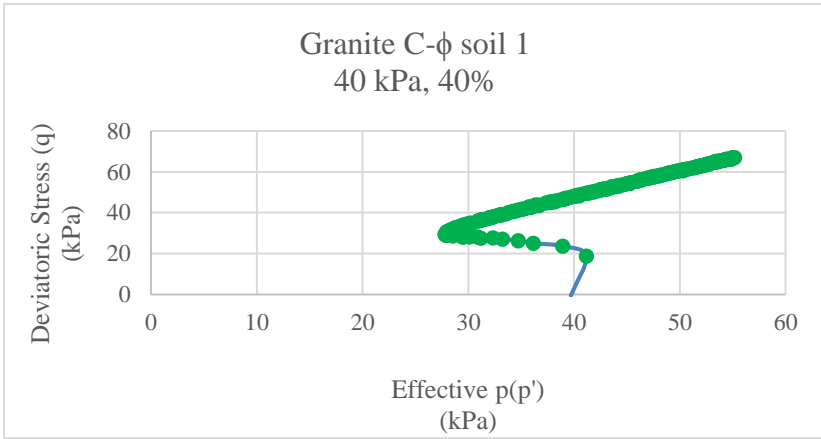
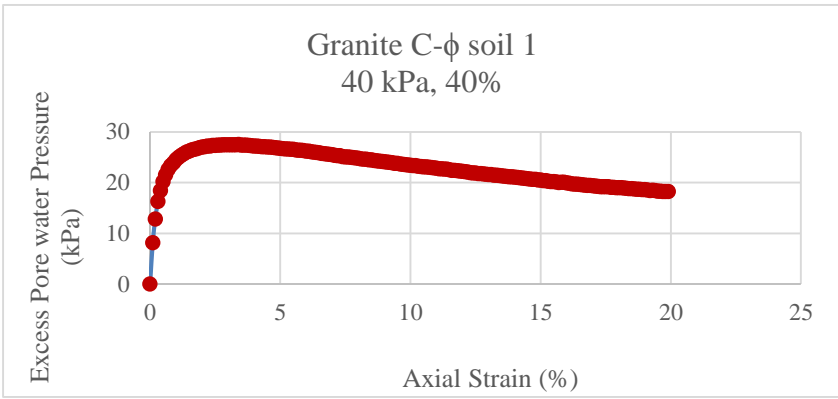
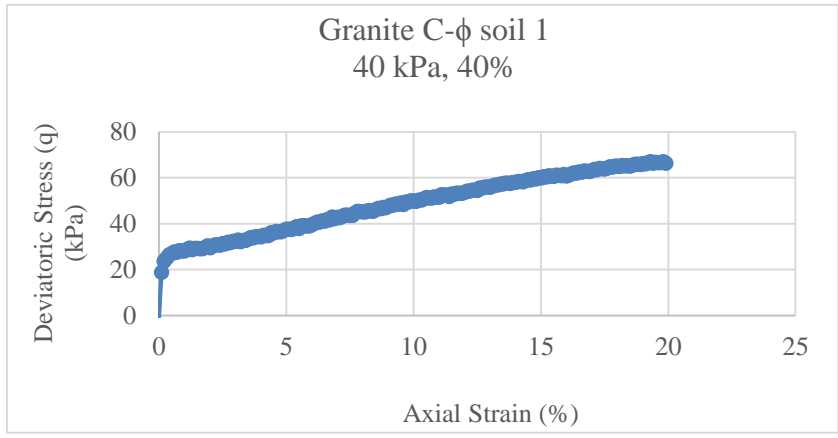


Figure 4-2. Atterberg Limit graph of Soil 1 (Granite Soil)

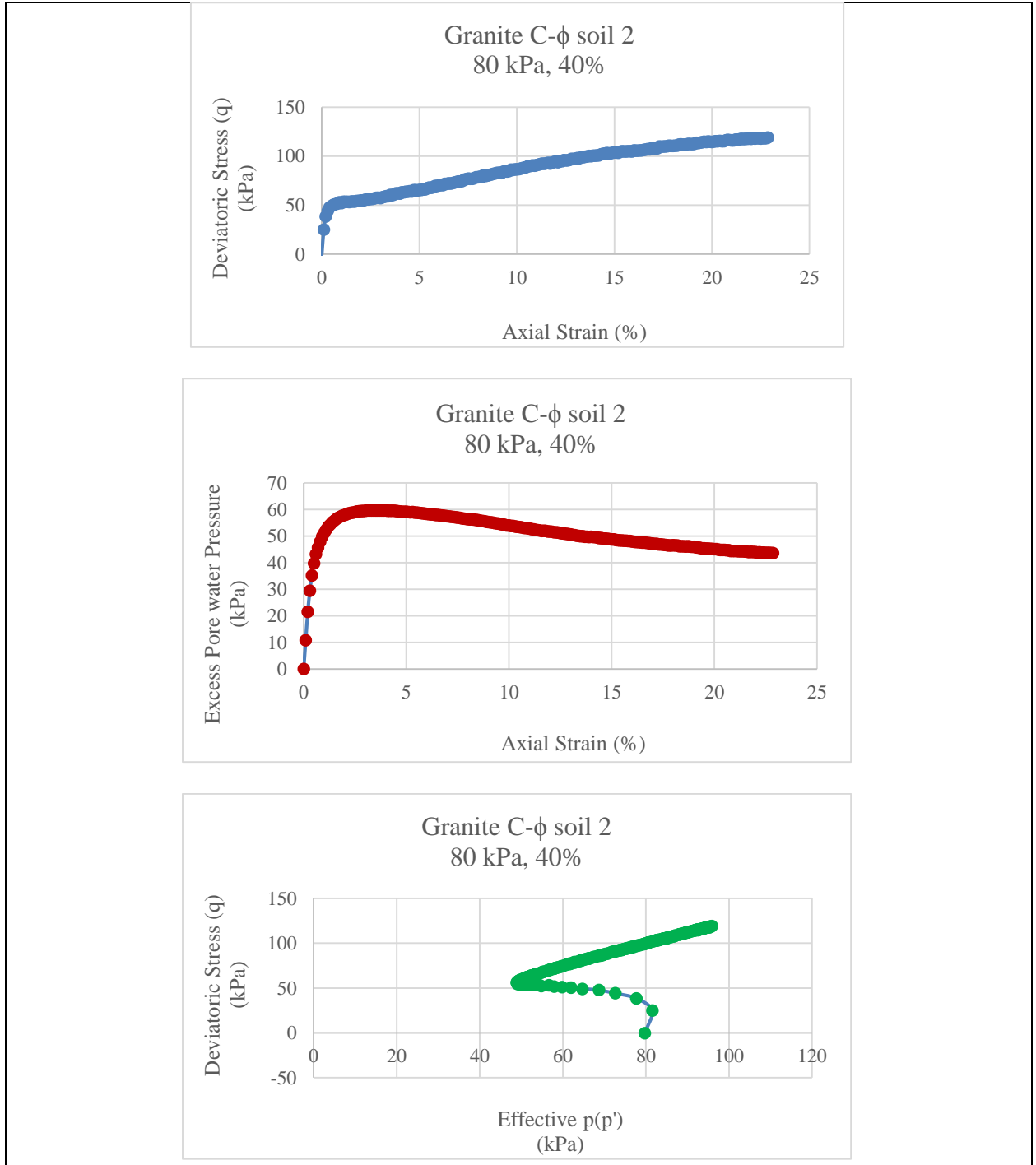
Figures 4-3 to Figures 4-11 show the results of the tests which illustrate Deviatoric stress versus Axial strain, Excess pore water pressure versus axial strain and Deviatoric stress versus Effective pressure for 40, 80 and 160 kP confining pressure of Granite soil in 40, 60 and 80% relative density.



Effective Consolidation pressure	40 kPa
Back Pressure	700 kPa
Initial Dry Density	15.89 kN/m ³

Results of Triaxial Test: Granite C-φ soil 1
Initial Relative Density: 40%
$\epsilon_{50} = 4.51 \%$

Figure 4-3. Triaxial test results of Granite Soil 1 Sample



Effective Consolidation pressure	80 kPa	Results of Triaxial Test: Granite C-φ soil 2	
Back Pressure	700 kPa	Initial Relative Density: 40%	
Initial Dry Density	15.89 kN/m ³	ε ₅₀ = 3.3 %	

Figure 4-4. Triaxial test results of Granite Soil 2 Sample

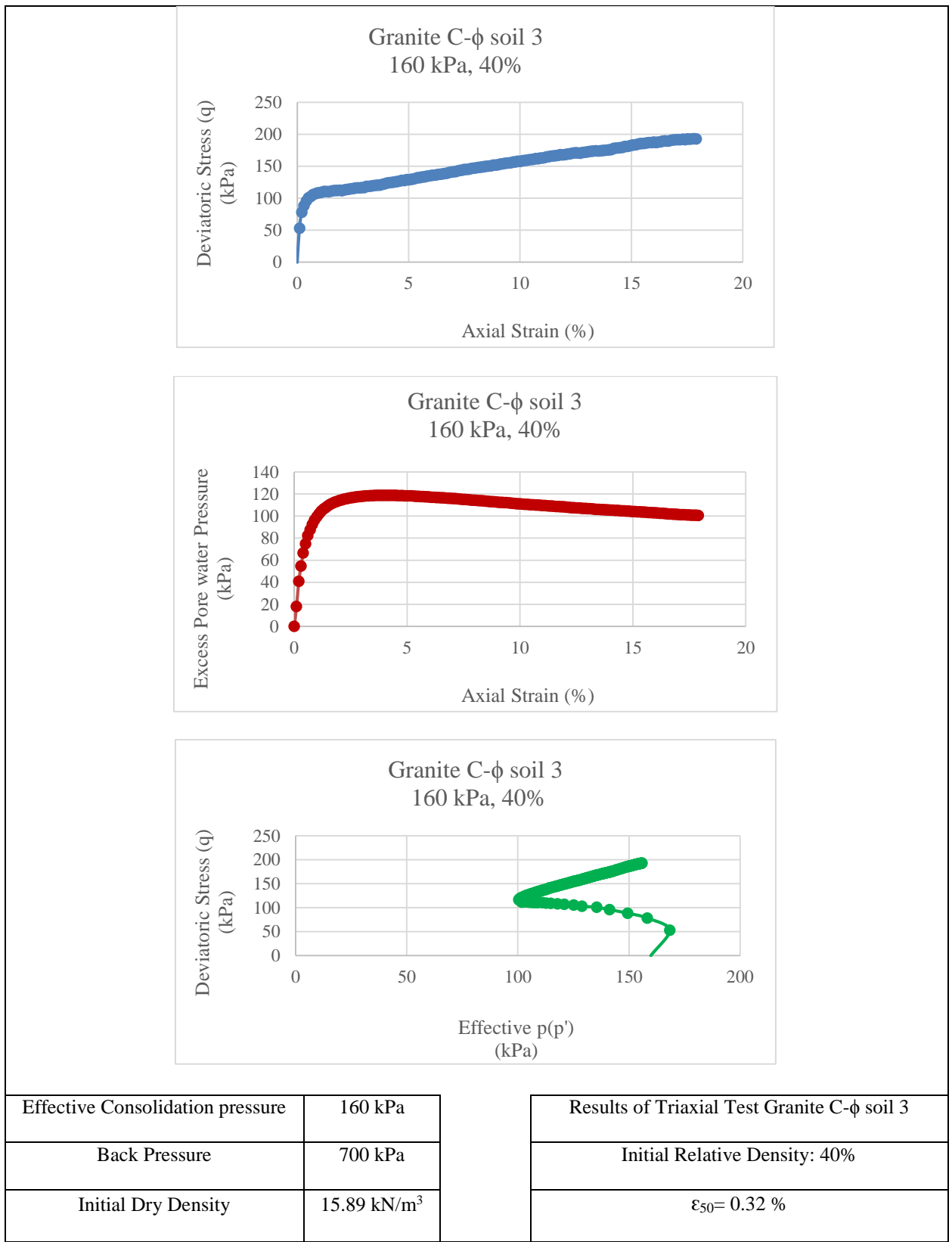


Figure 4-5. Triaxial test results of Granite Soil 3 Sample

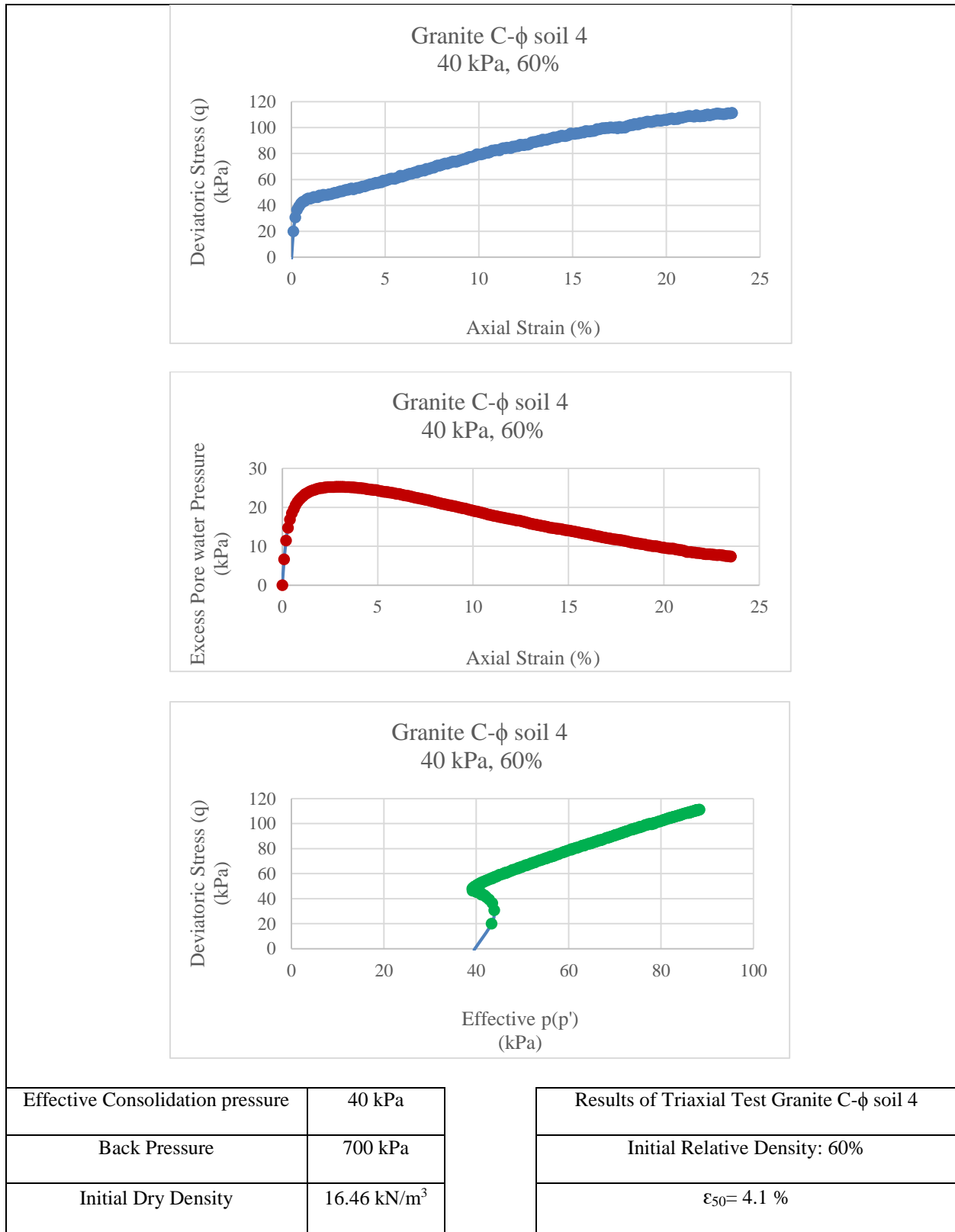


Figure 4-6. Triaxial test results of Granite Soil 4 Sample

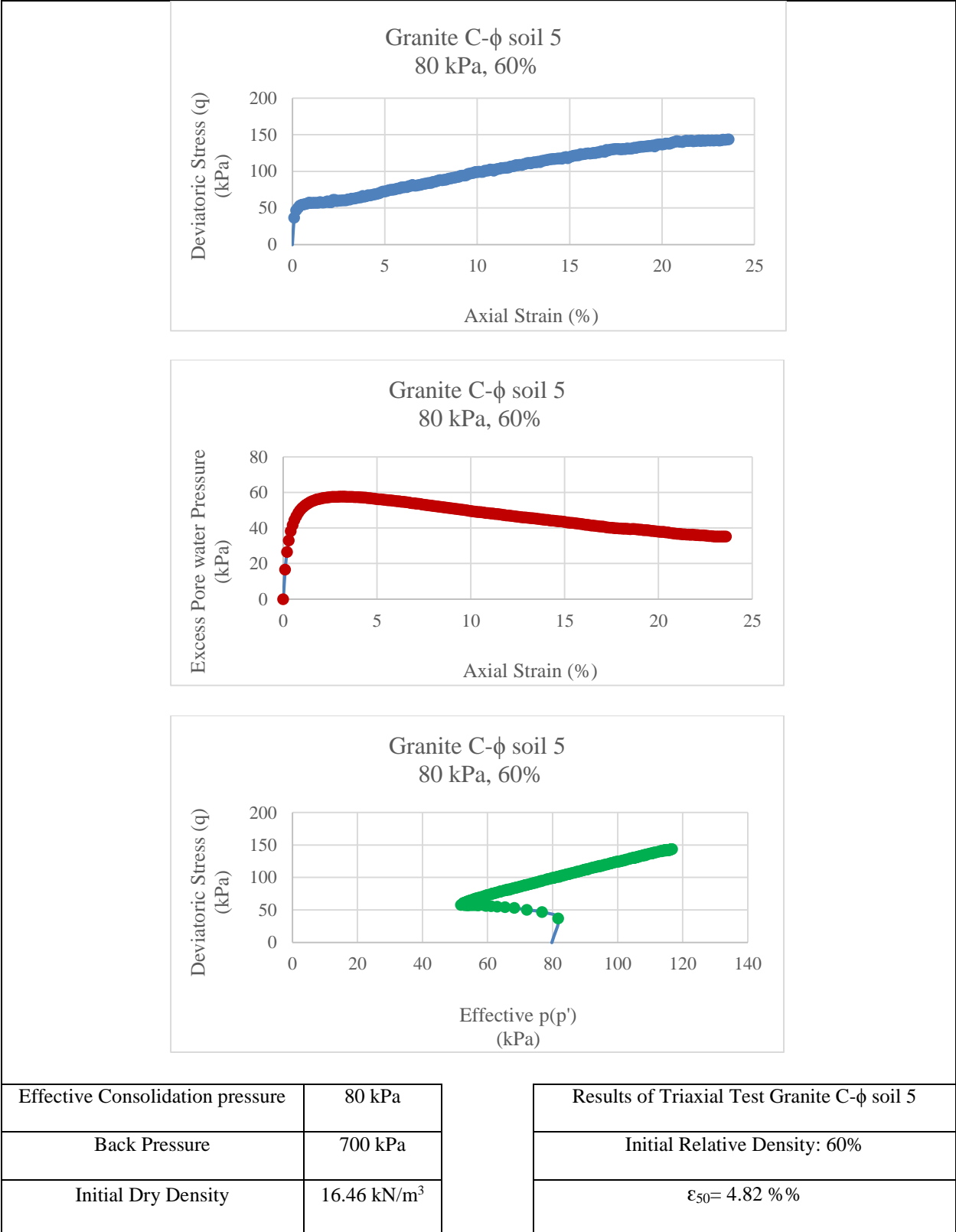


Figure 4-7. Triaxial test results of Granite Soil 5 Sample

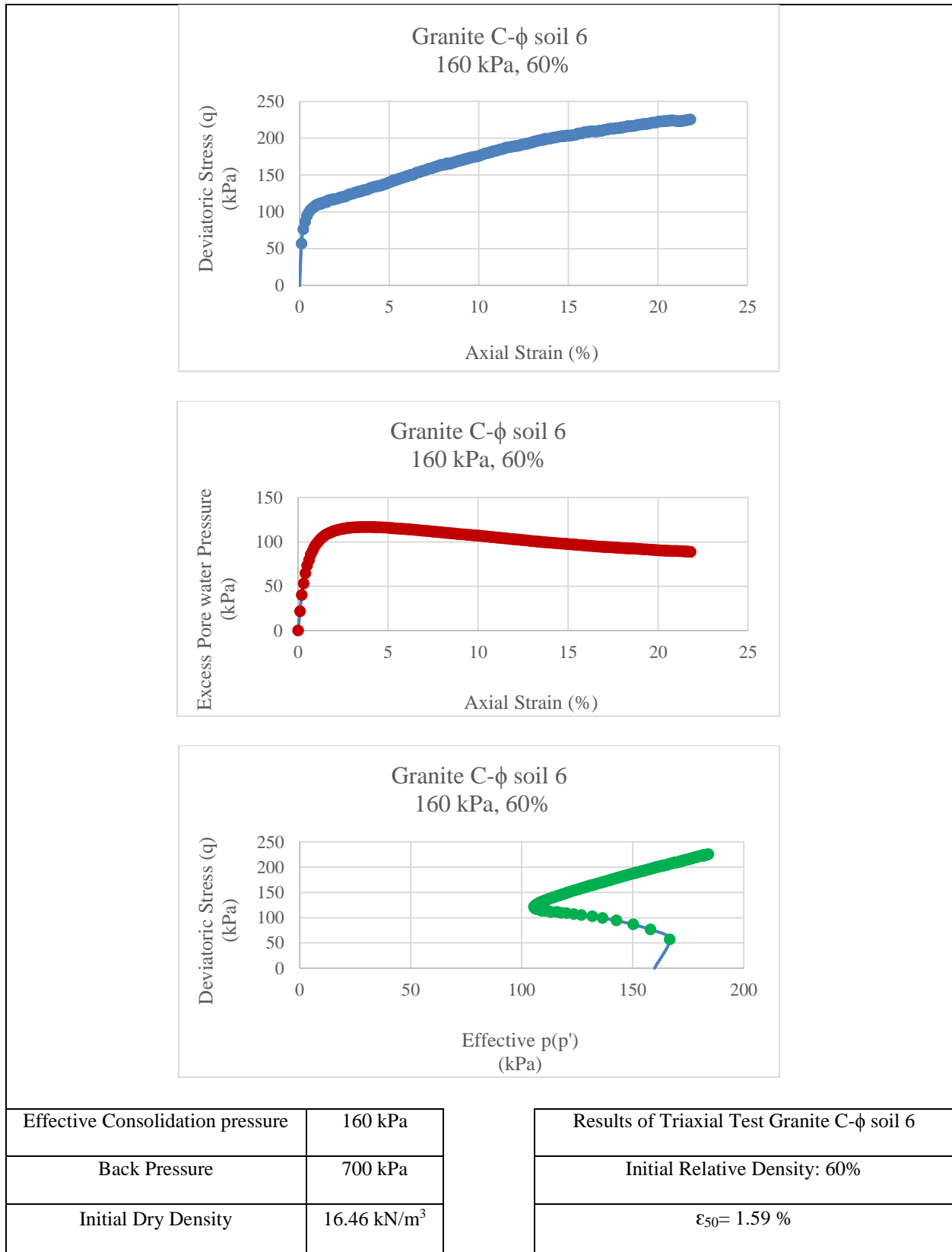
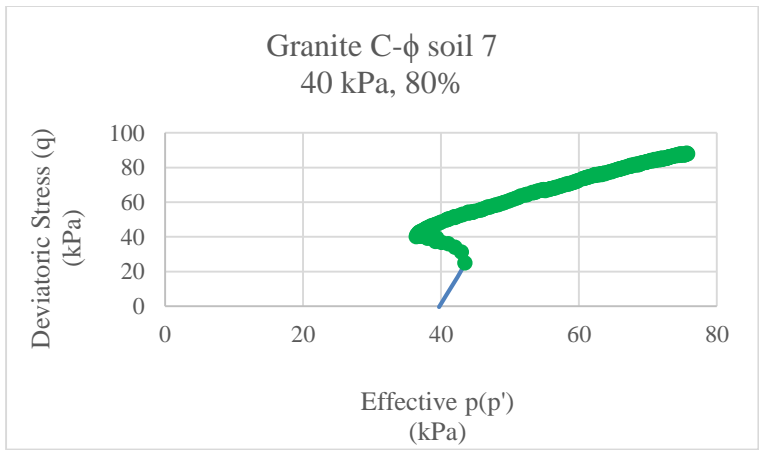
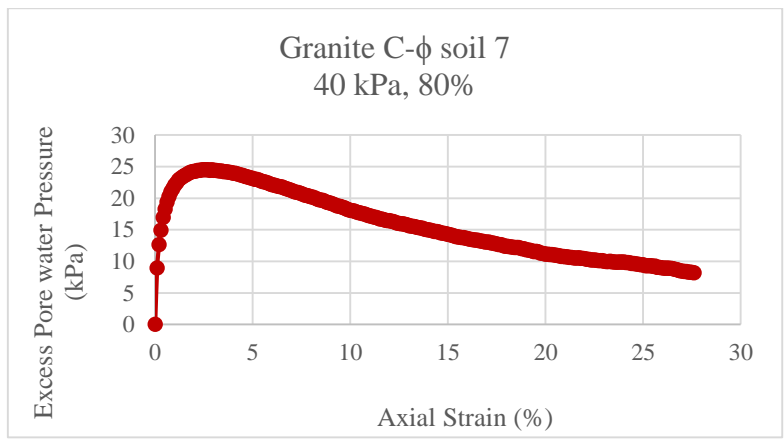
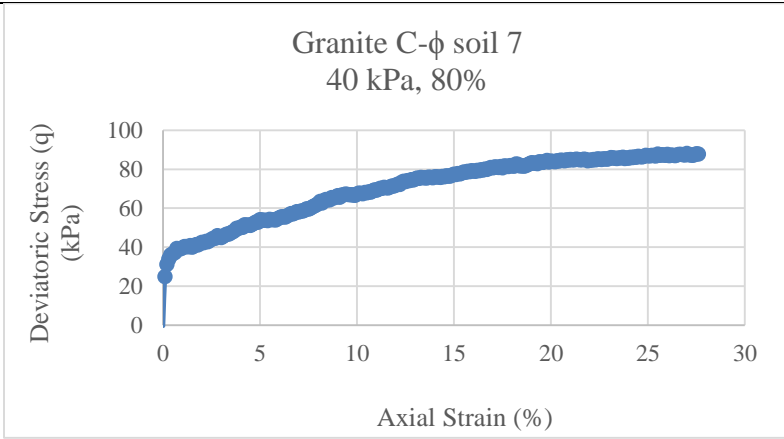


Figure 4-8 Triaxial test results of Granite Soil 6 Sample



Effective Consolidation pressure	40 kPa
Back Pressure	700 kPa
Initial Dry Density	17.08 kN/m ³

Results of Triaxial Test Granite C-φ soil 7
Initial Relative Density: 80%
$\epsilon_{50} = 2.48 \%$

Figure 4-9 Triaxial test results of Granite Soil 7 Sample

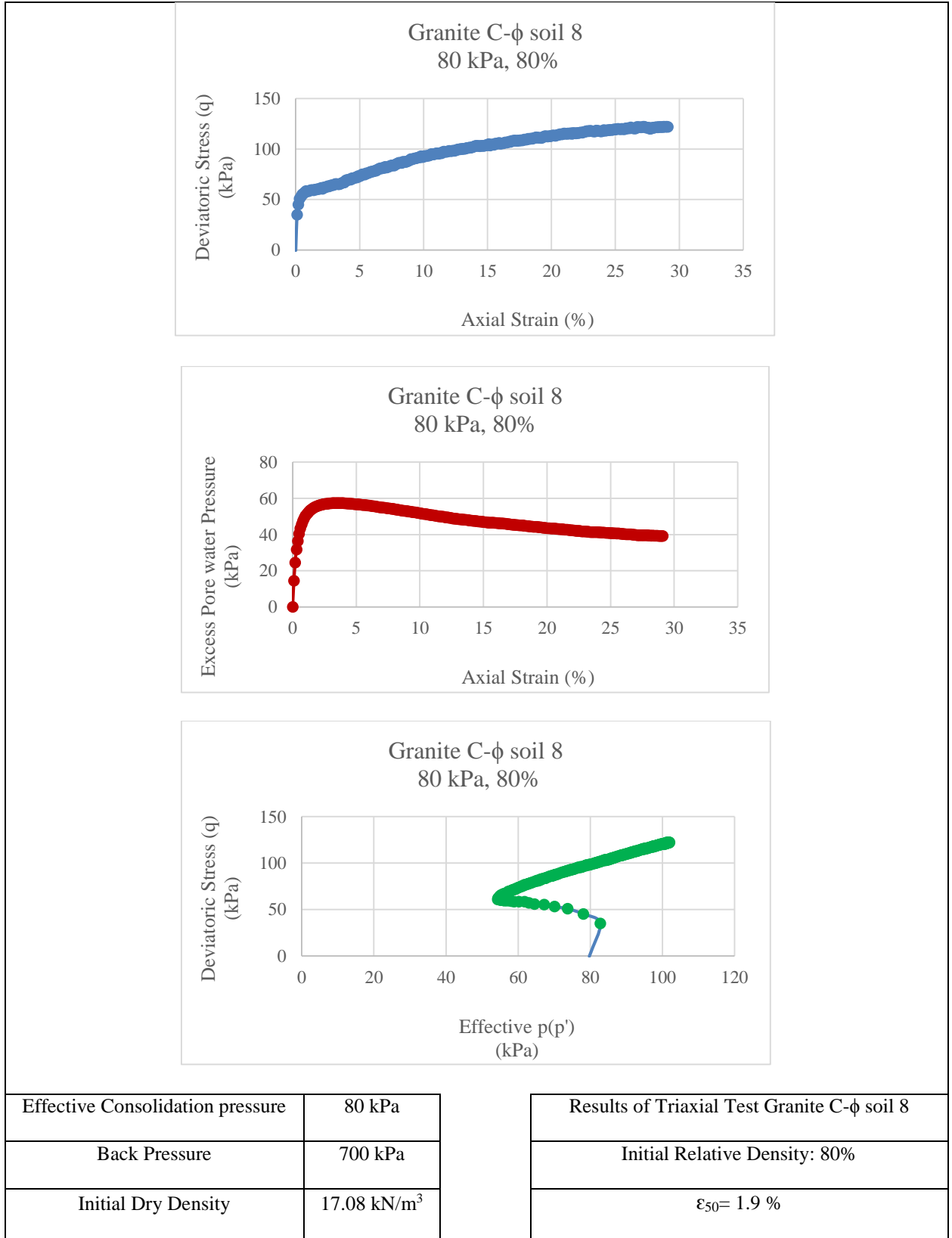
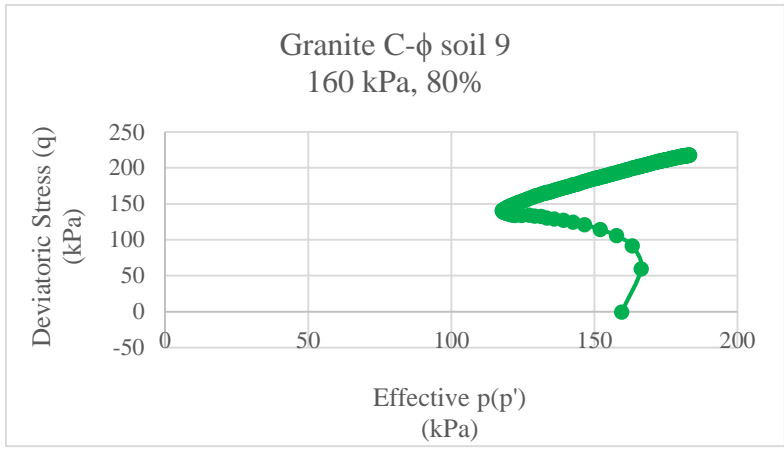
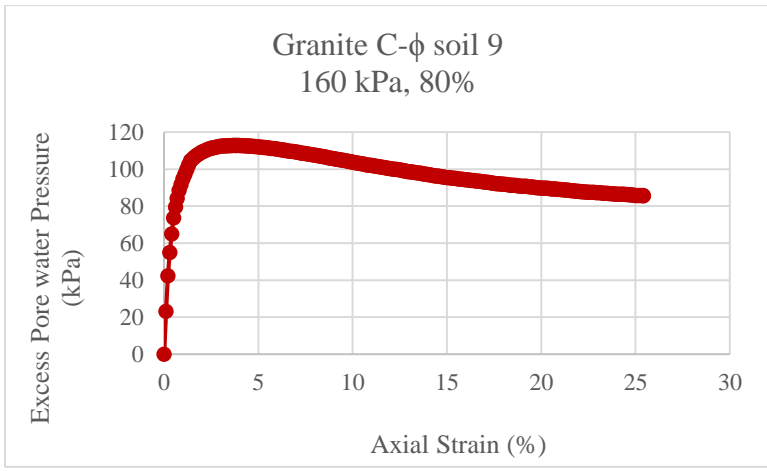
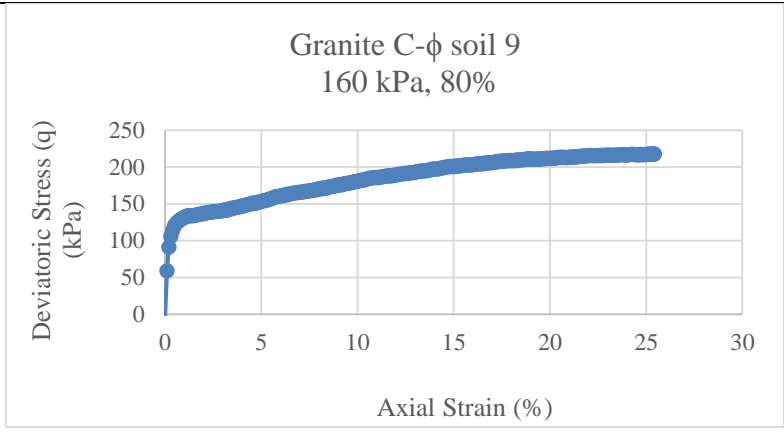


Figure 4-10 Triaxial test results of Granite Soil 8 Sample



Effective Consolidation pressure	160 kPa
Back Pressure	700 kPa
Initial Dry Density	17.08 kN/m ³

Results of Triaxial Test Granite C- ϕ soil 9
Initial Relative Density: 80%
$\epsilon_{50} = 3.8 \%$

Figure 4-11 Triaxial test results of Granite Soil 9 Sample

4.5.2 C- ϕ Soil 2 (Black Eagles)

Nine samples with 40%, 60% and 80% relative density on a C- ϕ soil 2 (Black Eagle) were prepared for CU tests. These tests were conducted on 40 kPa, 80 kPa and 160 kPa.

Table 4-17 shows the summary of Triaxial test data for this soil. In addition, Table 18 illustrates the required soil mass for sample preparation.

Table 4-17. Summary of Triaxial test data for C- ϕ Soil 2 (Black Eagle)

Soil Type	Target Dr (%)	d (inch)	h (inch)	Target gamma (kN/m ³)	V (mm ³)	M (gr)	gamma, max (kN/m ³)	gamma,min (kN/m ³)	M (gr)	Final gamma (kN/m ³)	Dr (%)
C- ϕ Soil 2 (Black Eagles)	40	2.817	6	13.633	612485.4	835	15.017	12.814	835	13.63297	40.95
C- ϕ Soil 2 (Black Eagles)	60	2.817	6	14.083	612485.4	862.6	15.017	12.814	863	14.09013	60.738
C- ϕ Soil 2 (Black Eagles)	80	2.817	6	14.564	612485.4	892	15.017	12.814	892	14.56361	80.892

Table 4-18. Required soil mass for sample preparation (Black Eagle Soil)

$\gamma_{d,max}$ (kN/m ³)	$\gamma_{d,min}$ (kN/m ³)	Dr (%)	γ_d (kN/m ³)	Average Sample Volume (ml.)	Soil Mass (gr)
15.017	12.814	40	13.633	612.485	835
15.017	12.814	60	14.083	612.485	862.6
15.017	12.814	80	14.564	612.485	892

Figure 4-12 and Figure 13 show the results of the gradation curve and Atterberg limit.

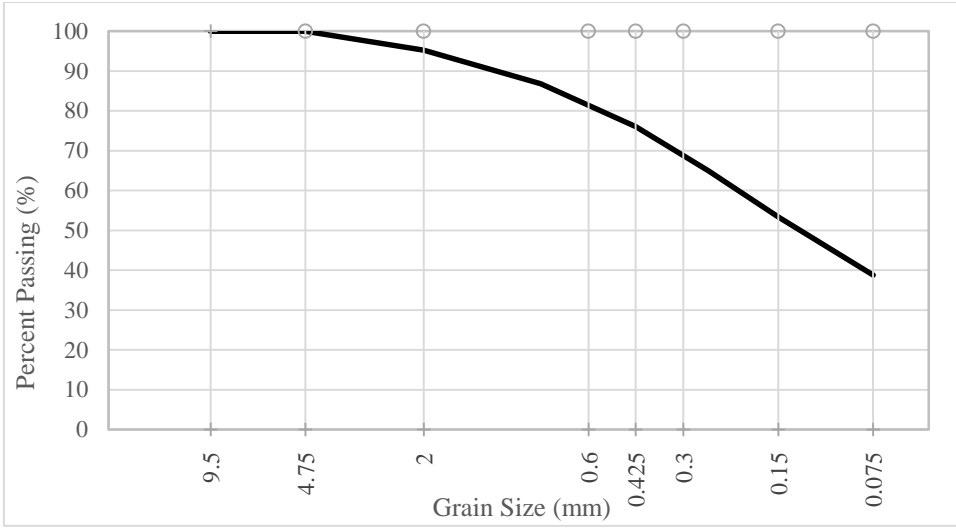


Figure 4-12. The gradation curve of Soil 2 (Black Eagle Soil)

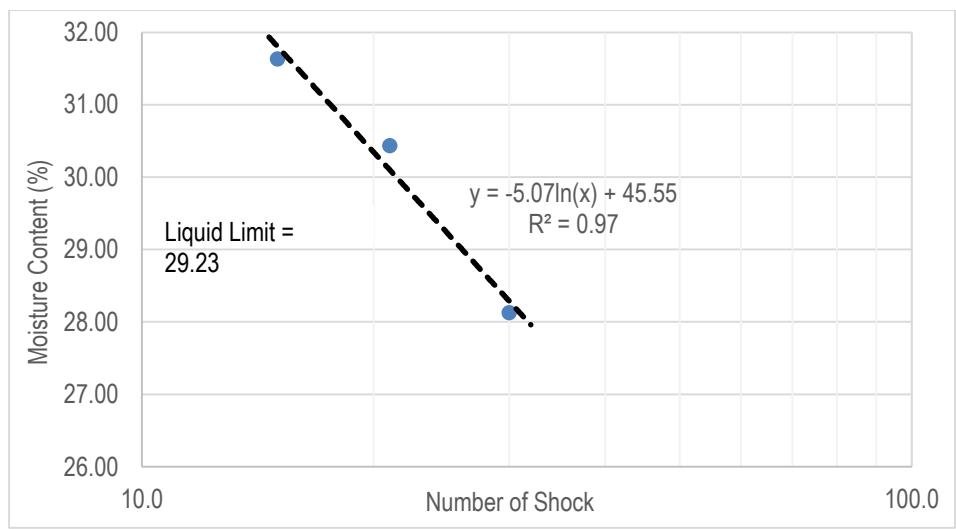
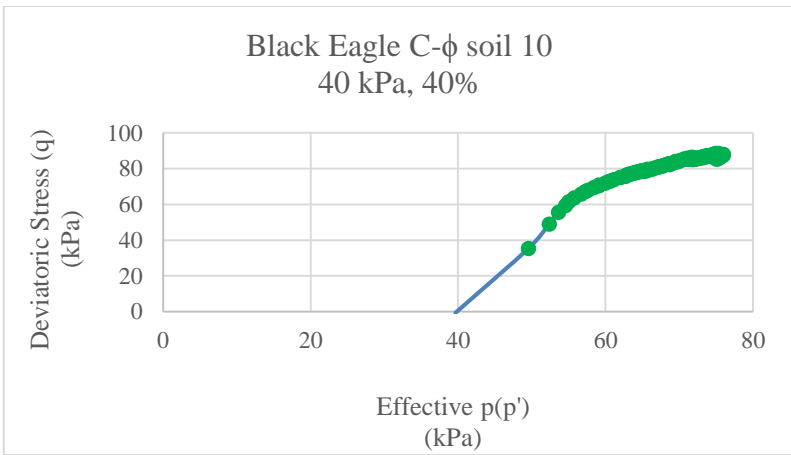
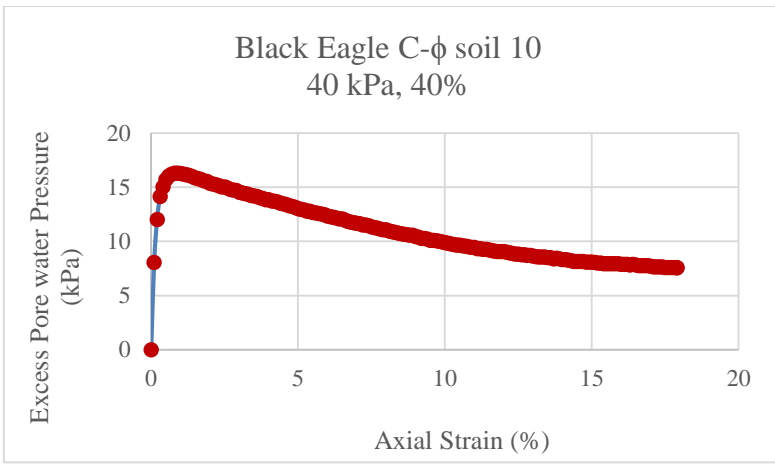
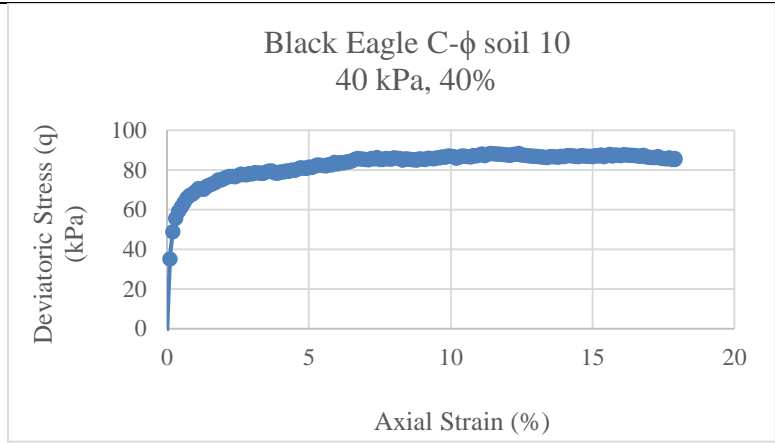


Figure 4-13. Atterberg Limit graph of Soil 2 (Black Eagle Soil)

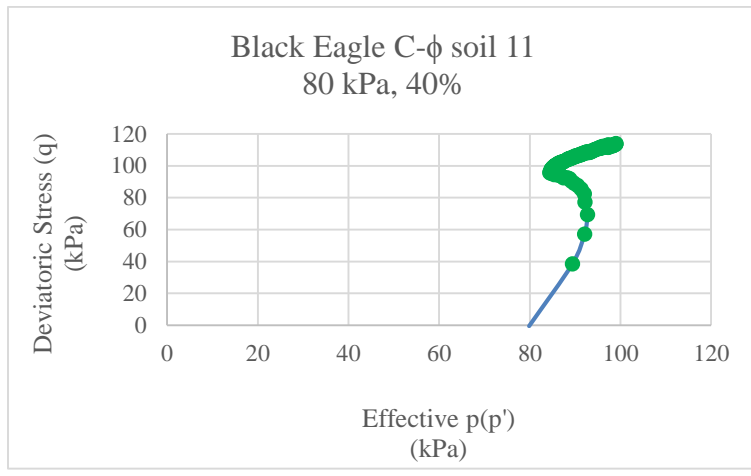
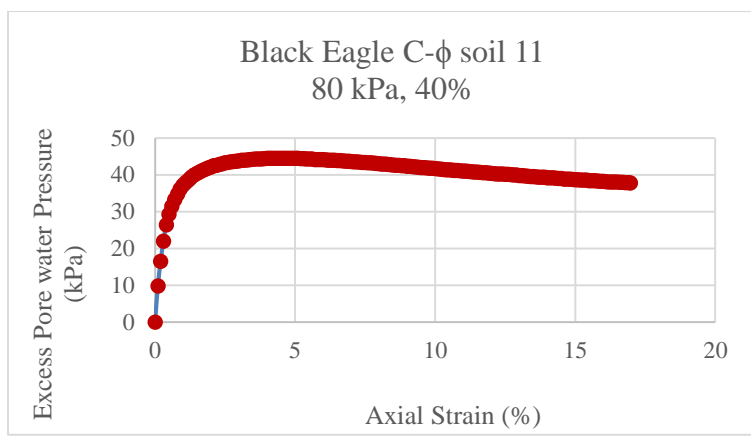
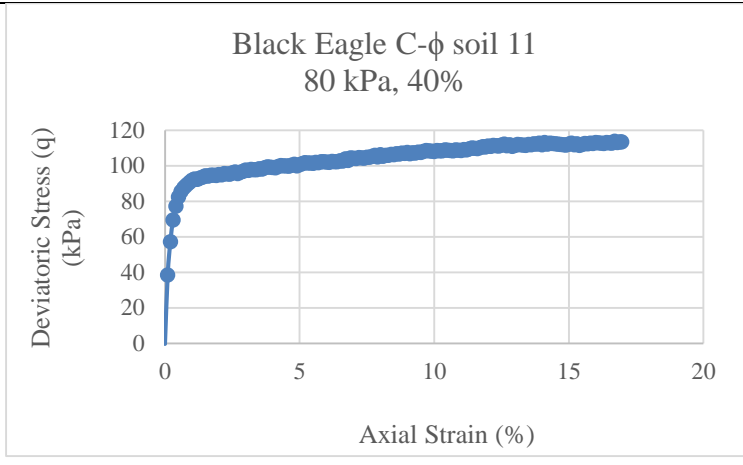
Figures 4-14 to 4-22 show the results of the tests which illustrate Deviatoric stress versus Axial strain, Excess pore water pressure versus axial strain and Deviatoric stress versus Effective pressure for 40, 80 and 160 kP Confining pressure of Black Eagle soil in 40, 60 and 80% relative density.



Effective Consolidation pressure	40 kPa
Back Pressure	700 kPa
Initial Dry Density	13.633 kN/m ³

Results of Triaxial Test BlackEagle C-φ soil10
Initial Relative Density: 40%
ε ₅₀ = 0.17 %

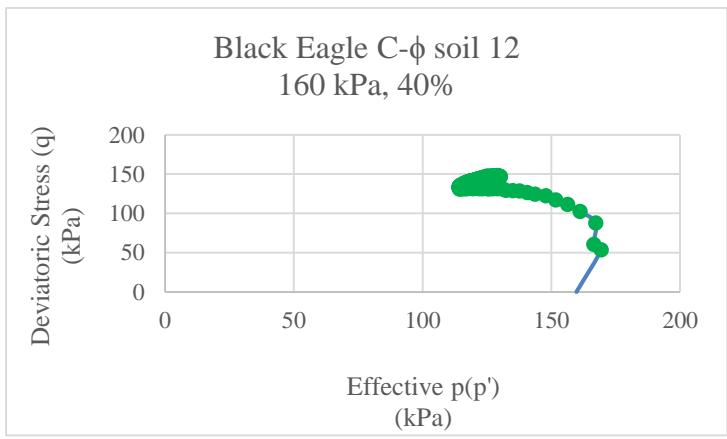
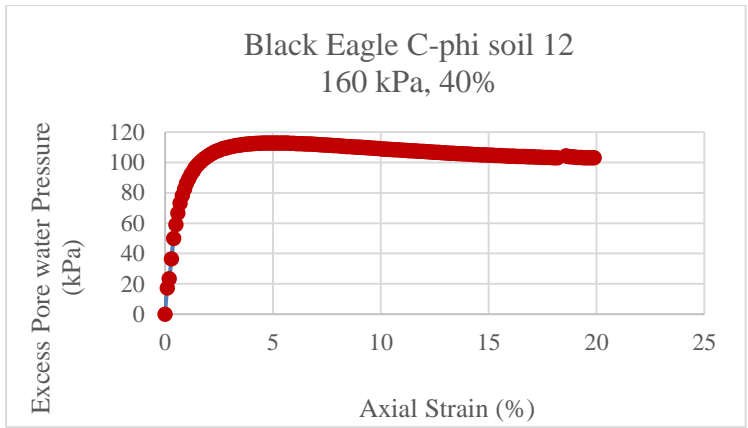
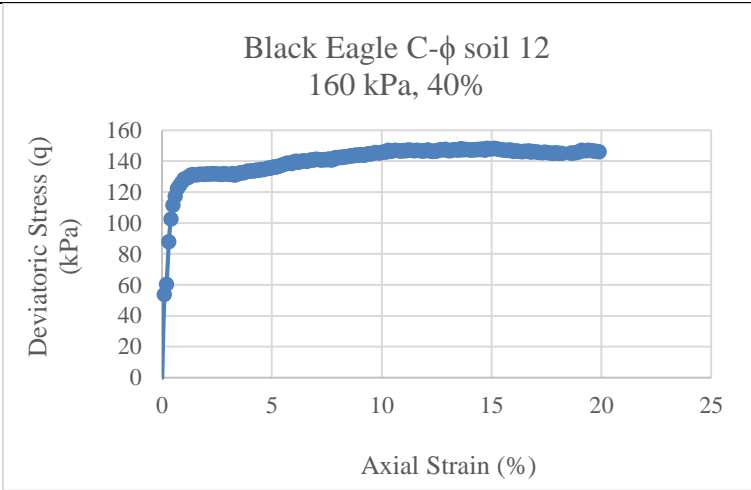
Figure 4-14 Triaxial test results of Black Eagle Soil 10 Sample



Effective Consolidation pressure	80 kPa
Back Pressure	700 kPa
Initial Dry Density	13.633 kN/m ³

Results of Triaxial Test BlackEagle C-φ soil11
Initial Relative Density: 40%
ε ₅₀ = 0.195 %

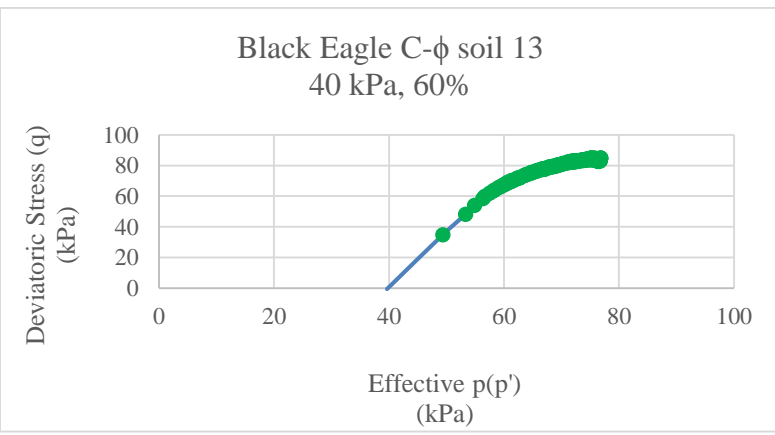
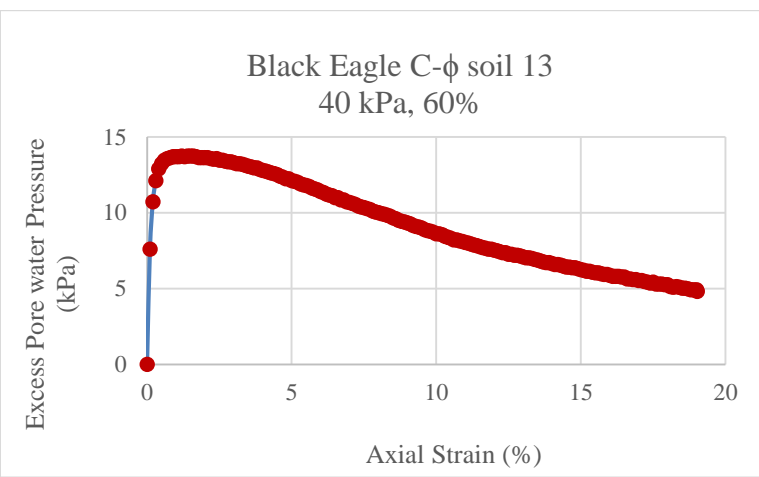
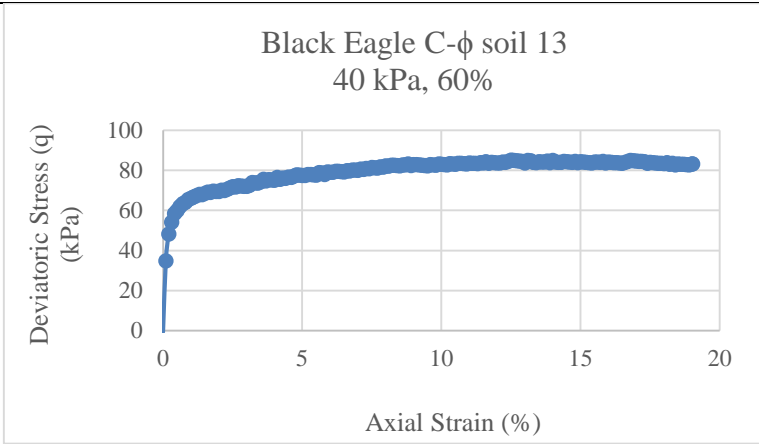
Figure 4-15 Triaxial test results of Black Eagle Soil 11 Sample



Effective Consolidation pressure	160 kPa
Back Pressure	700 kPa
Initial Dry Density	13.633 kN/m ³

Results of Triaxial Test BlackEagle C- ϕ soil12
Initial Relative Density: 40%
$\epsilon_{50} = 0.25 \%$

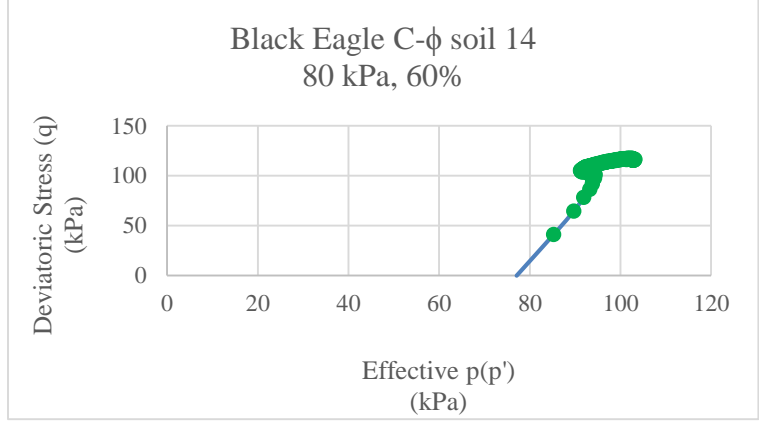
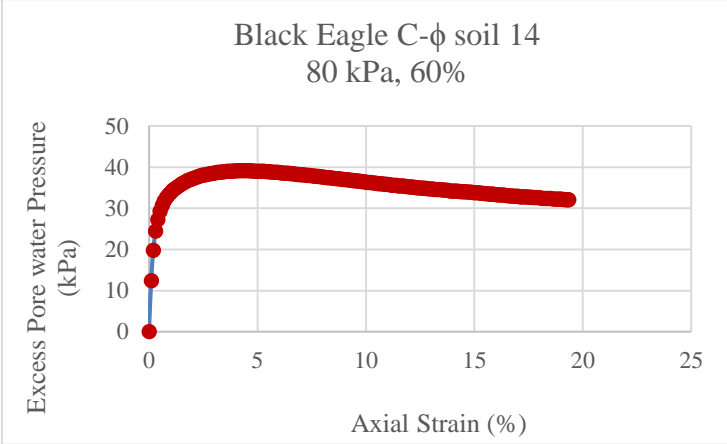
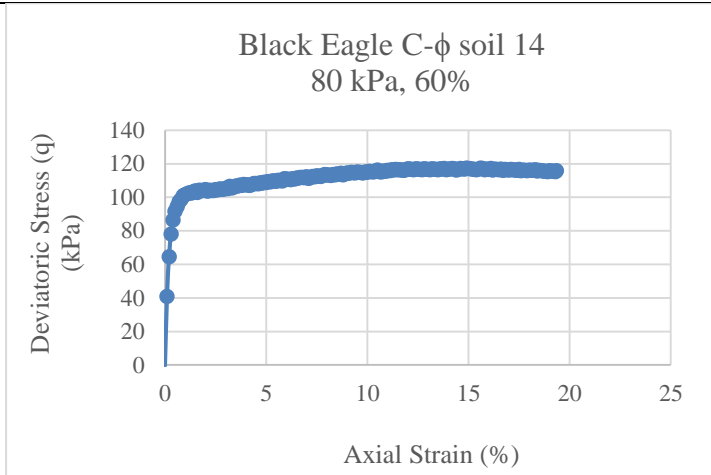
Figure 4-16 Triaxial test results of Black Eagle Soil 12 Sample



Effective Consolidation pressure	40 kPa
Back Pressure	700 kPa
Initial Dry Density	14.083 kN/m ³

Results of Triaxial Test BlackEagle C-φ soil13
Initial Relative Density: 60%
ε ₅₀ = 0.18 %

Figure 4-17 Triaxial test results of Black Eagle Soil 13 Sample



Effective Consolidation pressure	80 kPa
Back Pressure	700 kPa
Initial Dry Density	14.083 kN/m ³

Results of Triaxial Test BlackEagle C- ϕ soil14
Initial Relative Density: 60%
$\epsilon_{50} = 0.175 \%$

Figure 4-18 Triaxial test results of Black Eagle Soil 14 Sample

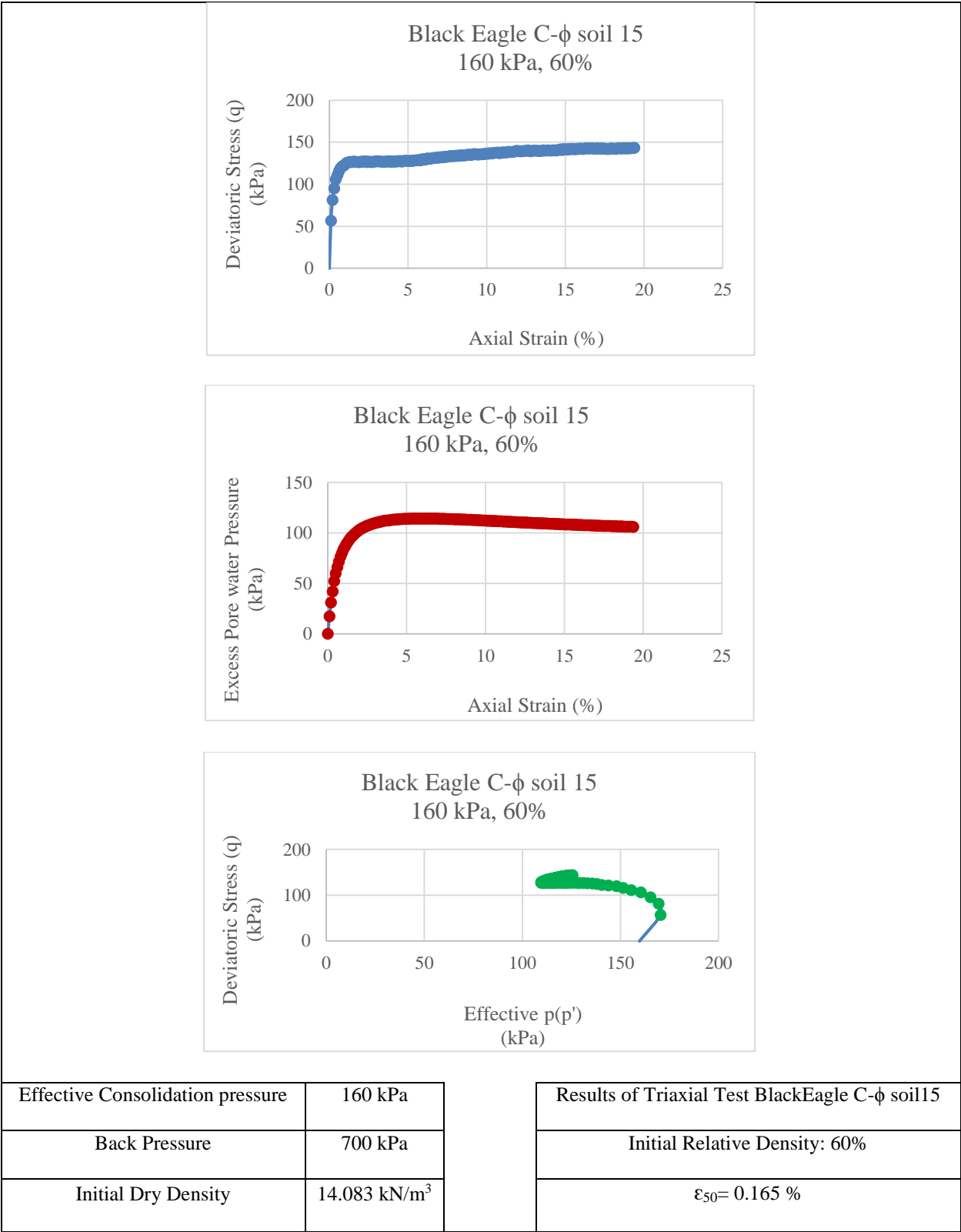


Figure 4-19 Triaxial test results of Black Eagle Soil 15 Sample

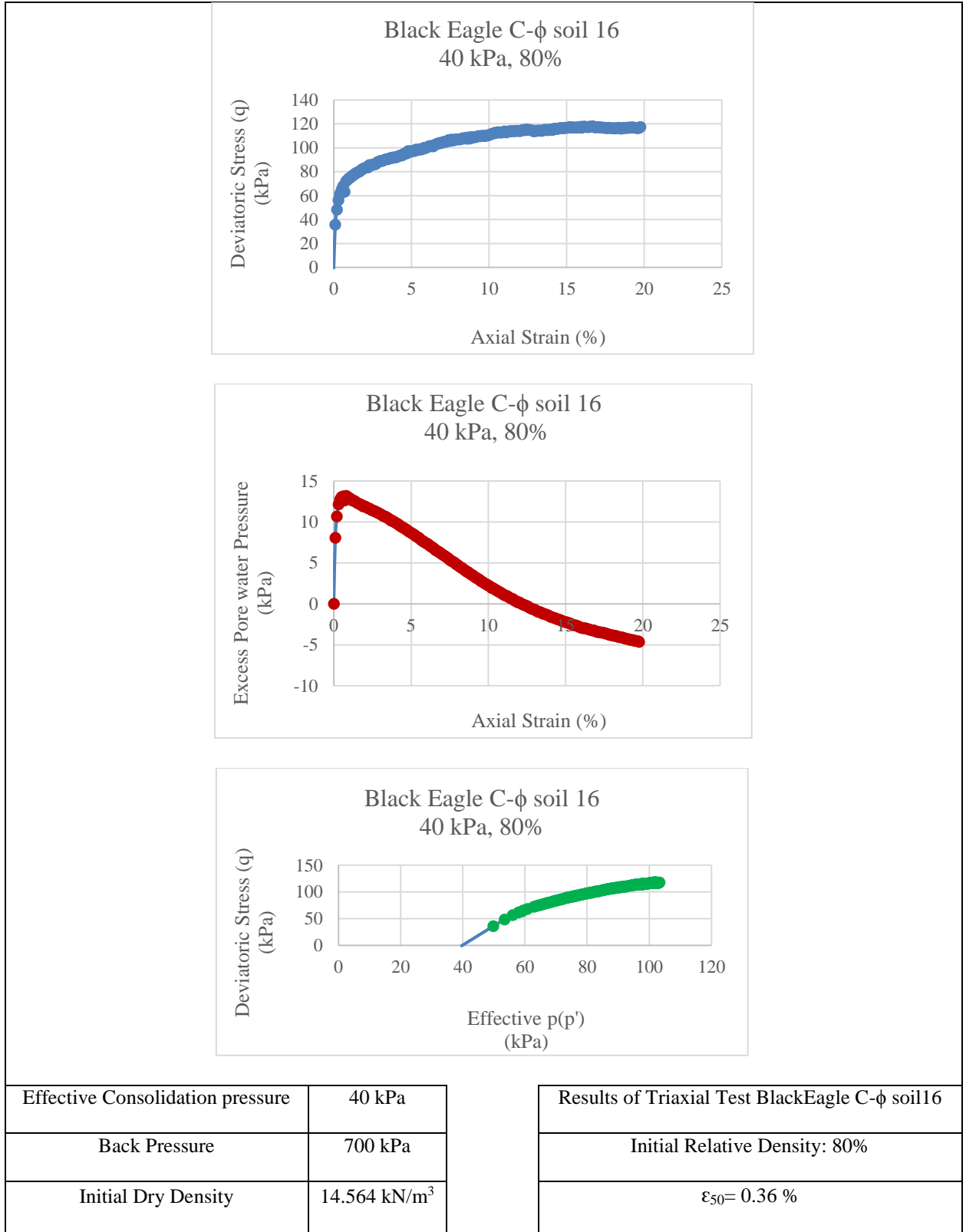
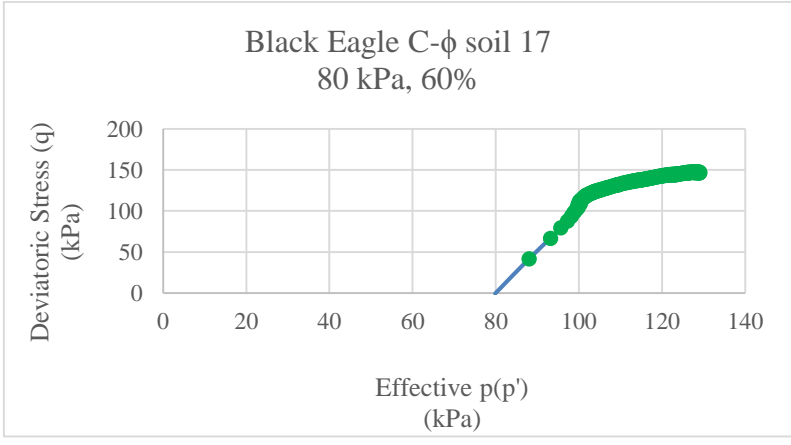
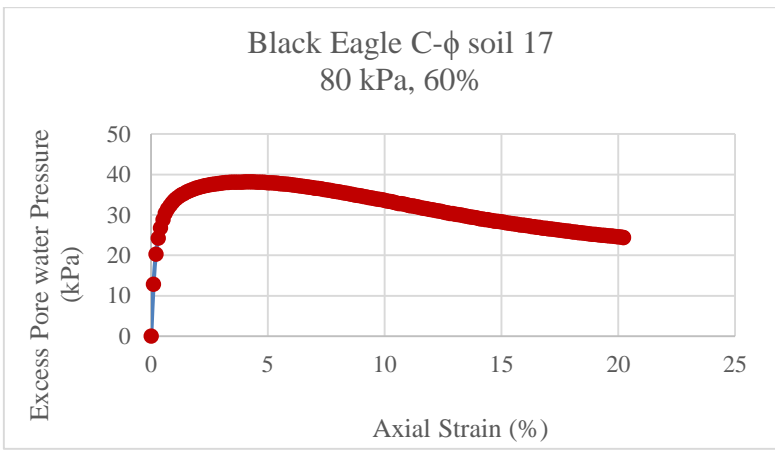
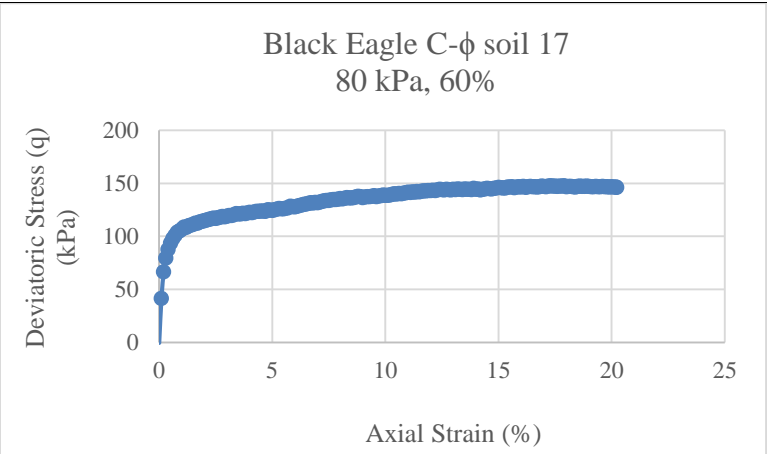


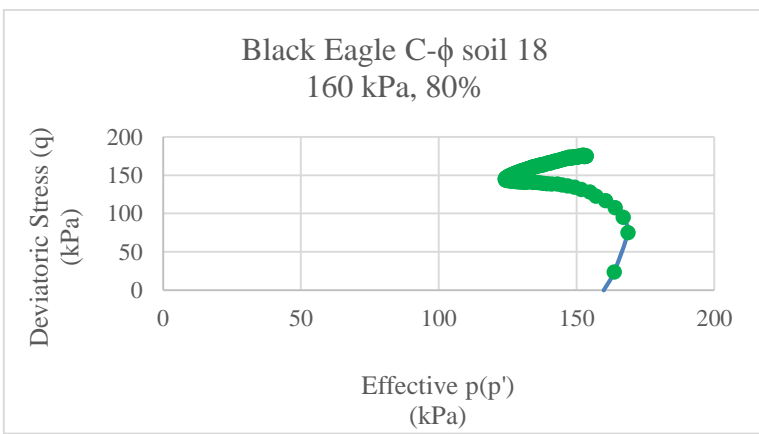
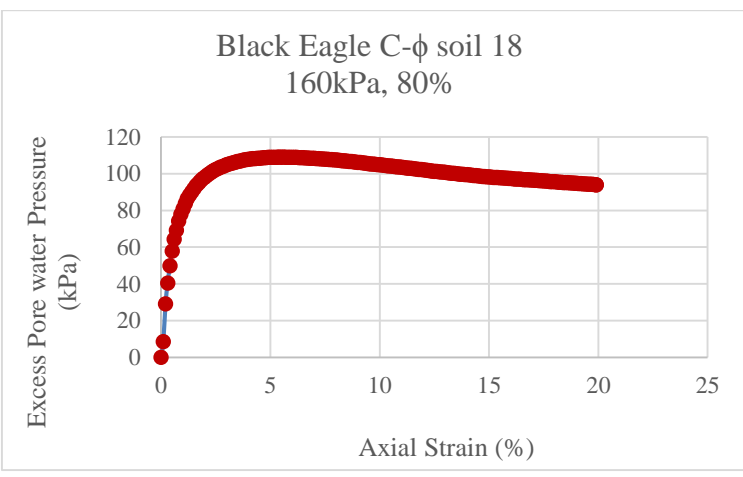
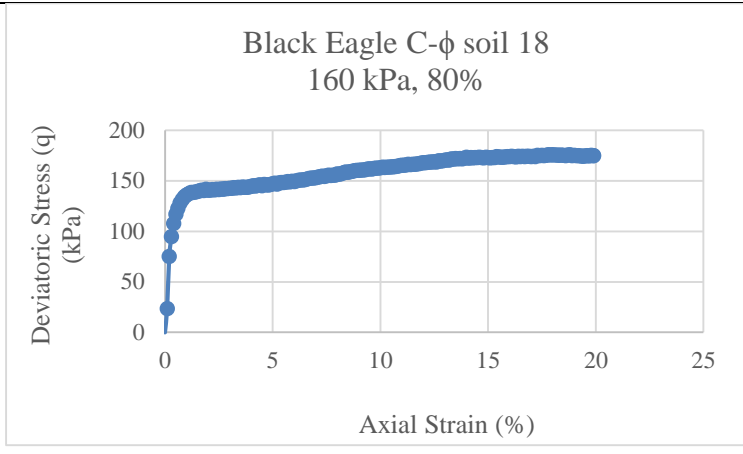
Figure 4-20 Triaxial test results of Black Eagle Soil 16 Sample



Effective Consolidation pressure	80 kPa
Back Pressure	700 kPa
Initial Dry Density	14.564 kN/m ³

Results of Triaxial Test BlackEagle C- ϕ soil17
Initial Relative Density: 80%
$\epsilon_{50} = 0.26 \%$

Figure 4-21 Triaxial test results of Black Eagle Soil 17 Sample



Effective Consolidation pressure	160 kPa
Back Pressure	700 kPa
Initial Dry Density	14.564 kN/m ³

Results of Triaxial Test BlackEagle C-φ soil18
Initial Relative Density: 80%
ε ₅₀ = 0.27 %

Figure 4-22 Triaxial test results of Black Eagle Soil 18 Sample

4.5.3 C- ϕ Soil 3 (Mixed Soil)

Nine samples with 40%, 60% and 80% relative density on a C- ϕ soil 3 were prepared for CU tests. These tests were conducted on 40 kPa, 80 kPa and 160 kPa.

Table 4-19 shows the summary of Triaxial test data for this soil. In addition, Table 4-20 illustrates the required soil mass for sample preparation.

Table 4-19. Summary of Triaxial test data for C- ϕ Soil 2 (Black Eagles)

Soil Type	Target Dr (%)	d (inch)	h (inch)	Target gamma (kN/m ³)	V (mm ³)	M (gr)	gamma, max (kN/m ³)	gamma,min (kN/m ³)	M (gr)	Final gamma (kN/m ³)	Dr (%)
C- ϕ Soil 3 (Mixed Soil)	40	2.817	6	14.856	612485.4	909.9	16.834	13.777	910	14.858	40.052
C- ϕ Soil 3 (Mixed Soil)	60	2.817	6	15.462	612485.4	947	16.834	13.777	947	15.462	60.005
C- ϕ Soil 3 (Mixed Soil)	80	2.817	6	16.119	612485.4	987.3	16.834	13.777	988	16.131	80.37

Table 4-20. Required soil mass for sample preparation (Mixed Soil)

$\gamma_{d,max}$ (kN/m ³)	$\gamma_{d,min}$ (kN/m ³)	Dr (%)	γ_d (kN/m ³)	Average Sample Volume (ml.)	Soil Mass (gr)
16.8335	13.777	40	14.856	612.485	909.91
16.8335	13.777	60	15.462	612.485	947.03
16.8335	13.777	80	16.119	612.485	987.27

Figure 4-23 and Figure 4-24 show the results of the gradation curve and Atterberg limit.

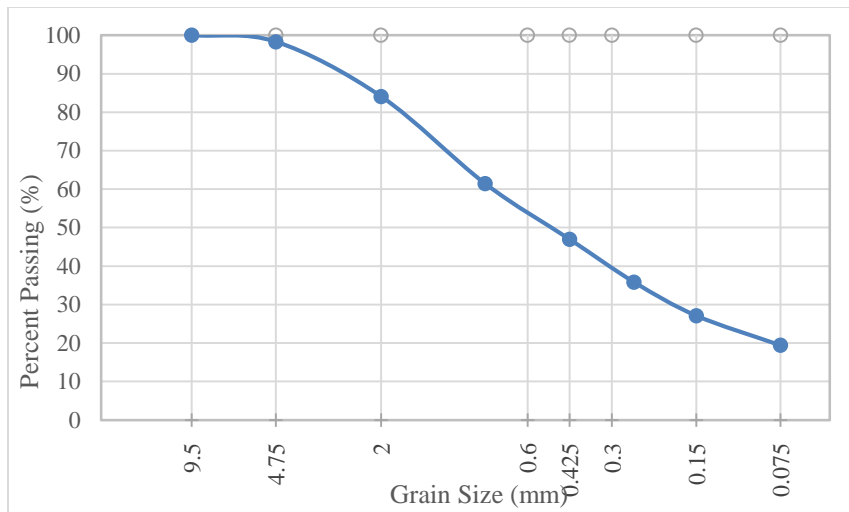


Figure 4-23. The gradation curve of Soil 3 (Mixed Soil)

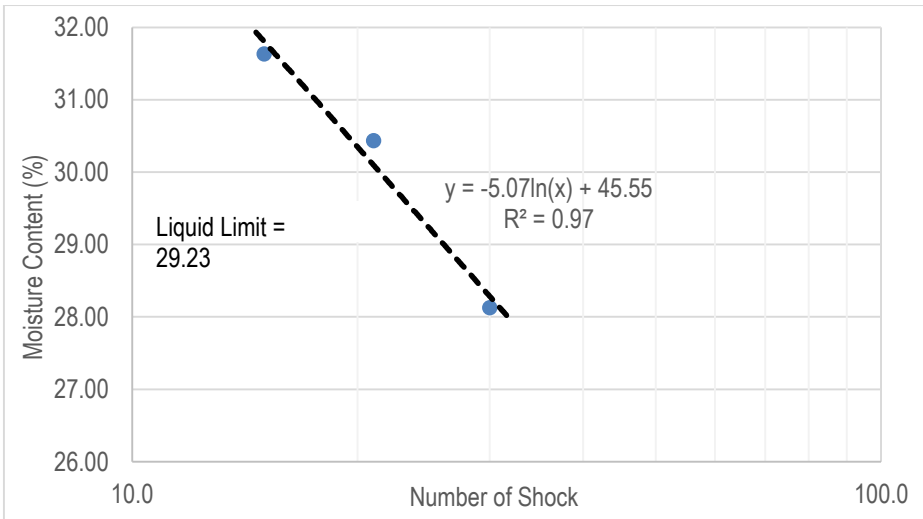


Figure 4-24. Atterberg Limit graph of Soil 3 (Mixed Soil)

Figures 4-25 to 4-33 show the results of the tests which illustrate Deviatoric stress versus Axial strain, Excess pore water pressure versus axial strain and Deviatoric stress versus Effective pressure for 40, 80 and 160 kP confining pressure of Mixed Soil in 40, 60 and 80% relative density.

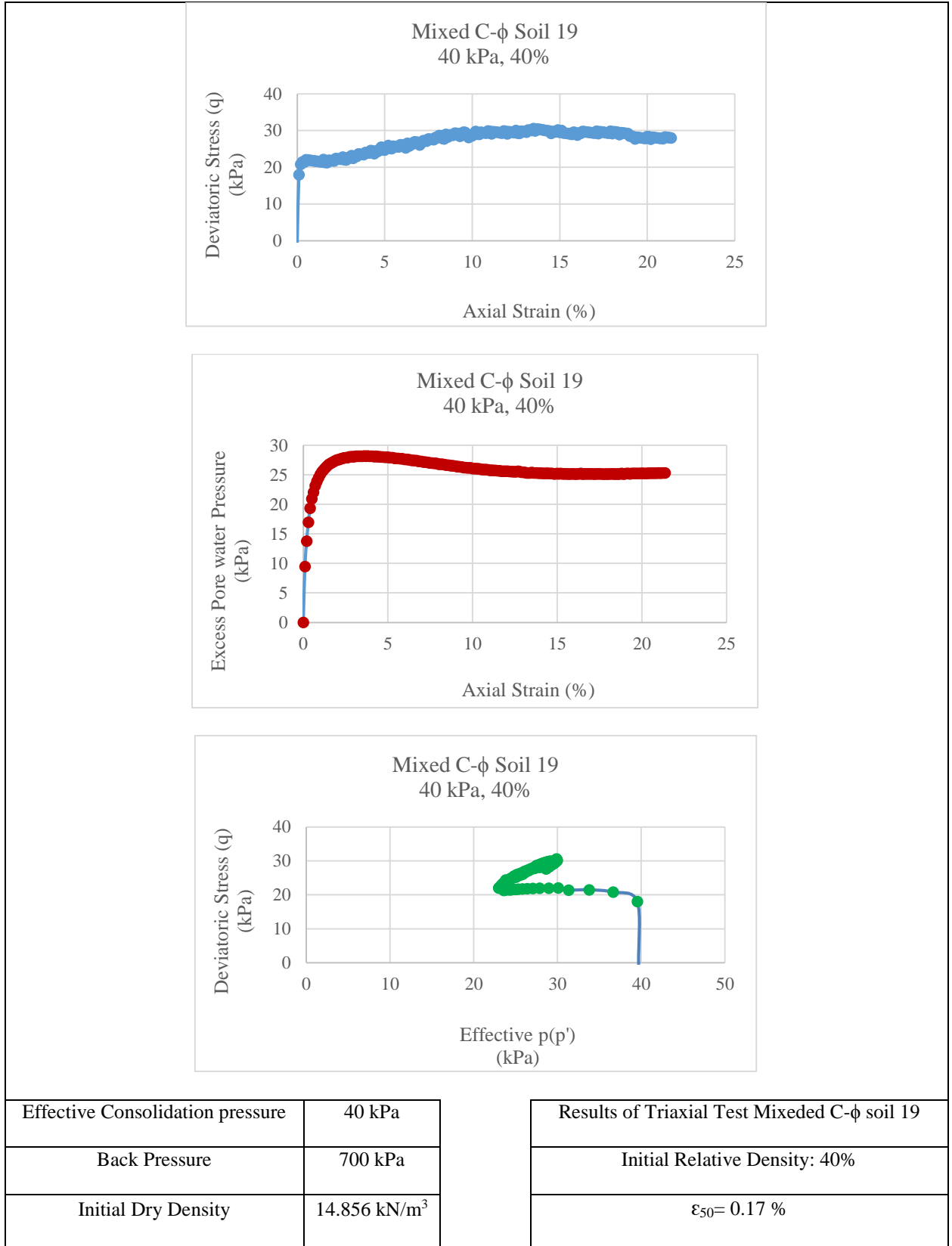


Figure 4-25 Triaxial test results of Mixed Soil 19 Sample

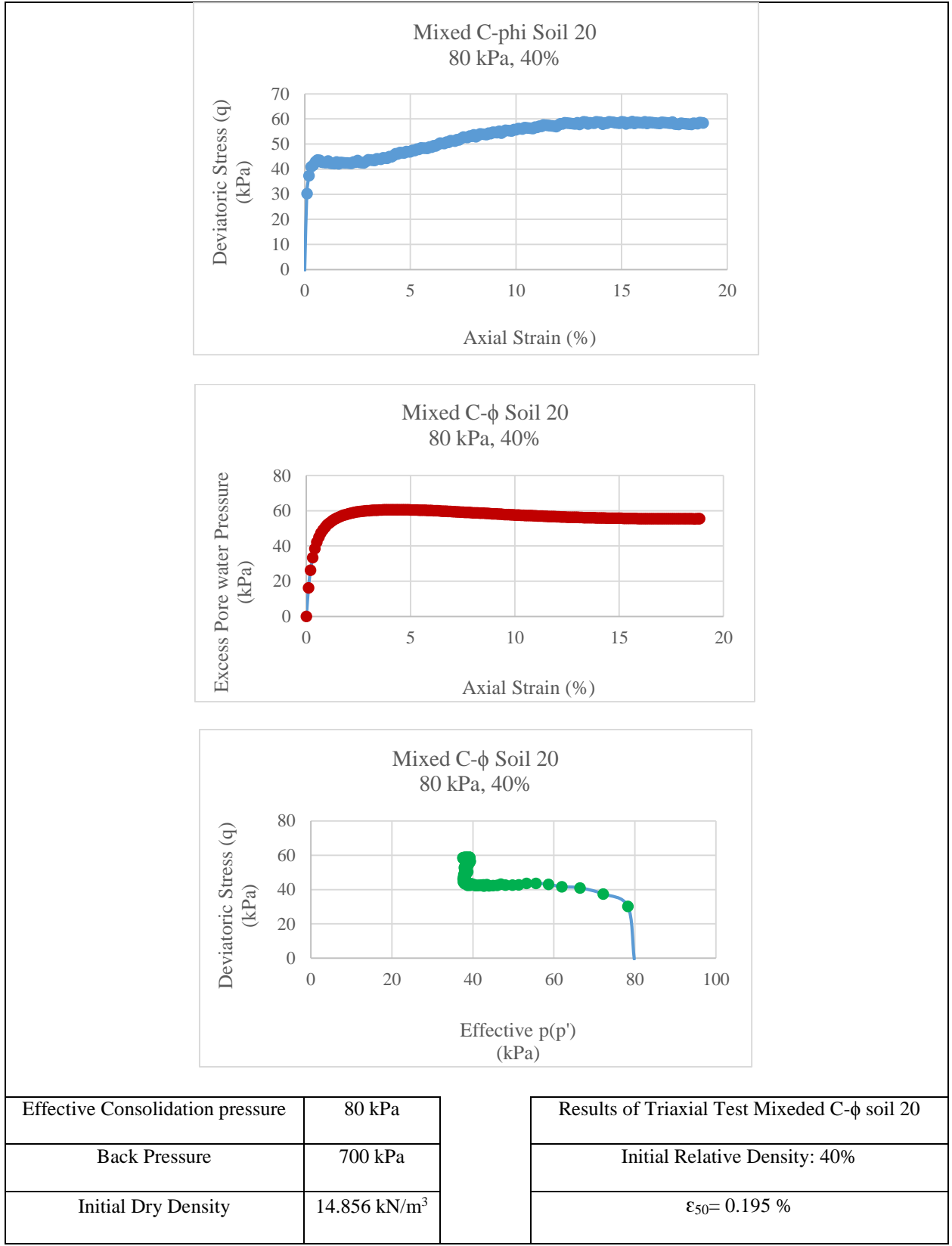


Figure 4-26 Triaxial test results of Mixed Soil 20 Sample

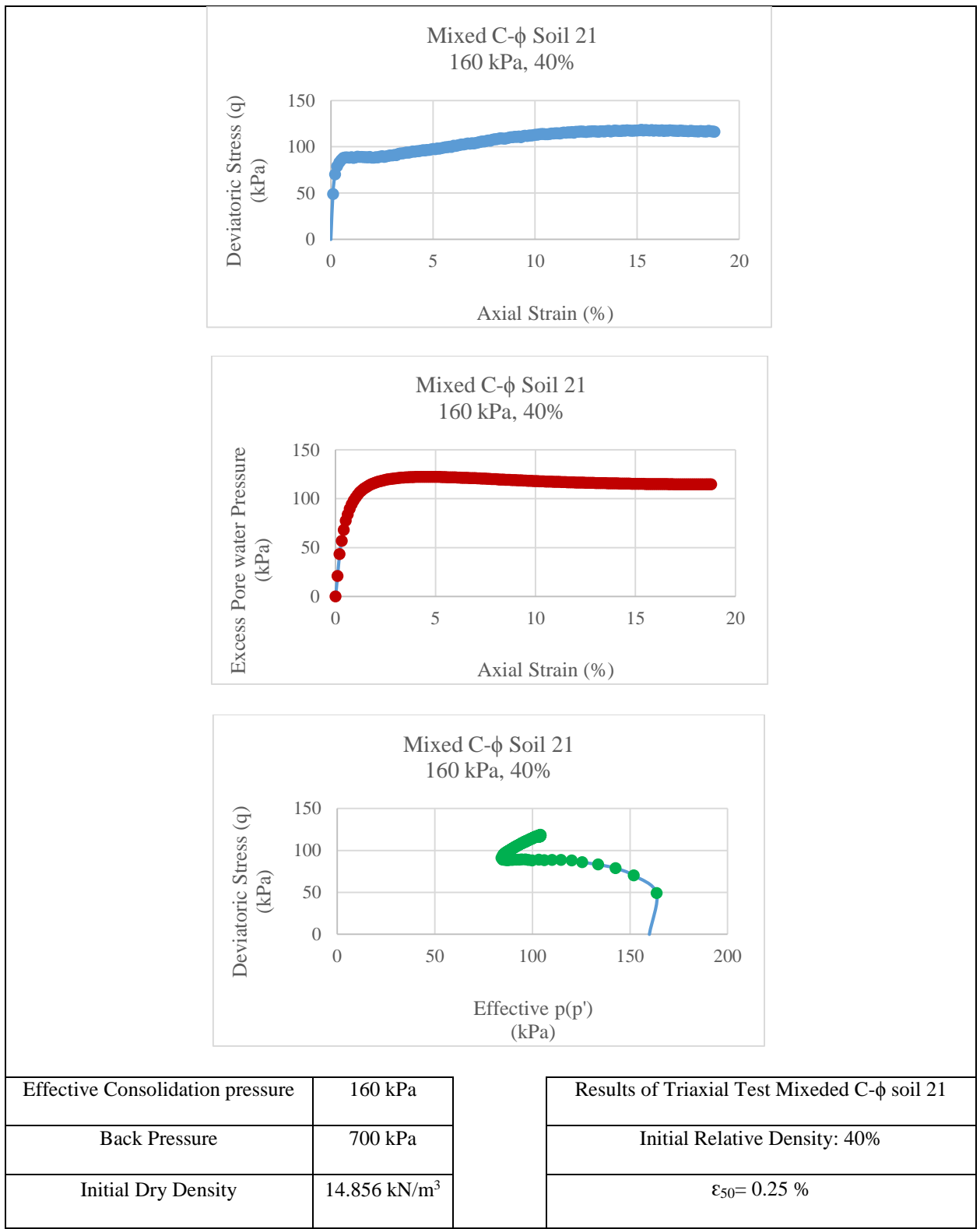


Figure 4-27 Triaxial test results of Mixed Soil 21 Sample

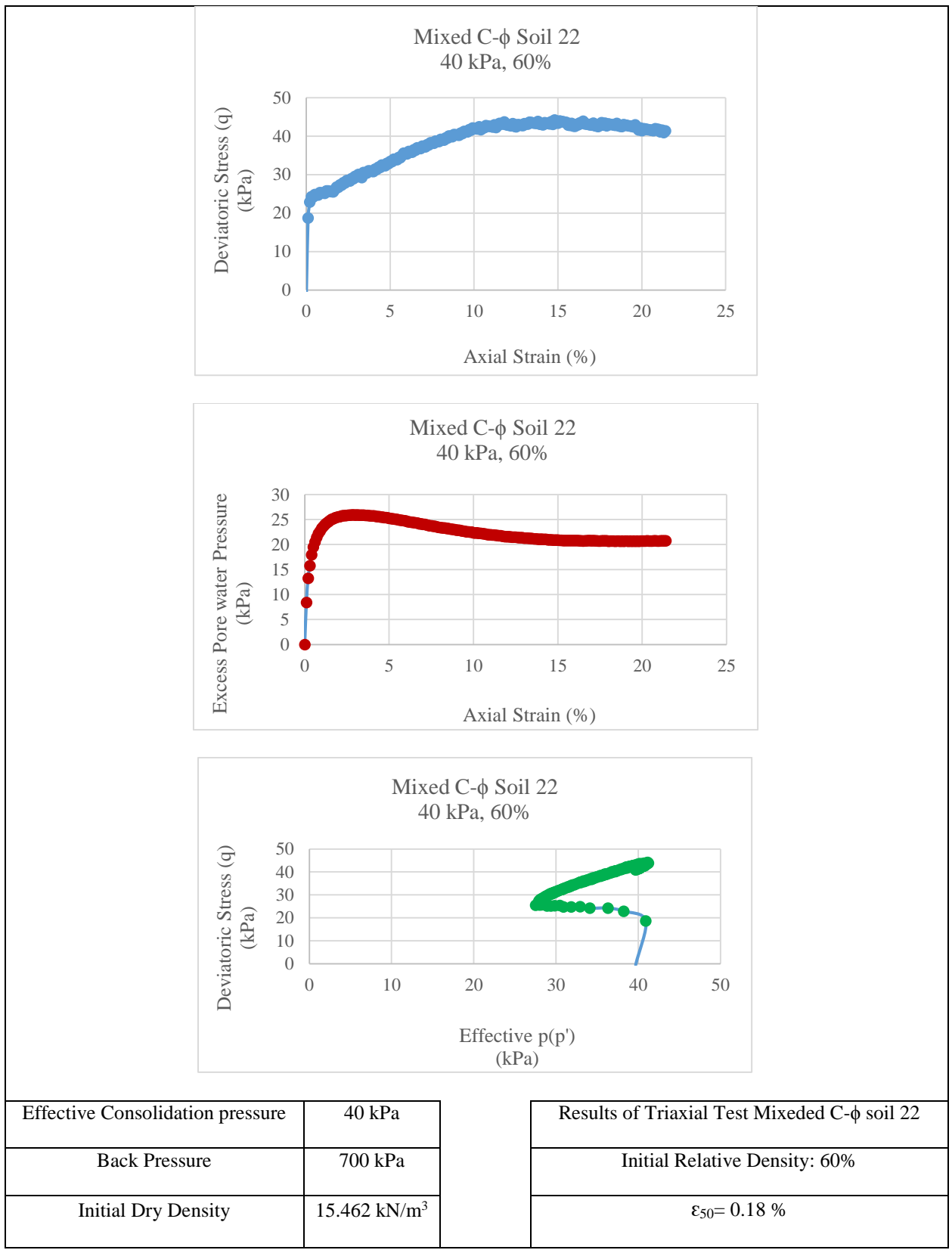


Figure 4-28 Triaxial test results of Mixed Soil 22 Sample

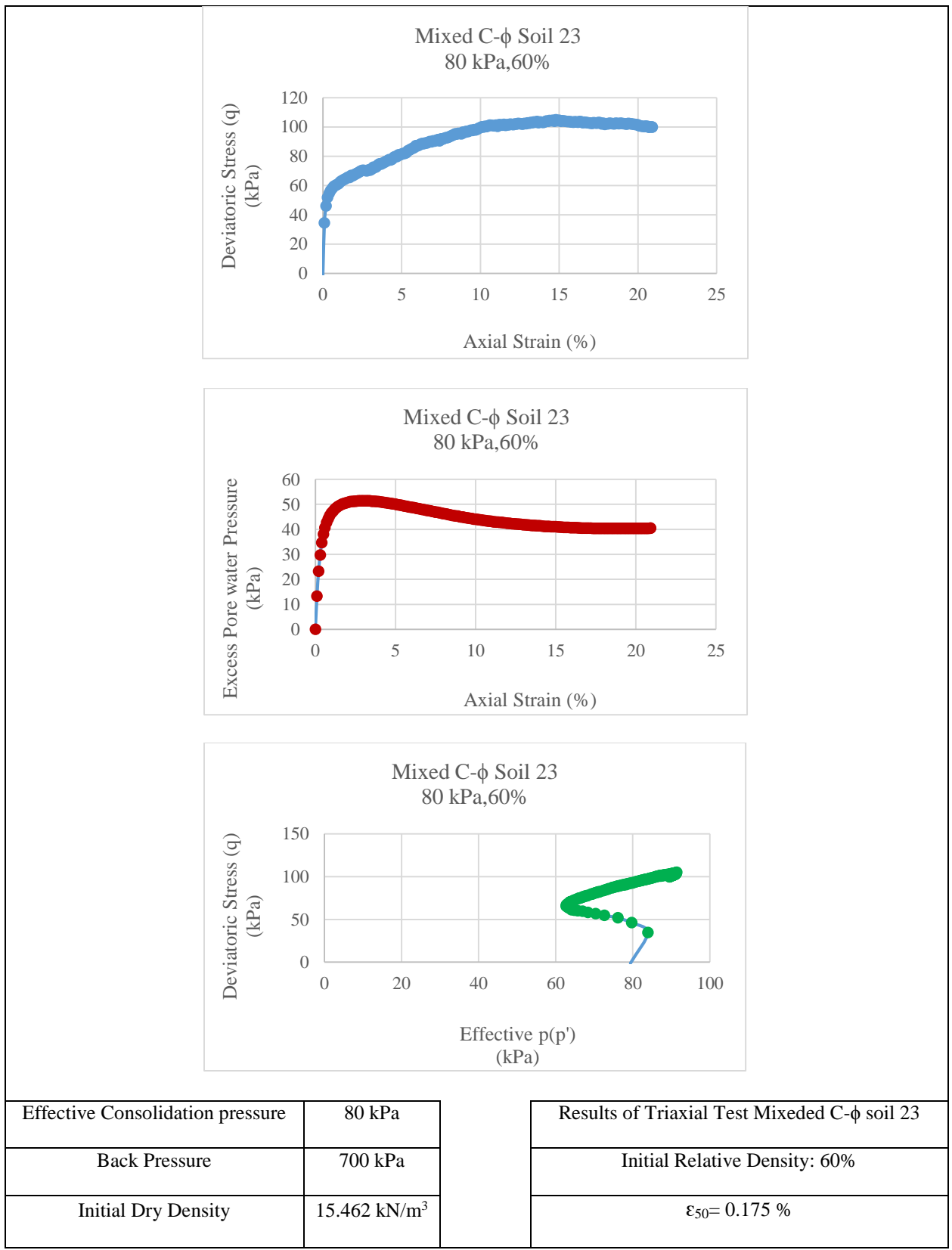


Figure 4-29 Triaxial test results of Mixed Soil 23 Sample

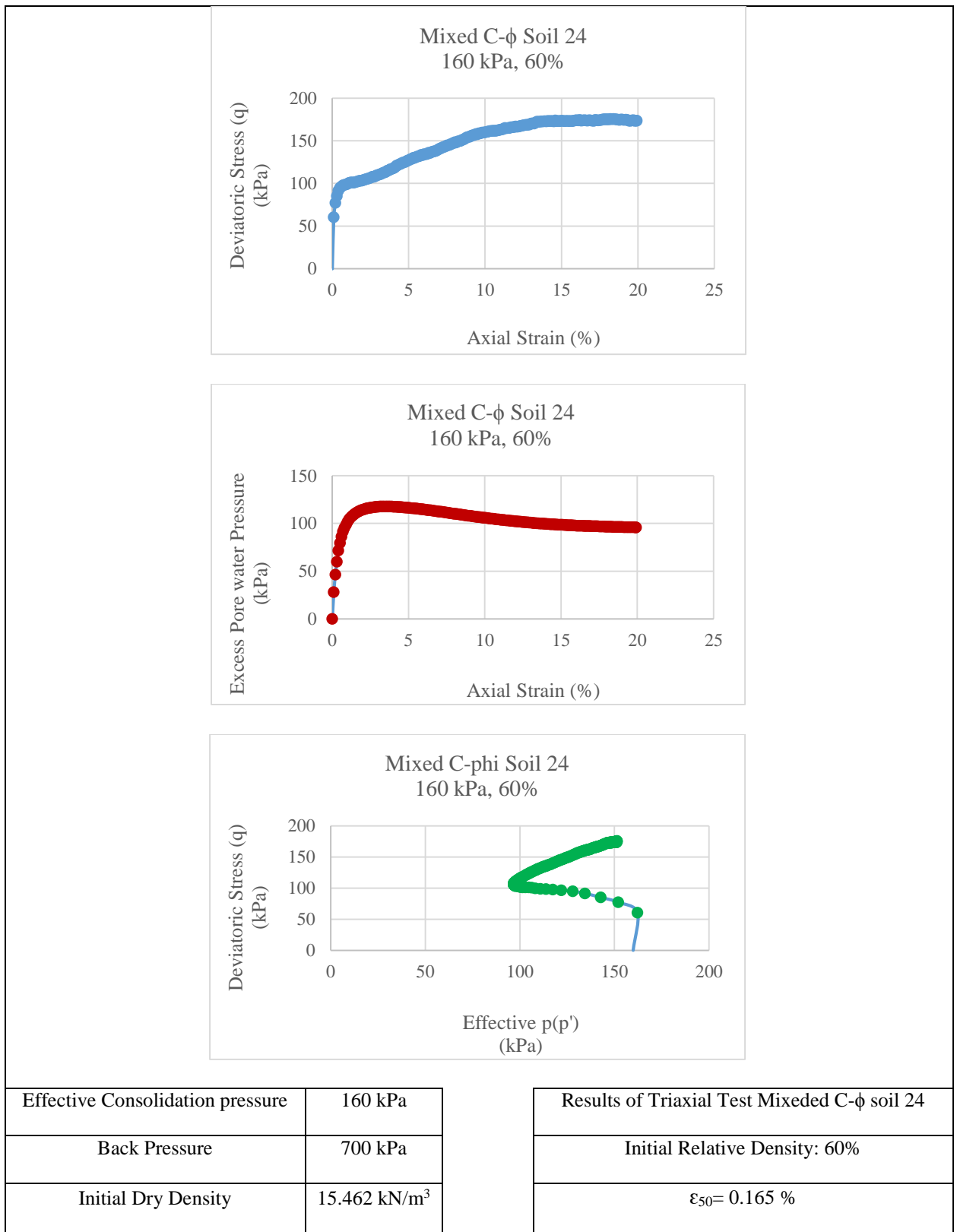


Figure 4-30 Triaxial test results of Mixed Soil 24 Sample

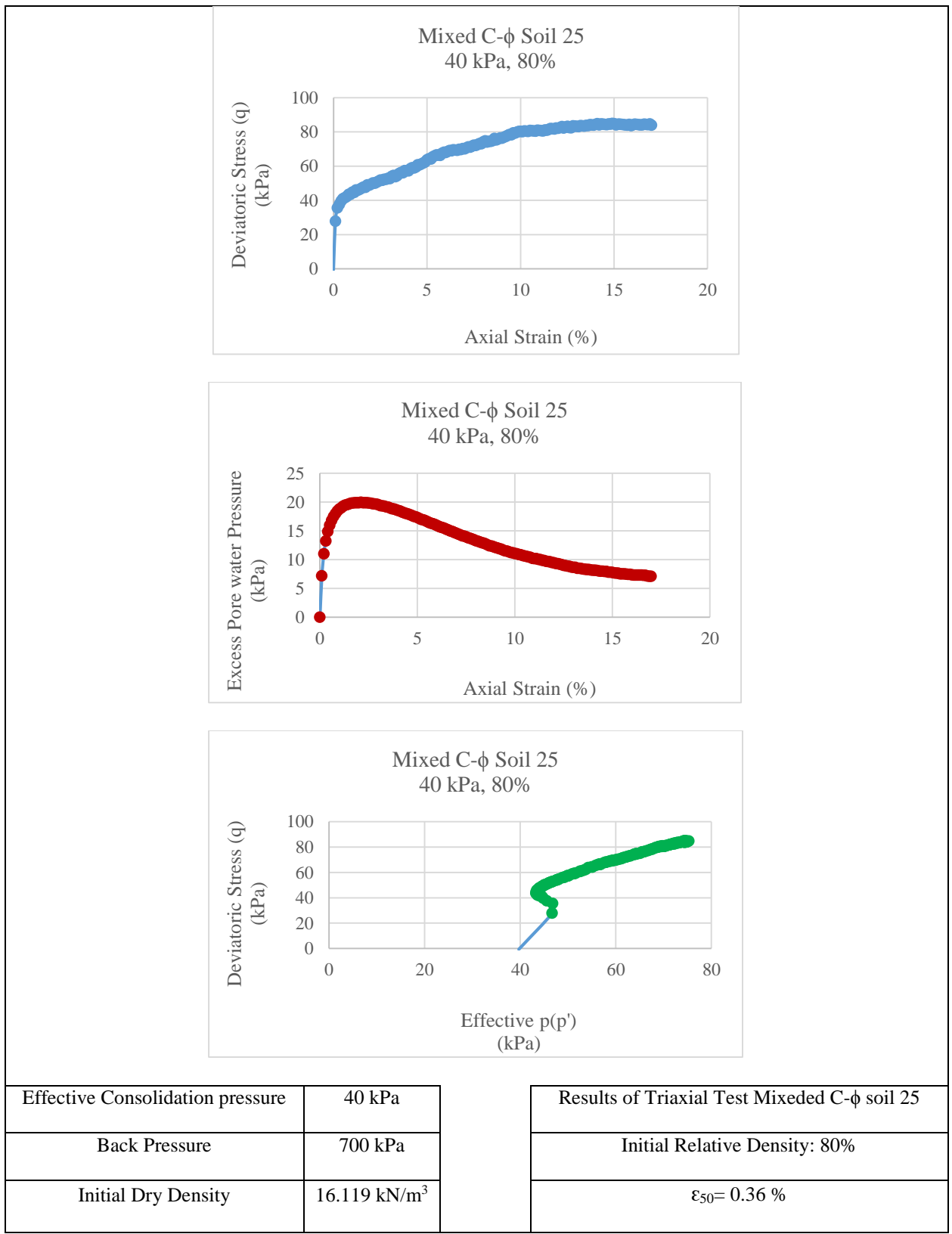


Figure 4-31 Triaxial test results of Mixed Soil 25 Sample

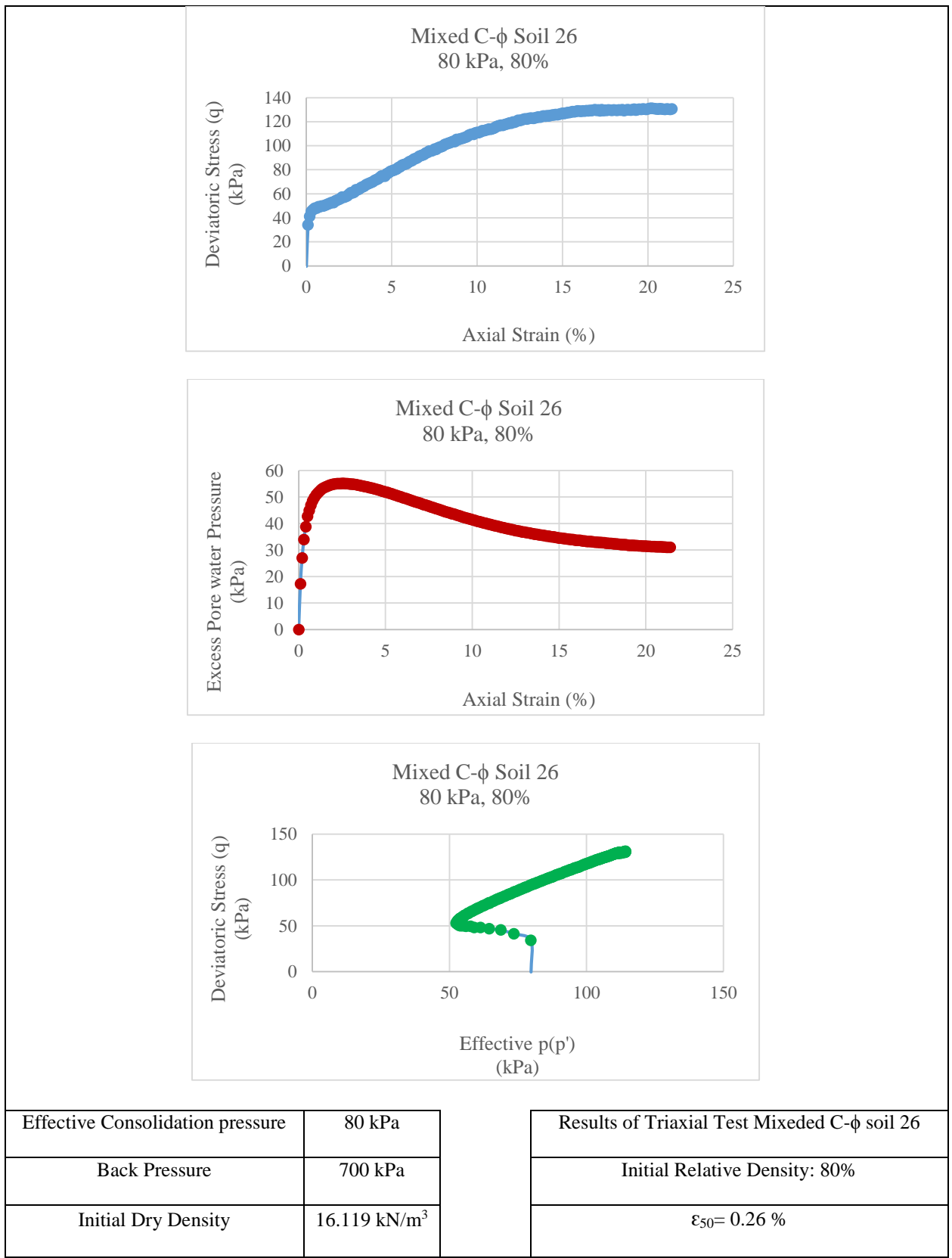


Figure 4-32 Triaxial test results of Mixed Soil 26 Sample

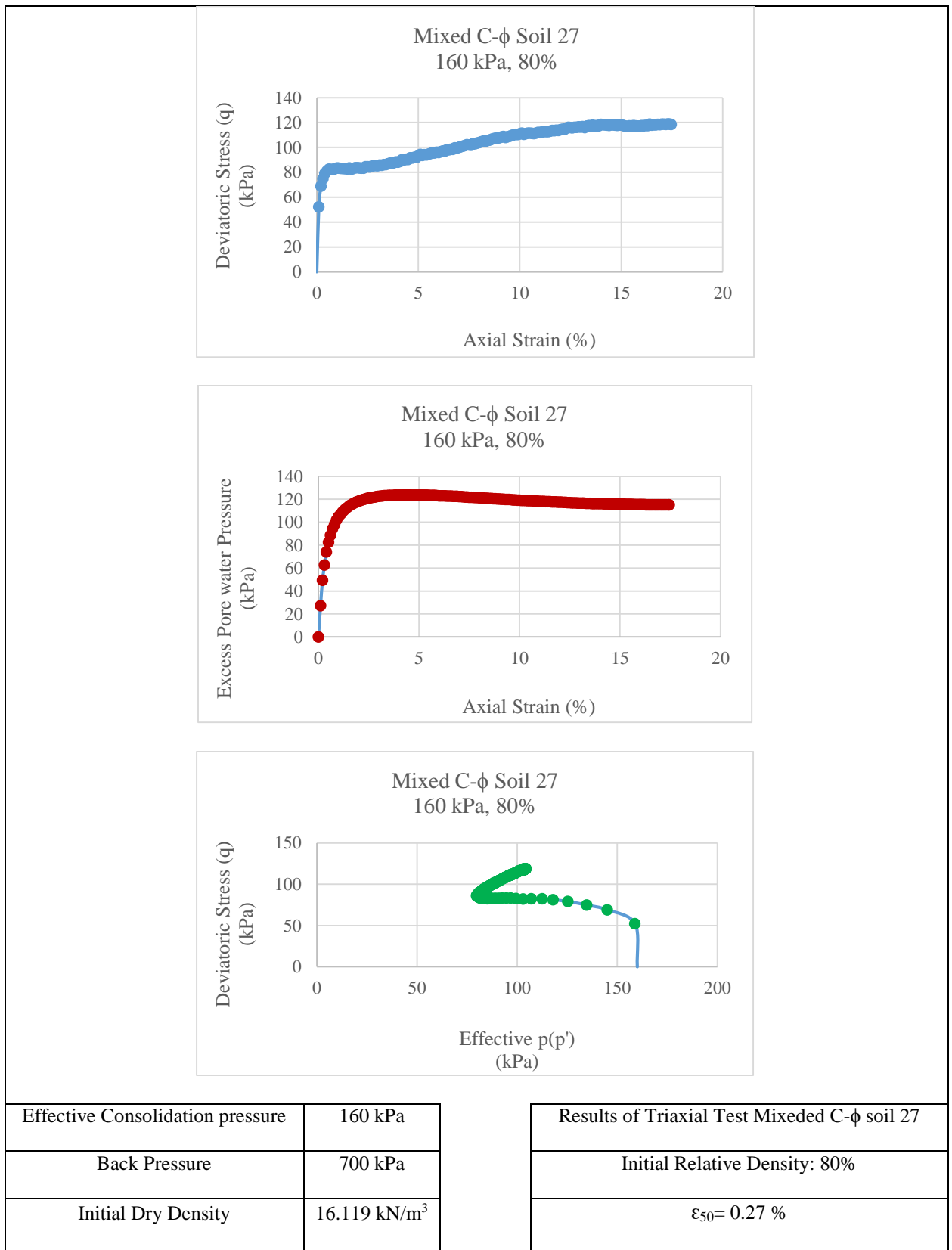


Figure 4-33 Triaxial test results of Mixed Soil 27 Sample

4.6 Data Obtained, Results, and Discussion

Figure 4-34, Figure 4-35 and figure 4-36 show the final Triaxial test results of Granite soil for 40%, 60% and 80% relative density, respectively. In addition, Figure 4-37 illustrates Mohr Circle results of Granite Soil.

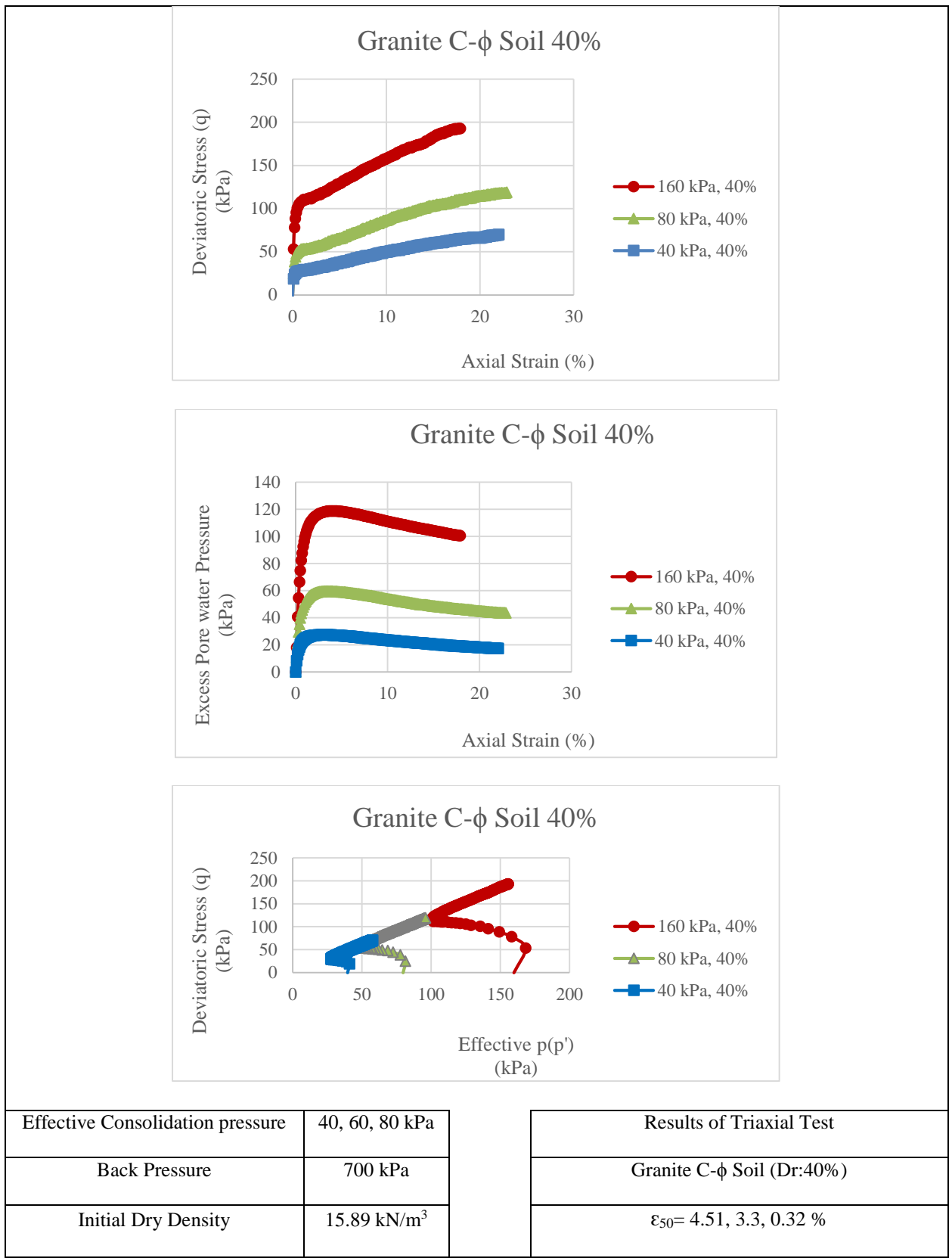


Figure 4-34 Triaxial test results of Granite Soil Sample (40% relative density)

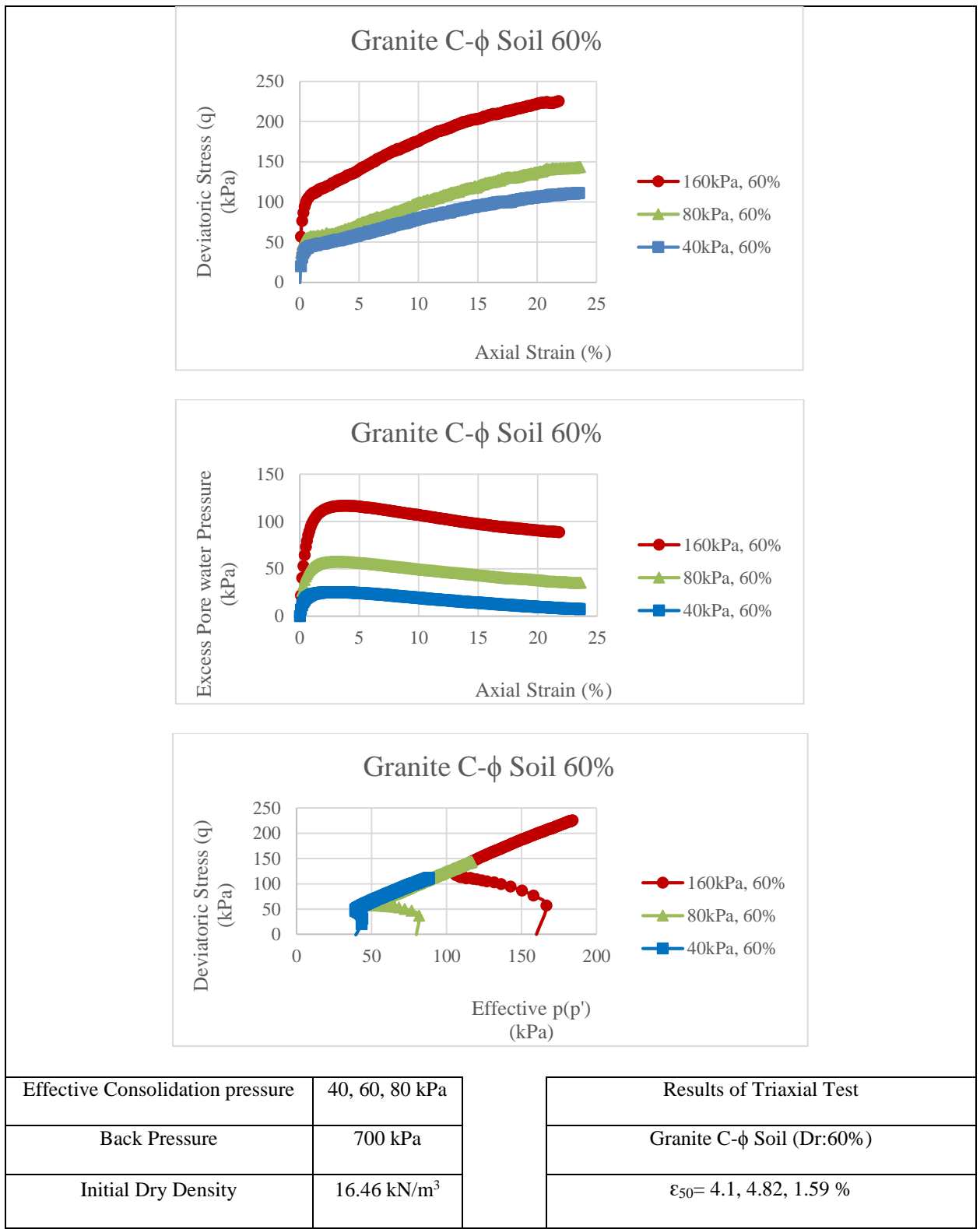


Figure 4-35 Triaxial test results of Granite Soil Sample (60% relative density)

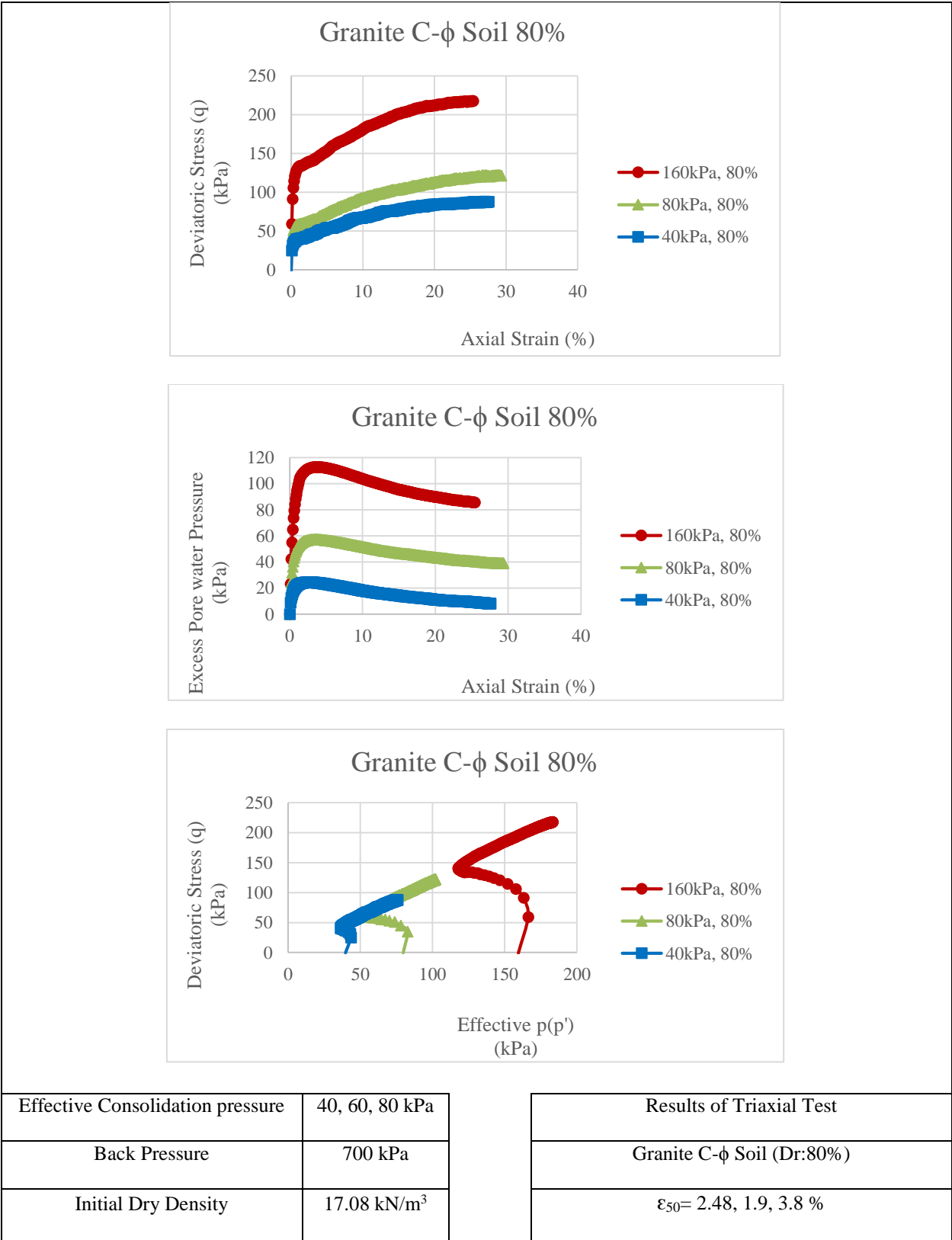


Figure 4-36 Triaxial test results of Granite Soil Sample (80% relative density)

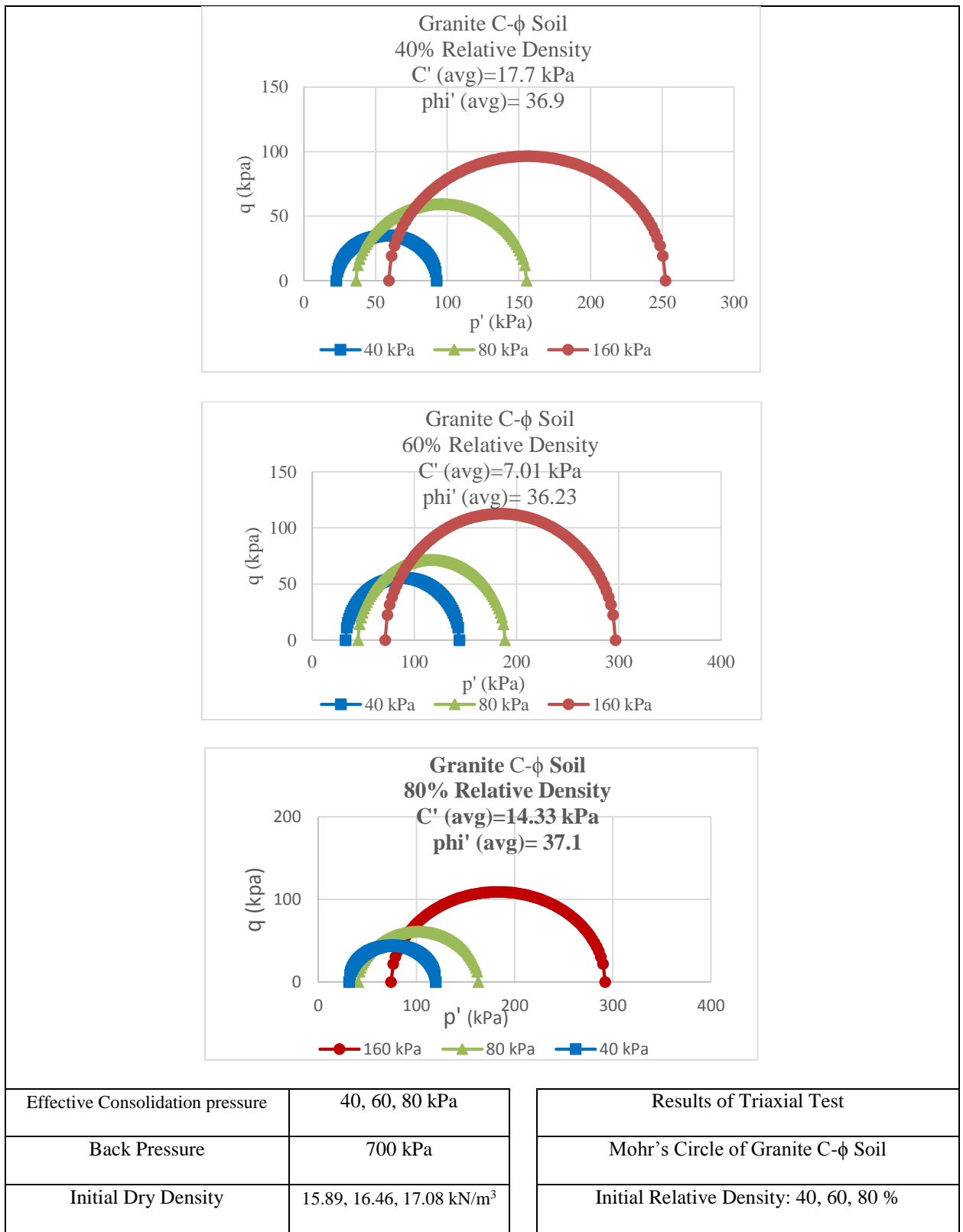


Figure 4-37 Triaxial test results of Granite Soil Sample (Mohr Circle)

Figure 4-38, Figure 4-39 and figure 4-40 show the final Triaxial test results of Black Eagle soil for 40%, 60% and 80% relative density, respectively. In addition, Figure 4-41 illustrates Mohr Circle results of Black Eagle Soil.

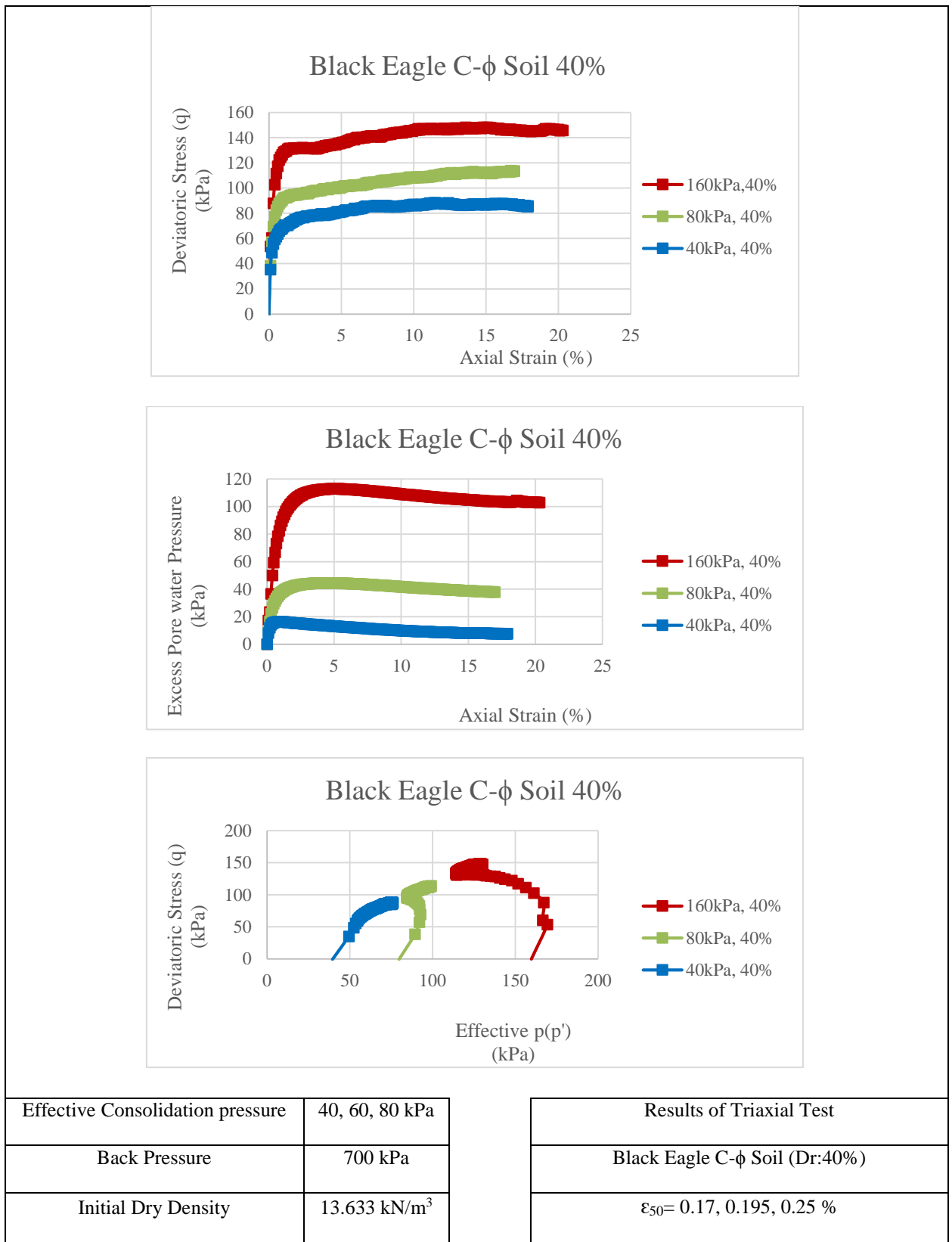
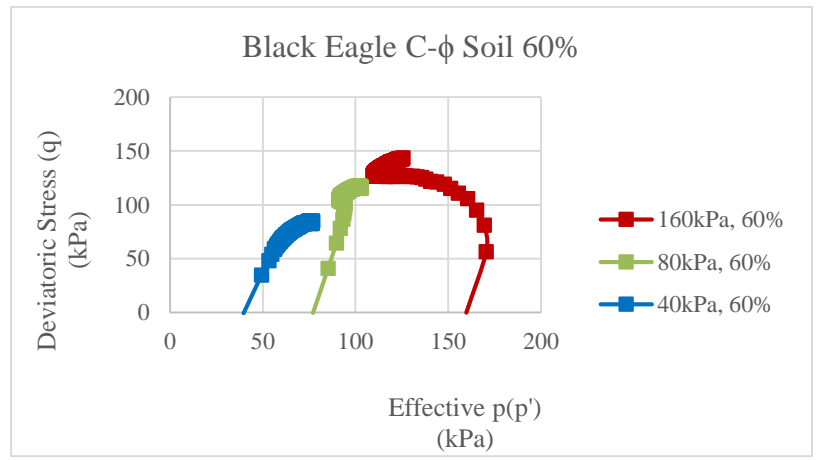
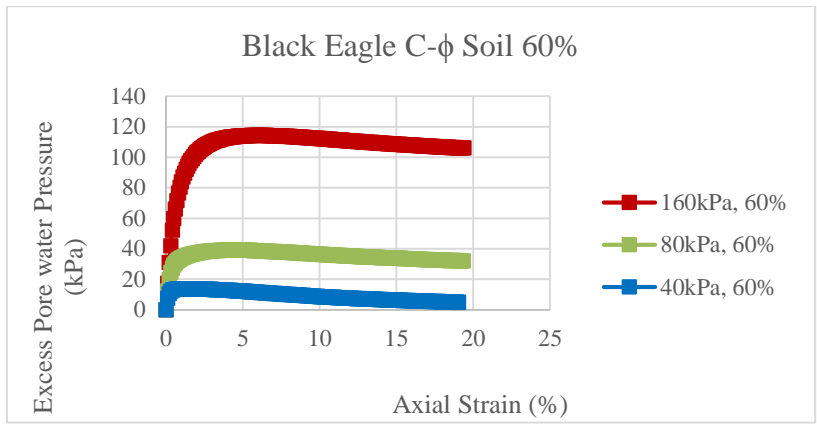
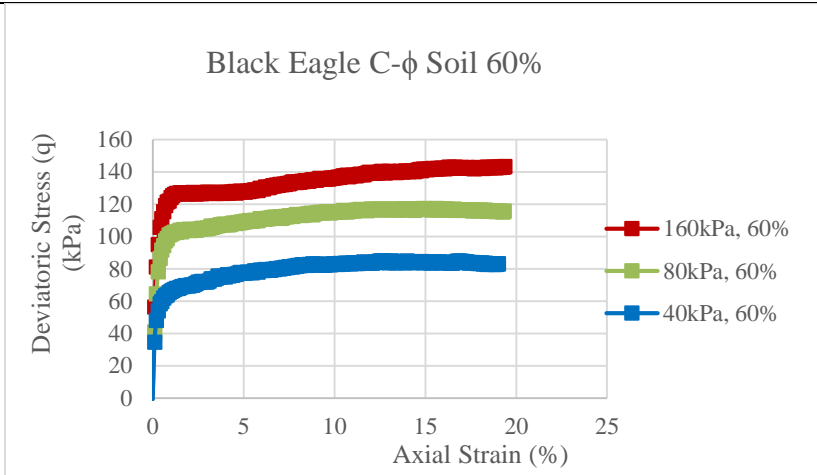


Figure 4-38 Triaxial test results of Black Eagle Soil Sample (40% relative density)



Effective Consolidation pressure	40, 60, 80 kPa
Back Pressure	700 kPa
Initial Dry Density	14.083 kN/m ³

Results of Triaxial Test
Black Eagle C-φ Soil (Dr:60%)
ε ₅₀ = 0.18, 0.175, 0.165 %

Figure 4-39 Triaxial test results of Black Eagle Soil Sample (60% relative density)

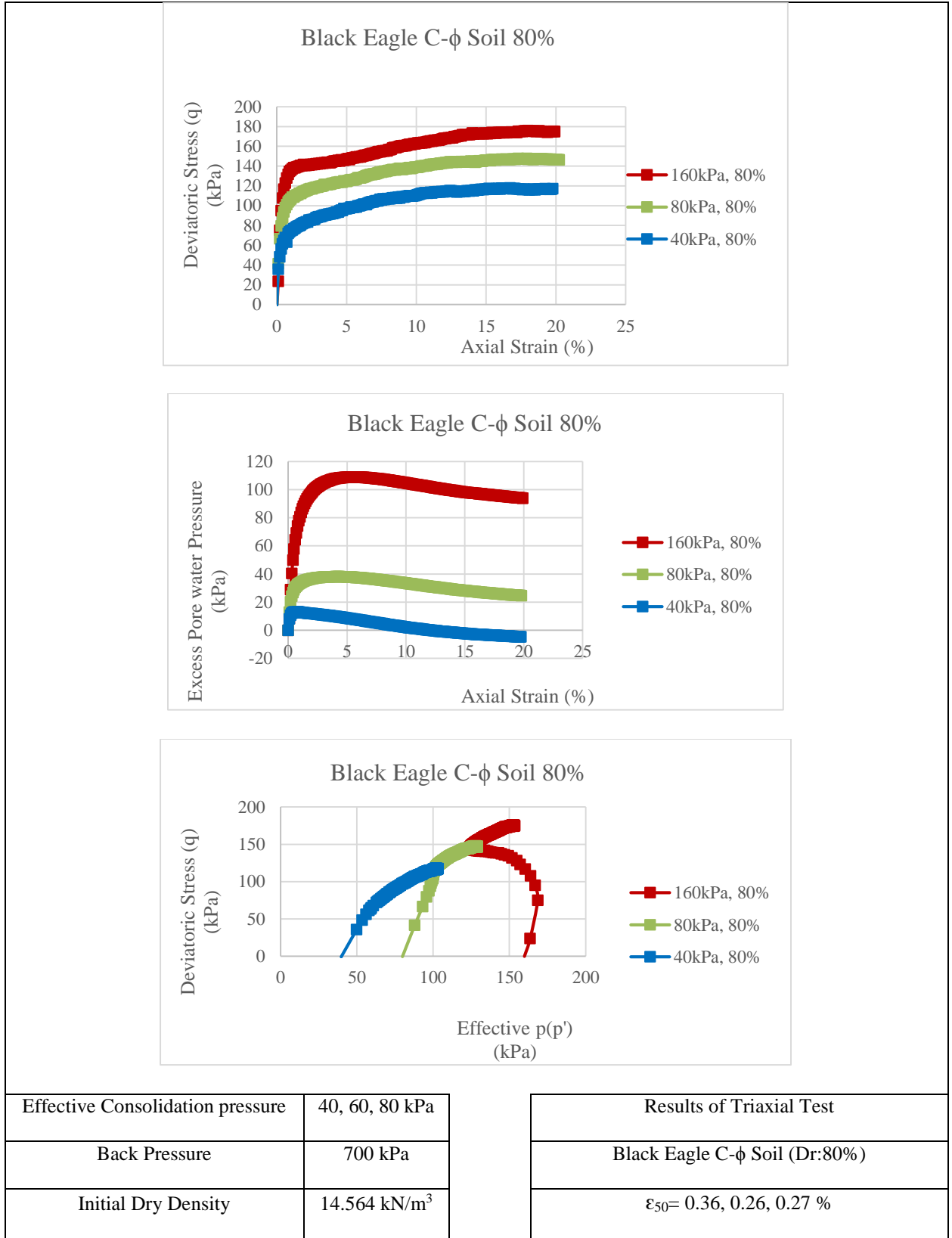


Figure 4-40 Triaxial test results of Black Eagle Soil Sample (80% relative density)

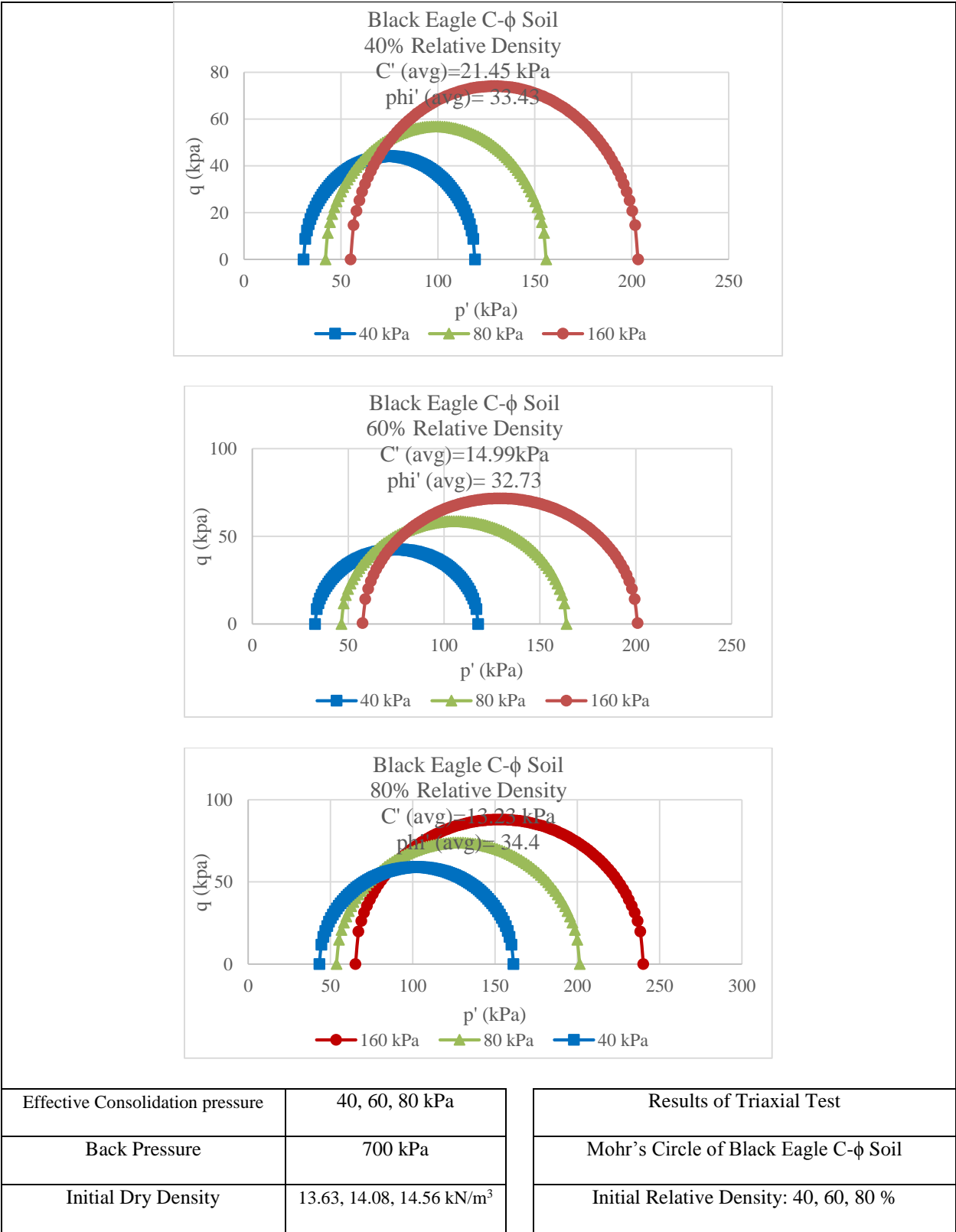


Figure 4-41 Triaxial test results of Black Eagle Soil Sample (Mohr Circle)

Figure 4-42, Figure 4-43 and figure 4-44 show the final Triaxial test results of Mixed Soil for 40%, 60% and 80% relative density, respectively. In addition, Figure 4-45 illustrates Mohr Circle results of Mixed Soil.

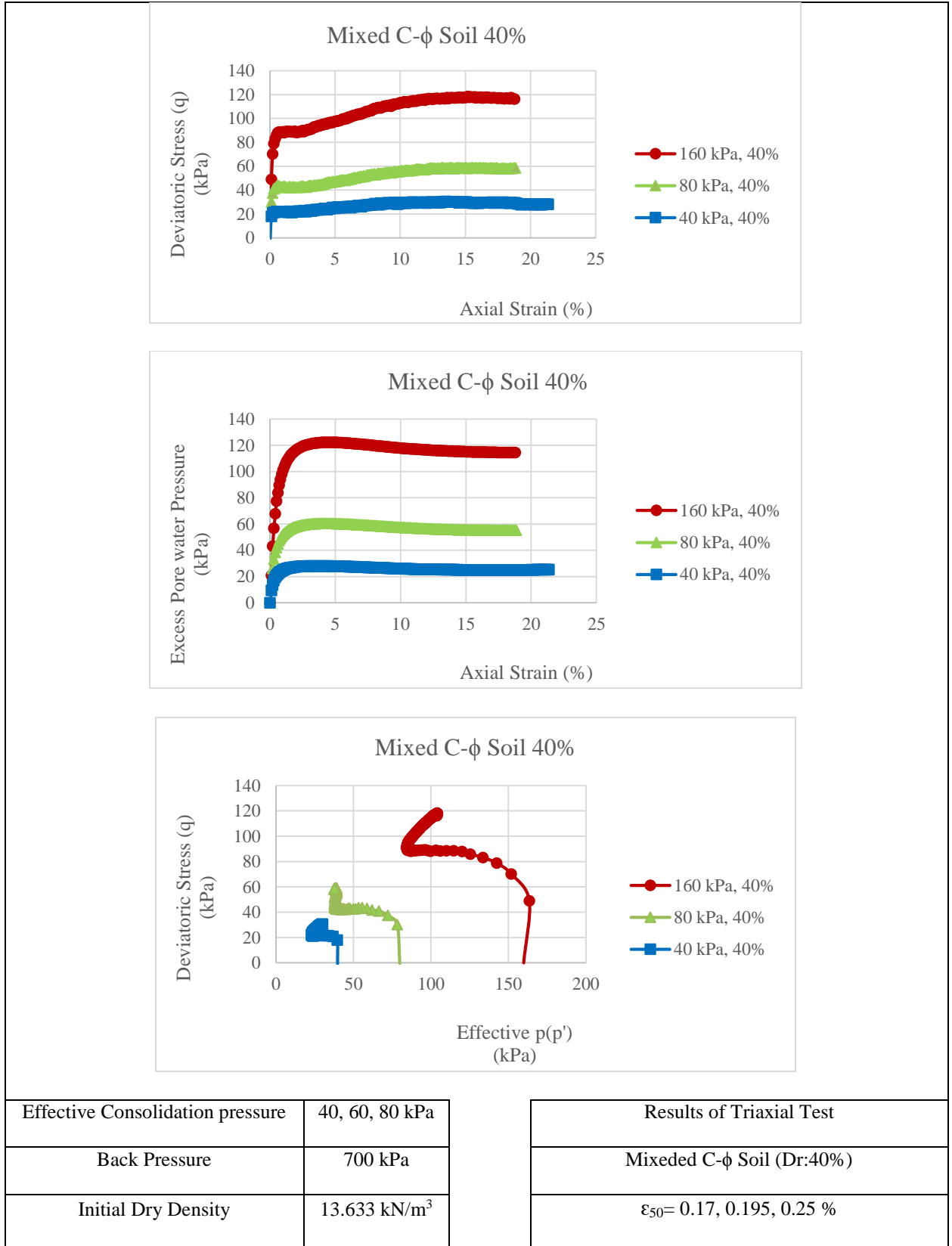
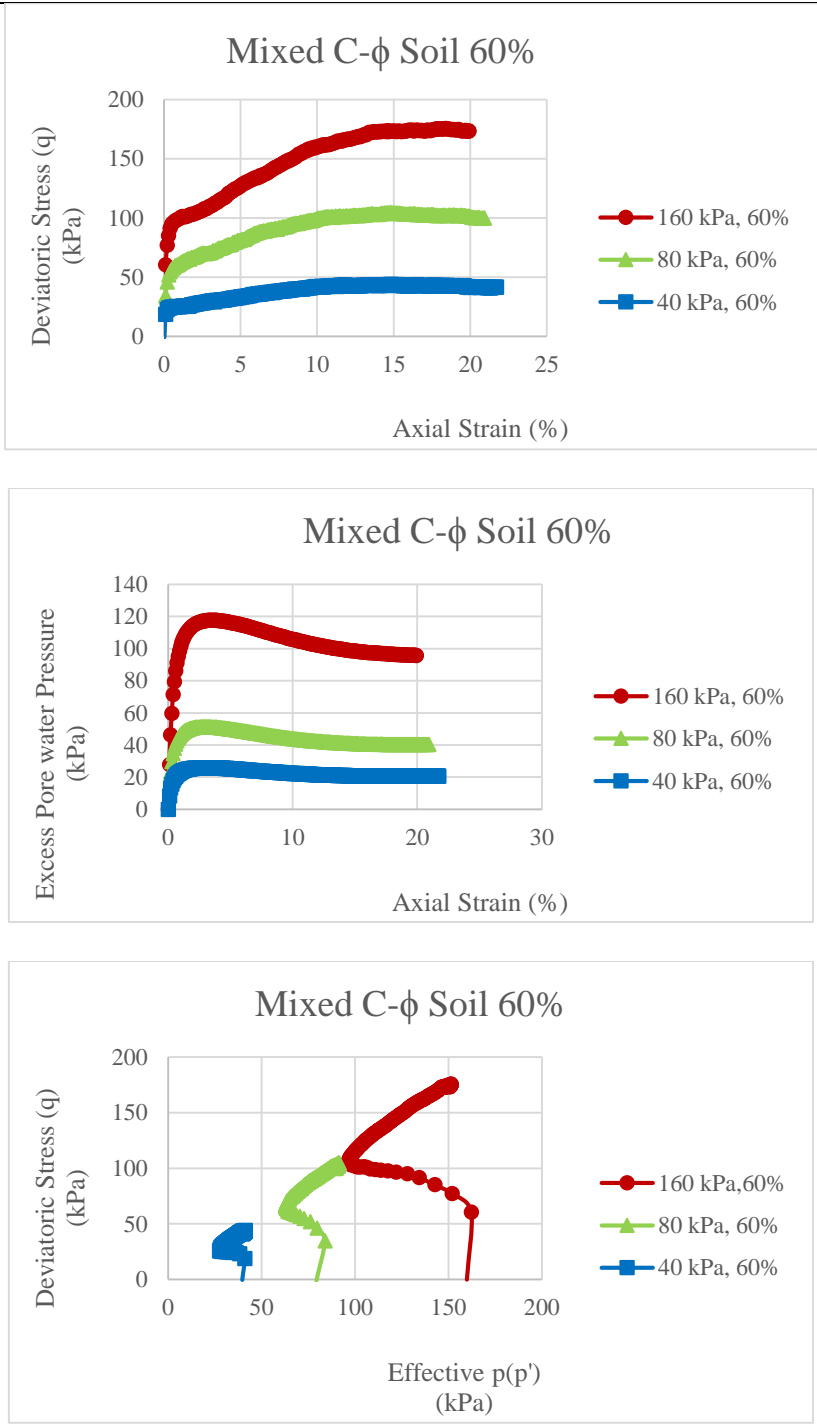


Figure 4-42 Triaxial test results of Mixed Soil Sample (40% relative density)



Effective Consolidation pressure	40, 60, 80 kPa
Back Pressure	700 kPa
Initial Dry Density	14.083 kN/m ³

Results of Triaxial Test
Mixed C-φ Soil (Dr:60%)
ε ₅₀ = 0.18, 0.175, 0.165 %

Figure 4-43 Triaxial test results of Mixed Soil Sample (60% relative density)

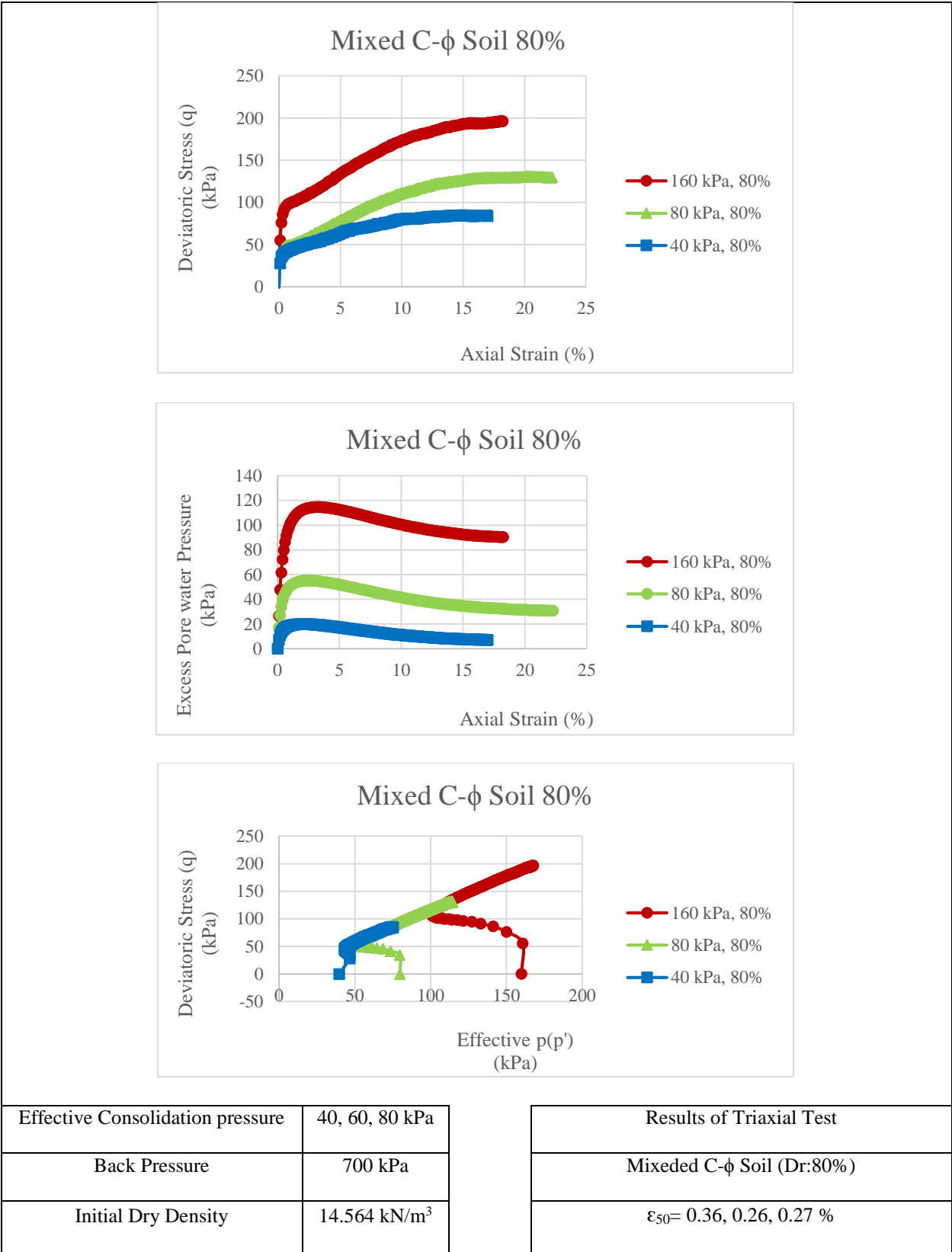
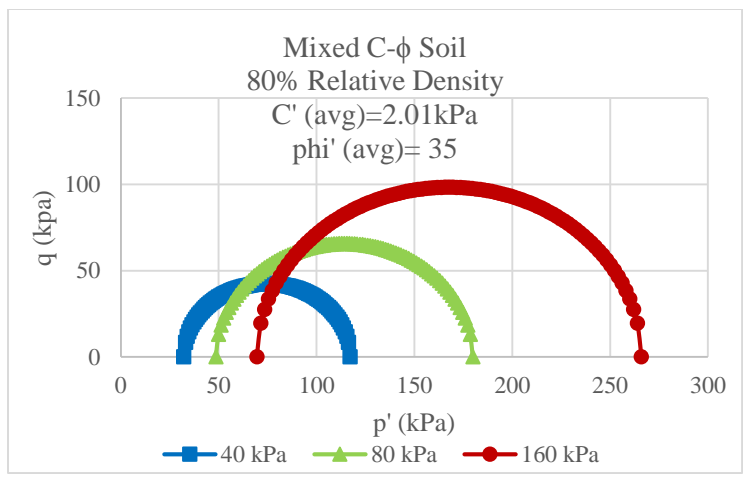
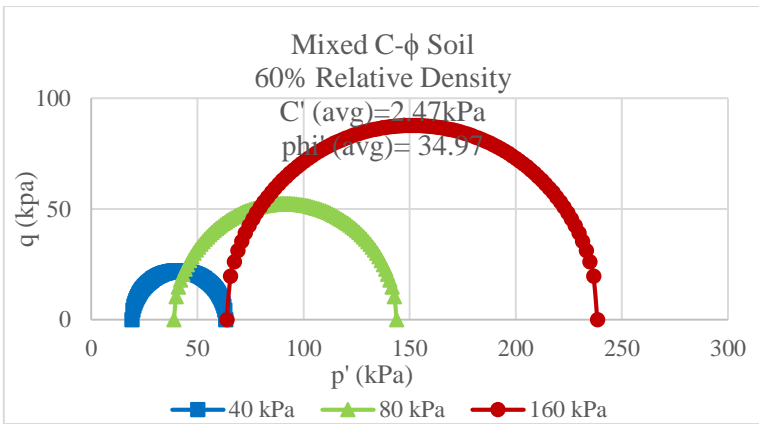
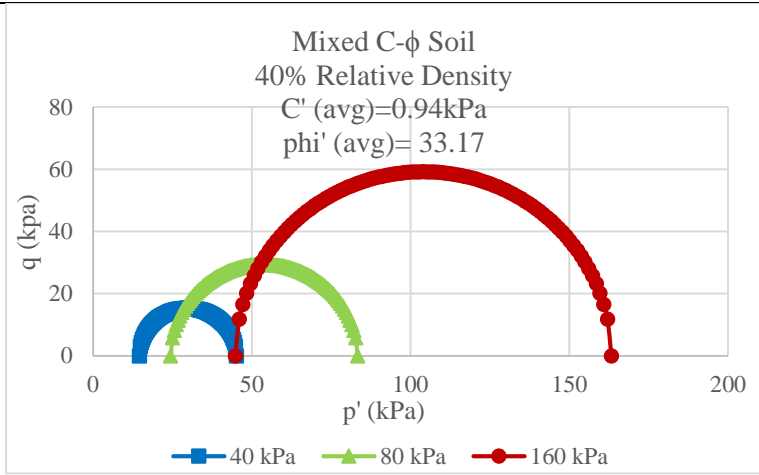


Figure 4-44 Triaxial test results of Mixed Soil Sample (80% relative density)



Effective Consolidation pressure	40, 60, 80 kPa
Back Pressure	700 kPa
Initial Dry Density	13.63, 14.08, 14.56 kN/m ³

Results of Triaxial Test
Mohr's Circle of Mixeded C-phi Soil
Initial Relative Density: 40, 60, 80 %

Figure 4-45 Triaxial test results of Mixed Soil Sample (Mohr Circle)

In total, 27 triaxial tests were run and Table 4-21 presents the calculation cohesion (C) and internal friction angle (ϕ) of tested soils for relative densities 40%, 60%, and 80%.

Table 4-21 The amount of C and ϕ for these three kinds of C- ϕ soils

Soil Type	Relative Density	C (kPa)	ϕ (°)
Soil 1	40%	17.7	36.9
	60%	7.01	36.23
	80%	14.33	37.1
Soil 2	40%	21.45	33.43
	60%	14.99	32.73
	80%	13.23	34.4
Soil 3	40%	0.94	33.17
	60%	2.47	34.97
	80%	2.01	35

Table 4-22 shows the amount of ϵ_{50} for different relative density and confining pressure of Granite soil. Figure 4-46 and 4-47 illustrate the amount of ϵ_{50} versus relative density and confining pressure, respectively for Granite Soil.

Table 4-22. The amount of ϵ_{50} for different relative density and confining pressure (Granite soil)

Granitte Soil			
Dr (%)	$\epsilon_{50}(\%)$ [40 kPa]	$\epsilon_{50}(\%)$ [80 kPa]	$\epsilon_{50}(\%)$ [160 kPa]
40	4.51	3.3	0.32
60	4.1	4.82	1.59
80	2.48	1.9	3.8

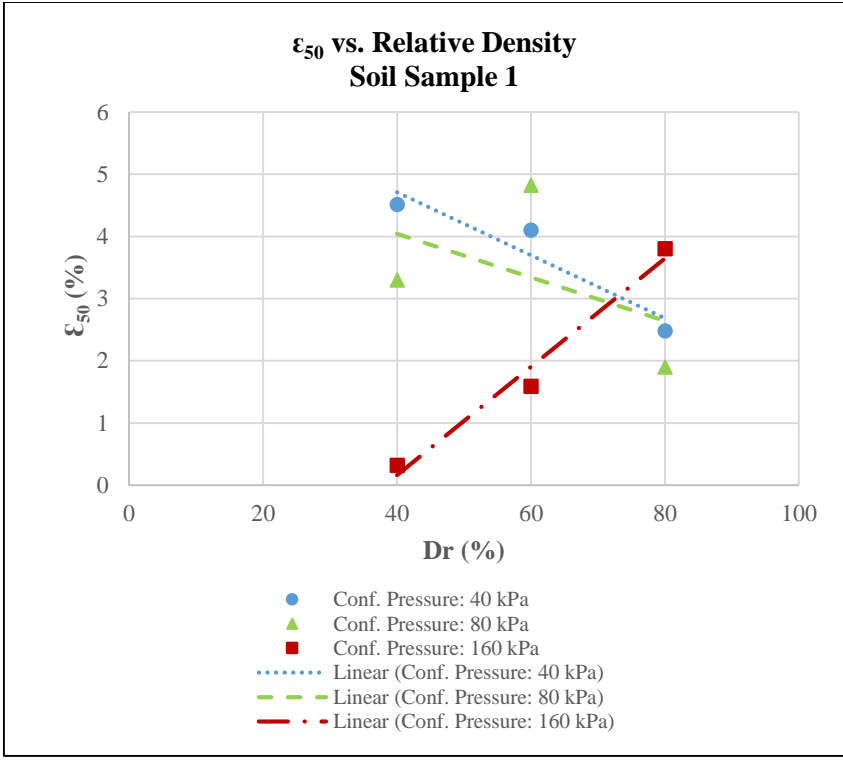


Figure 4-46. The amount of ε₅₀ versus relative density (Granite Soil)

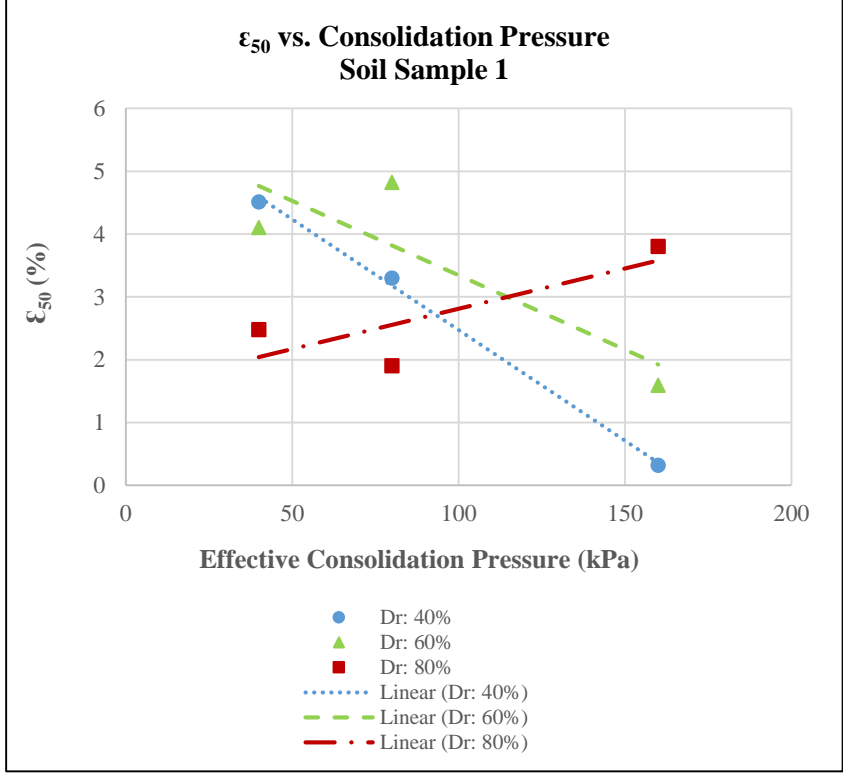


Figure 4-47. The amount of ε₅₀ versus confining pressure (Granite Soil)

Table 4-23 shows the amount of ϵ_{50} for different relative density and confining pressure of Black Eagle soil. Figure 4-48 and 4-49 illustrate the amount of ϵ_{50} versus relative density and confining pressure, respectively for Black Eagle Soil.

Table 4-23. The amount of ϵ_{50} for different relative density and confining pressure (Black Eagle soil)

Black Eagle Soil			
Dr (%)	ϵ_{50} (%) [40 kPa]	ϵ_{50} (%) [80 kPa]	ϵ_{50} (%) [160 kPa]
40	0.17	0.195	0.25
60	0.18	0.175	0.165
80	0.36	0.26	0.27

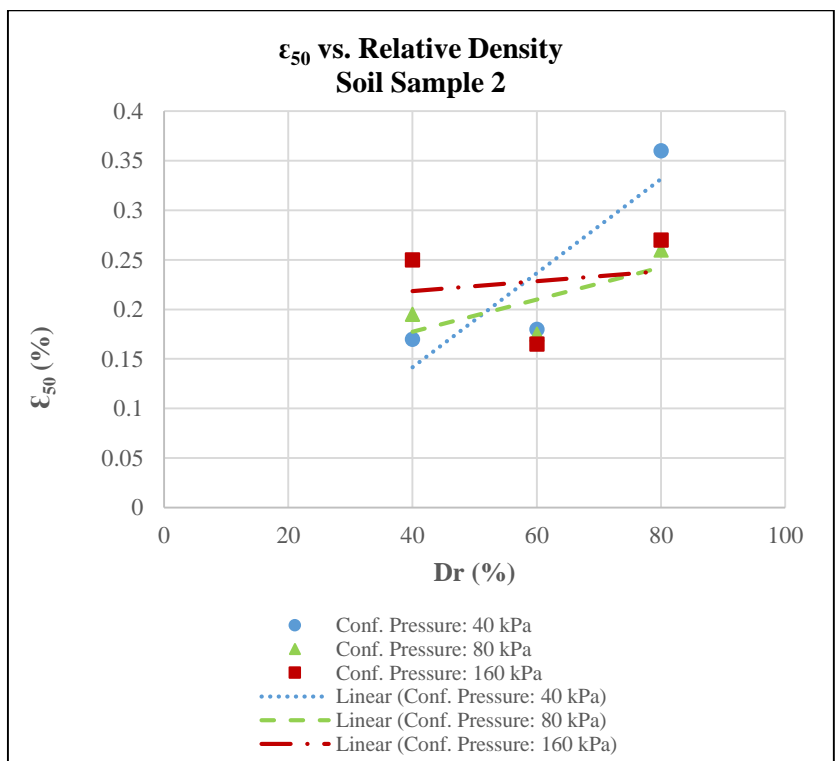


Figure 4-48. The amount of ϵ_{50} versus relative density (Black Eagles Soil)

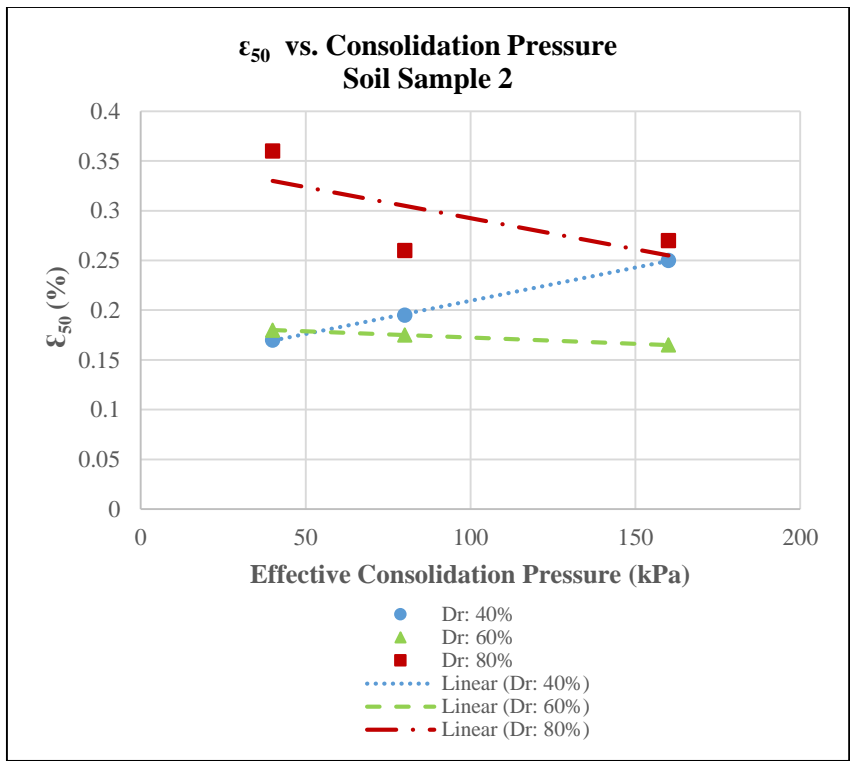


Figure 4-49. The amount of ϵ_{50} versus confining pressure (Black Eagle Soil)

Table 4-24 shows the amount of ϵ_{50} for different relative density and confining pressure of Mixed Soil. Figure 4-50 and 4-51 illustrate the amount of ϵ_{50} versus relative density and confining pressure, respectively for Mixed Soil.

Table 4-24. The amount of ϵ_{50} for different relative density and confining pressure (Mixed Soil)

Mixed Soil			
Dr (%)	ϵ_{50} (%) [40 kPa]	ϵ_{50} (%) [80 kPa]	ϵ_{50} (%) [160 kPa]
40	0.097	0.1	0.145
60	0.2	0.32	0.34
80	0.71	3.29	0.8

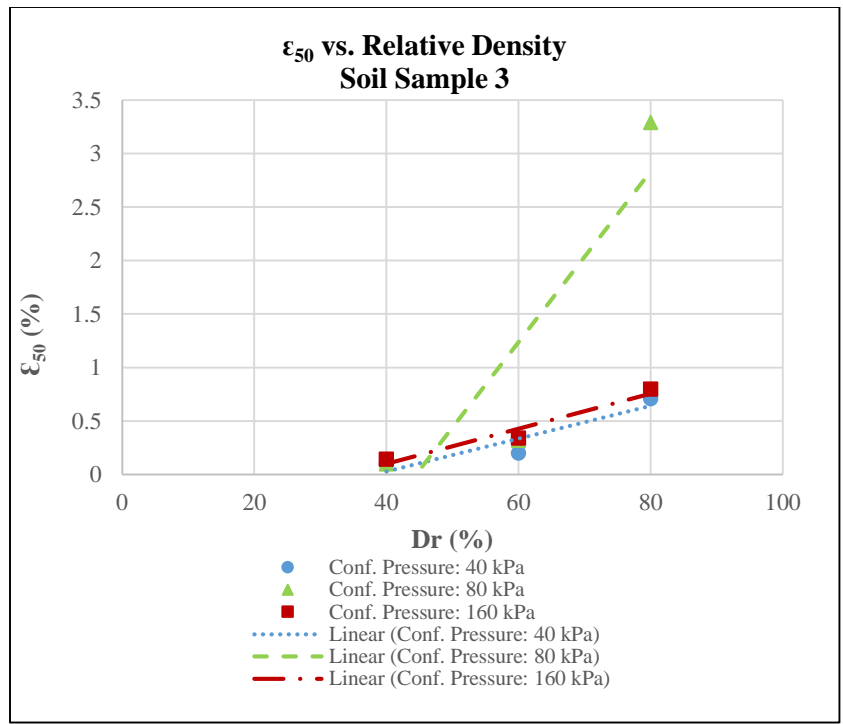


Figure 4-50. The amount of ε₅₀ versus relative density (Mixed Soil)

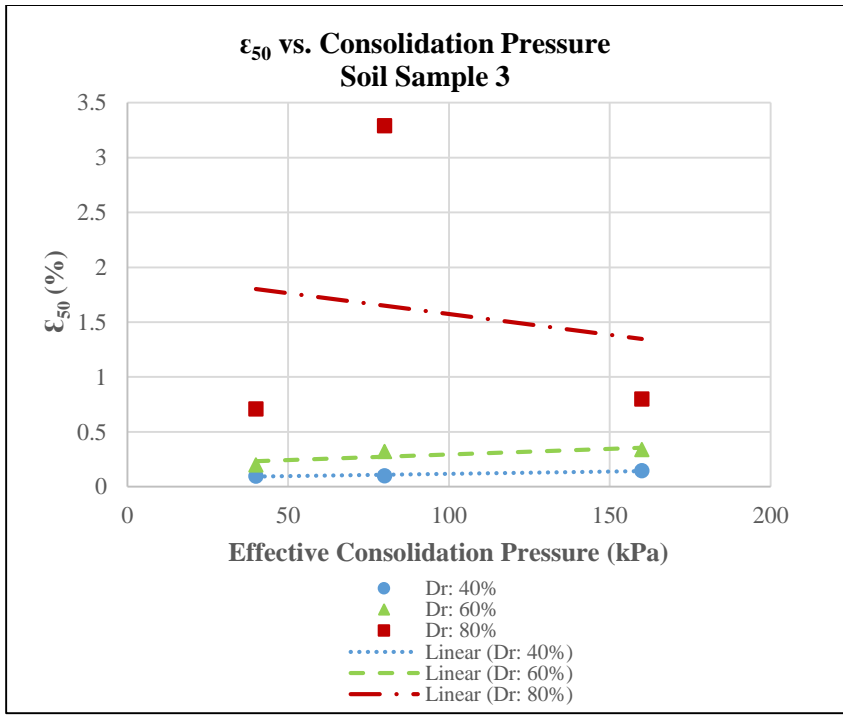


Figure 4-51. The amount of ε₅₀ versus confining pressure (Mixed Soil)

As it can be seen in following figures, the behavior of these $c-\phi$ soils do not show the linear or arranged action. Fluctuation in the amount of ε_{50} can be observed for different confining pressure as well as various relative density. Hence, it seems not to be able to explore any correlation for $c-\phi$ soils and the only way for gaining the amount of ε_{50} is preparing samples and conducting triaxial tests.

5 Case Study of Pile Axial Load Testing

5.1 Introduction

The computer program CGI-DFSAP (Computers and GeoEngineering Inc., 2011) was employed to carry out a class A prediction of a full scale load test on a bored pile (drilled shaft) conducted for the International Pile Prediction Event, supported by ISSMGE. This software estimates axial load-settlement behavior with a unique type of t - z analysis which is outlined in Ashour and Helal (2012) and Ashour et al. (2010). The procedure involves the implementation of a semi-empirical model for the stress-strain behavior of soils to derive load transfer curves for both side-shear and end-bearing in cohesive, cohesionless, rock and c - ϕ materials. This approach was selected because it has shown promise in recent studies (Motamed et al., 2015; Stanton et al., 2015).

A blind prediction of the load-settlement response of an axially loaded drilled shaft in Santa Catarina, Brazil, was carried out in June of 2015. The original results were developed using “best-estimate” soil properties within a t - z analysis framework developed by Norris (1986) and modified by Ashour et al. (1998). However, this approach relies heavily on the estimation of the axial strain at 50% of maximum deviatoric stress, termed ϵ_{50} . Thus, a thorough literature review (chapter 2) was carried out on published ϵ_{50} values and empirical relationships. The original estimates of ϵ_{50} were also varied in this study to explore how sensitive the prediction results are in this regard. It was found the average root mean squared error between the predicted and measured results were significantly affected by changes in ϵ_{50} and that the t - z style predictions were substantially influenced by the estimates of ϵ_{50} , highlighting the need for proper and careful estimation of this important parameter.

5.2 Experimental testing site

Six testing piles were conducted with different technology (bored, with bentonite or polymer mud, and Continuous Flight Auger, CFA), lengths (15 to 24 m) and diameters (0.7 to 1.0 m). All piles were instrumented by wire stain gauges and steel tubes.

5.3 In Situ testing

A comprehensive in situ investigation was started at the Experimental Testing Site, including several geotechnical and geophysical techniques.

These tests involved 13 CPTUs, 3 SPTs and 2 SDMTs. Additional laboratory tests were performed on disturbed samples to determine soil grading and natural water content.

5.4 CGI-DFSAP

CGI-DFSAP (Computers and GeoEngineering Inc., 2011) is the computer program employed to perform a class A prediction of a full scale load test on a drilled shaft, supported by ISSMGE. DFSAP estimates axial load-settlement behavior with a unique type of t - z analysis (outlined in Ashour and Helal (2012), and Ashour et al. (2010)). A semi empirical model for the stress-strain behavior of soils was carried out to derive load transfer curves for both sideshear and end-bearing in cohesive, cohesionless, rock and c - ϕ materials.

Based on the material type, there are required input parameters for CGI-DFSAP. The values for the effective unit weight (γ') and the strain at 50% of the peak deviatoric stress (ϵ_{50}) are some of the input parameters. The undrained shear strength of clay and the effective friction angle of sand are additional essential properties. The value of ϵ_{50} is estimated using correlations with the coefficient of uniformity and void ratio for sand (Norris, 1977) and with undrained shear strength for clay (Evans and Duncan, 1982). Because it can be determined internally by the program, it has a crude approximation and causes minimizing prediction errors.

The test shaft (ET5) with a diameter of 1 m and an embedded length of 24.4 m was modeled as a circular reinforced concrete section. Based on the data in question, 1.44% was assumed for the reinforcing steel to concrete ratio (A_s/A_c) and 0.18 m for the thickness of concrete cover.

Additionally, a free head fixity condition was assumed for the shaft model.

5.5 Material Properties

With the spreadsheet, which was developed for the important step of describing material properties in the CGI-DFSAP model, several empirical and theoretical relationships were used to estimate the required input parameters for the following data types: Cone Penetration Test (CPT), shear wave velocity (V_s) and Standard Penetration Test (SPT).

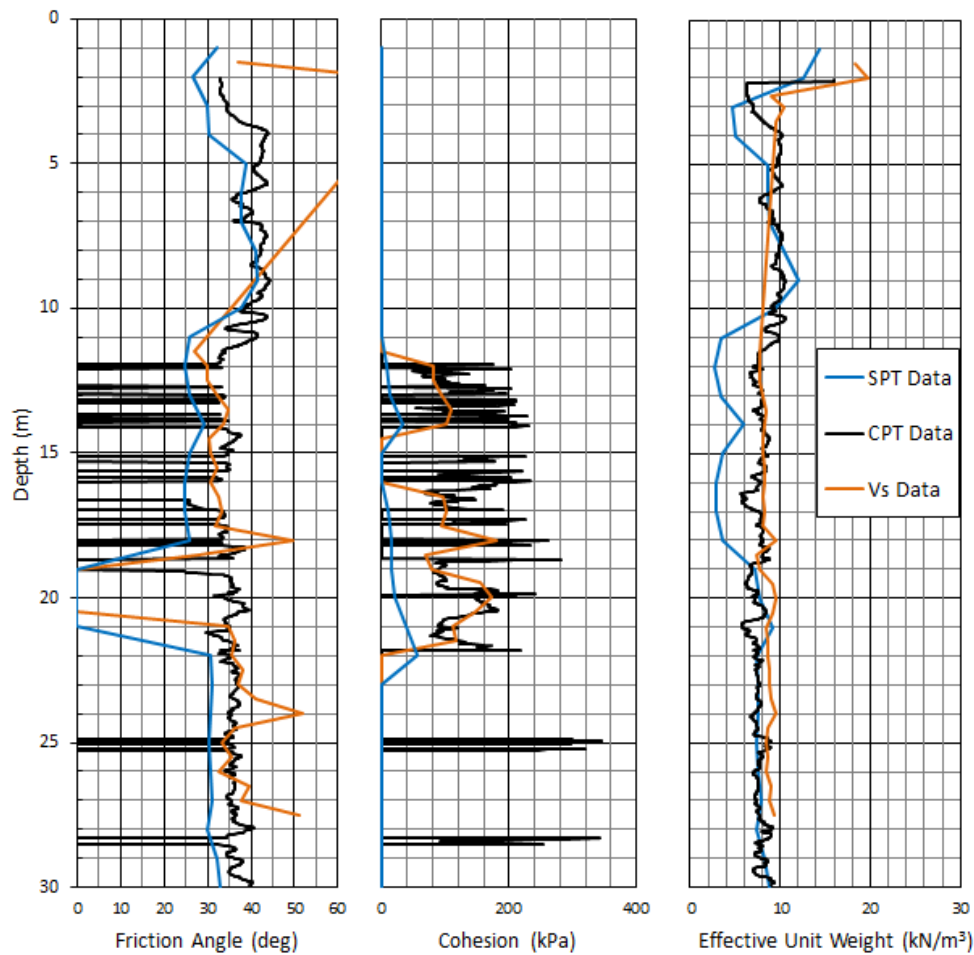


Figure 5-1. Comparison of soil properties estimated using CPT, SPT and V_s data.

Figure 5-1 shows the comparison of soil properties using CPT, SPT and V_s . The comparison of the implied soil index and strength parameters illustrate the correlations from the V_s and CPT

data are commonly in adjacent agreement. Although the SPT data correlations were considerably low between the depth of 10 m and 20 m for cohesion and unit weight, they matched well for friction angle. Figure 5-1 is discussed in the following sub-sections in detail.

5.5.1 CPT Data

In this research, the Robertson (2009) methodology is updated to recognize the implied soil behavior types (SBT). Normalizing measured resistance values for correcting the effects of overburden pressure and providing more accurate evaluations of SBT than provided by the Robertson (1986) approach were part of this research procedure. Figure 5-2 shows the comparison of Robertson's suggestion (1986) for SBT and Robertson's suggestion (2009) for this site. In addition, using the normalized SBT resulted in more layers being assumed to reveal cohesive properties that the older approach could build on.

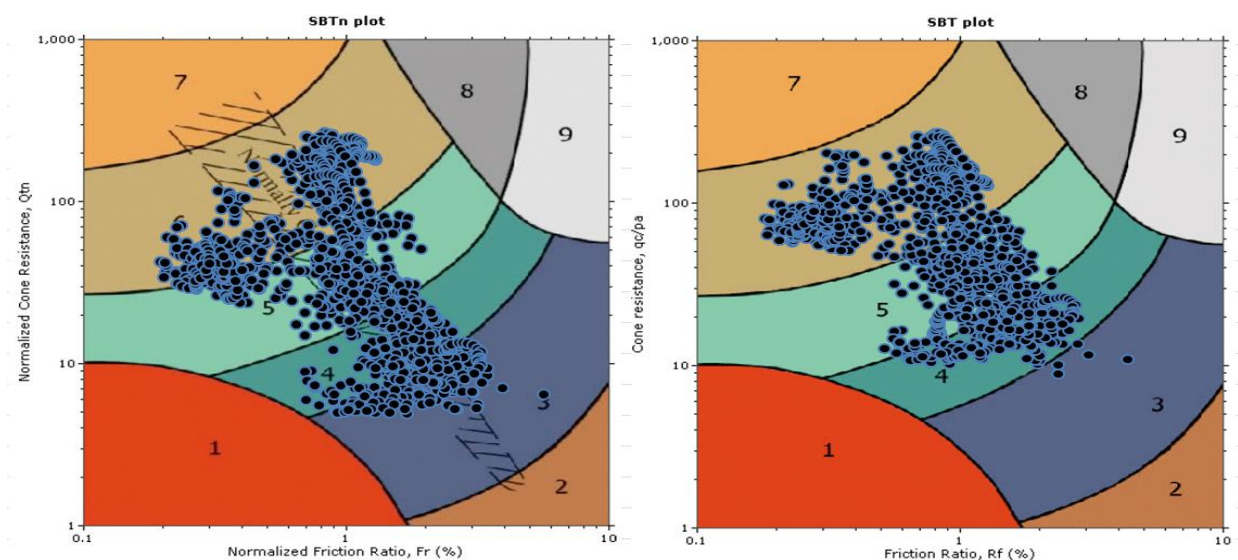


Figure 5-2. Comparison of soil behavior types suggested by Robertson (1986) (right) and Robertson (2009) (left) for CPT-03.

Empirical correlations were employed to assess the soil unit weight (Robertson and Cabal, 2010), undrained shear strength (Robertson, 2012), internal friction angle (Mayne, 2007),

overconsolidation ratio (Robertson, 2009), relative density (Robertson and Cabal, 2010) and void ratio (Novo Tech Software, 2011). An iterative process which was shown in the aforementioned spreadsheet was required for determination of soil unit weight and the normalized cone resistance. Moreover, based on the visual manual classifications given in the boring logs and by inspecting the available sample images for SPT-03, the coefficient of uniformity of sand layers was estimated.

5.5.2 Shear Wave Velocity Data

The previously discussed required parameters were estimated by using the V_s data from SDMT-03. An iterative procedure was employed to estimate unit weights and overburden pressure was estimated by an iterative procedure so that values could be changed to normalized shear wave velocity as in Mayne (2007). This allowed for the estimation of friction angle (Hatanaka and Uchida, 1996) and undrained shear strength (Dickenson, 1994). It should be noted that the determination of friction angle required that the V_s data first be converted to SPT blow counts corrected for hammer efficiency (N_{60}) using relationships given in Bellana (2009).

The SPT and CPT data was also related to V_s and normalized V_s (V_{s1}) to understand which data sets were the most consistent. This was fulfilled using the recommendations from Wair et al. (2012) and Robertson (2012) for SPT and CPT, respectively. All in all, CPT correlation matched the measured V_s data more closely at shallow to medium depths. In addition, those from SPT matched better for deeper layers.

5.5.3 Standard Penetration Data

Unit weight using recommendation from Bowles (1988) is the most important parameter related to the SPT data which enabled the approximation of friction angle (Hatanaka and Uchida, 1996) and undrained shear strength (Kulhawy and Mayne, 1990). Furthermore, the V_s and CPT data

were transformed to SPT blow counts corrected for hammer energy and overburden stress ($N_{1,60}$) which was reached using guidelines given in Bellana (2009) for V_s and Lunne et al. (1997) for CPT. CPT correlation matched very closely at all depths; however, the estimation of SPT was very high at shallower depth (less than 10 m and between 20 m and 25 m).

5.5.4 Finalized Soil Profile

Table 5-1 shows the assumed soil profile modeled in CGI-DFSAP. Based on the previous explanation about material properties using the CPT, SPT and V_s data, the most reliable test data was CPT for layer discretization, friction angles and undrained shear strength. It indicated that except for depths between 3.5 m and 11.5 m where no V_s measurements were recorded, the soil unit weights were based equally on the V_s and CPT data.

Table 5-1. Assumed soil layering and properties for blind prediction

Base Depth (m)	Mean Normalized SBT	Assumed Soil Type	γ' (kN/m ³)	ϕ' (deg)	Su (kPa)	ε_{50} (%)
2.15	5	Silty Sand	16.02	32.9	0	1
3.8	5.14	Silty Sand	7.17	35.2	0	0.8
5.9	6	Silty Sand	9.77	42.4	0	0.55
7.05	5.68	Silty Sand	8.61	38.2	0	0.75
9.6	6	Silty Sand	9.95	42.5	0	0.6
11.55	5.64	Silty Sand	9.26	39	0	0.75
14.1	4.19	Clayey Silt	7.62	33.1	145	0.5
16	4.77	Clayey Silt	8.12	34.8	0	0.6
16.9	3.71	Silty Clay	6.53	26.2	117.8	0.6
18.69	4.88	Clayey Silt	7.99	34.2	189.7	0.5
19.85	3.17	Silty Clay	6.8	34	106	0.55
20.5	4.09	Clay	7.63	0	170	0.5
21.7	3.17	Clay	6.89	0	110.5	0.8
30	5.64	Silty Sand	7.44	35.9	170.5	0.7

5.5.5 Blind Prediction Results.

The results of blind prediction are summarized in Figure 5-3, Figure 5-4, and Table 5-2 below. Note that w is the shaft head settlement, Q is the total axial load, z is the depth below the ground surface and N is the amount of load carried between a given depth and the base of the shaft (24.4

m depth). Also, Q_s and Q_b are the components of axial load carried in side-shear and end-bearing respectively.

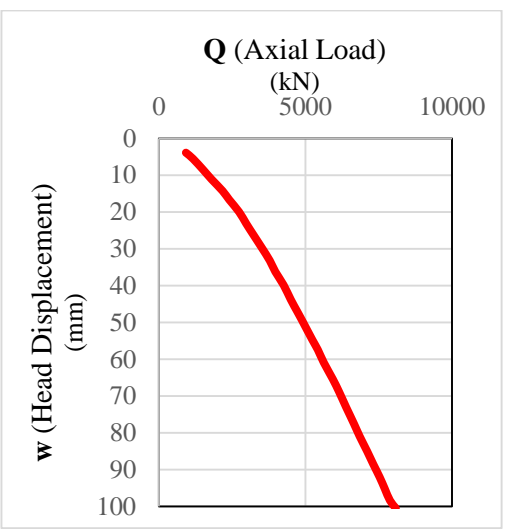


Figure 5-3 Predicted axial shaft head load-settlement response

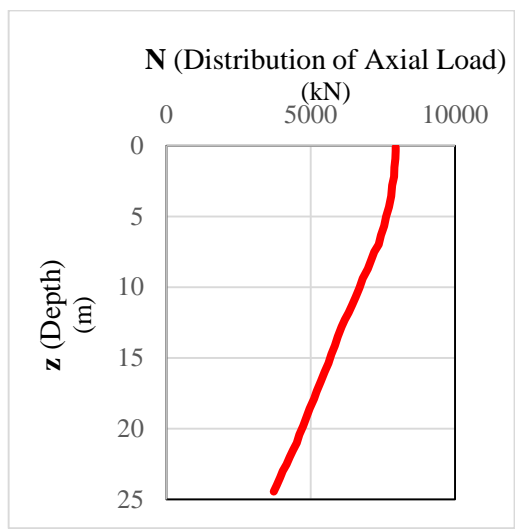


Figure 5-4. Load distribution for a settlement equal to 10% of the shaft diameter

Table 5-2. Predicted loads at failure ($w/D=10\%$)

Component	Load (kN)
Q (total)	7920.76
Q_s (side-shear)	4375.00
Q_b (end-bearing)	3545.76

5.6 Sensitivity Analysis

In order to evaluate the sensitivity of the shaft response to ε_{50} , a thorough literature review (chapter 2) was carried out to collect the recommended ε_{50} values in published literature for different soil types. The reviewed papers included: Kondner et al. (1963), Sullivan et al. (1979), Reese and Sullivan (1980), Evans et al. (July 1982), Dunnavant et al. (1989), Jeong et al. (2007); Kim et al. (2009), Javadi et al. (2009), Zhang et al. (2013), McClellan (2013), Ebrahimian et al. (2015). According to the reviewed literature, a range for the ε_{50} was determined considering the soil type, depth, undrained shear strength, friction angle, and unit weight for each layer.

Table 5-2 presents the summary of different ranges of ε_{50} based on Table 5-1's assumed soil profile. A summary of the predicted range for ε_{50} is presented in Table 5-3 which illustrates the range for the ε_{50} for each soil layer. As it can be seen in this table, the selected ε_{50} values for the blind prediction exercise are comparable to the range selected for the sensitivity study. Overall, the range of ε_{50} increases when soil type changes from clayey silt to silty sand and clay, respectively. Furthermore, the range of ε_{50} generally increases when unit weight, undrained shear strength and friction angle also increase.

Table 5-3. Assumed soil layering and properties for sensitivity analysis

Layer No.	Base Depth (m)	Assumed Soil Type	ε_{50} (%) for blind prediction	Range of ε_{50} in sensitivity analysis (%)
1	2.15	Silty Sand	1	0.3-4.7
2	3.8	Silty Sand	0.8	0.1-3.5
3	5.9	Silty Sand	0.6	0.15-3.5
4	7.05	Silty Sand	0.8	0.1-3.5
5	9.6	Silty Sand	0.6	0.15-3.5
6	11.55	Silty Sand	0.8	0.15-3.5
7	14.1	Clayey Silt	0.5	0.4-1.5
8	16	Clayey Silt	0.6	0.5-3.5
9	16.9	Silty Clay	0.6	0.3-1.5
10	18.69	Clayey Silt	0.5	0.5-3.5
11	19.85	Silty Clay	0.6	0.3-1.5
12	20.5	Clay	0.5	0.5-7
13	21.7	Clay	0.8	0.5-1.5
14	30	Silty Sand	0.7	0.5-1.5

The sensitivity study results are summarized in Figure 5-5 and Figure 5-6 below which include the axial load vs. head displacement for the lower limit range of ε_{50} , the upper limit range of ε_{50} , the original estimate of ε_{50} (blind prediction), and the measured field load test during the Araquari field test.

As can be seen in Figure 5-5, all the measured and predicted results show an increase in higher load with rising the head displacement. However, these values are higher for the measured results. In addition, the upper limit range of ε_{50} have a mild increase in comparison with the blind prediction and the lower limit range of ε_{50} .

For the distribution of axial load vs. depth, the measured results are usually between the upper limit range of ε_{50} and the lower limit range of ε_{50} . However, the behaviour of the blind prediction is smaller than the measured results before 9.6 meters depth and it shows greater values at the upper depth (Figure 5-6). Figure 5-6 illustrates the distribution of axial loads as an output.

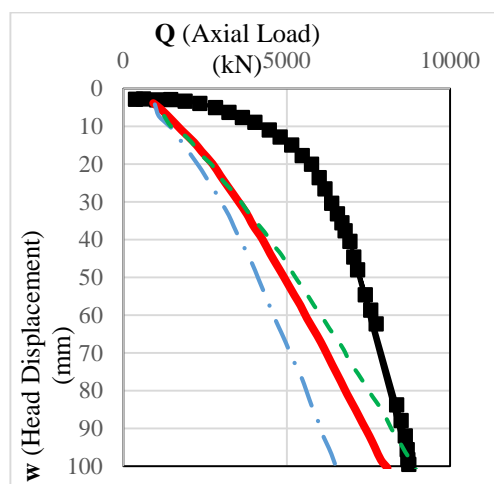


Figure 5-5. Comparison chart for predicted axial shaft head load-settlement response

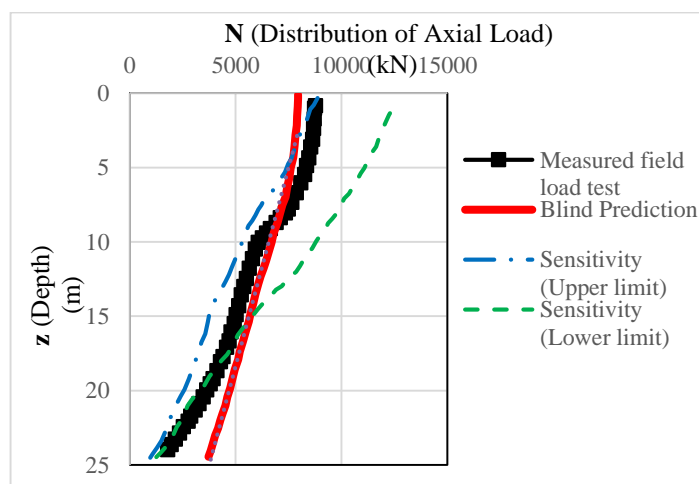


Figure 5-6. Comparison chart for predicted load distribution for a settlement equal to 10% of the shaft diameter

To gain further insight from the sensitivity analyses, Figure 5-7 and Figure 5-8 illustrate the root mean square error (RMSE) between the predicted and measured results. To calculate RMSE, the square root of the sum of the squared residual errors between the predicted and measured results were taken.

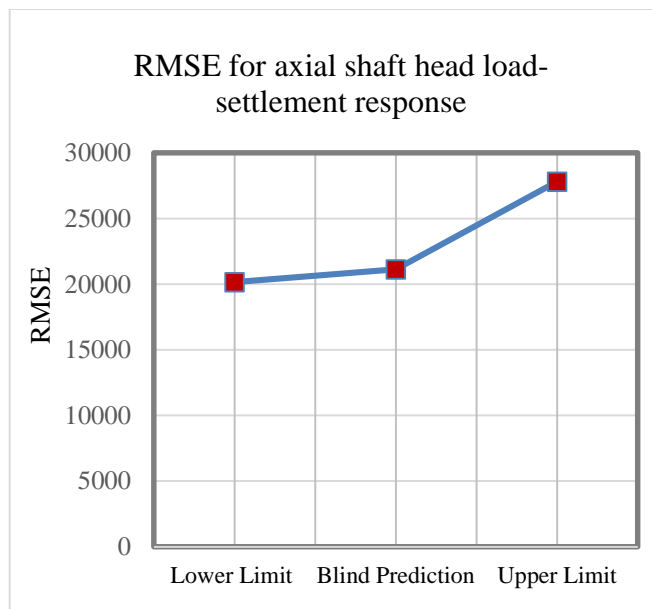


Figure 5-7. Average root mean square error (RMSE) between the predicted and measured results for axial shaft head load-settlement response

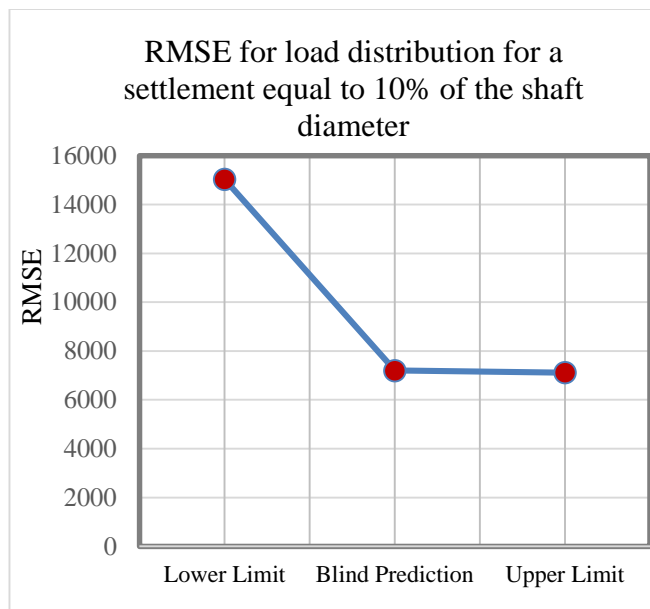


Figure 5-8 Average root mean square error (RMSE) between the predicted and measured results for a settlement equal to 10% of the shaft diameter

Based on Figure 5-7, the overall error increases as ϵ_{50} increases for axial shaft head load-settlement response. Otherwise, for the load distribution, the lower limit of ϵ_{50} makes a much greater error than the blind prediction and the upper limit of ϵ_{50} (Figure 5-8). While this seems counterintuitive, it would actually be reasonable for the two conceptions of the results to react in such seemingly different ways to ϵ_{50} . The nature of the load-transfer method is such that the resistance offered by one layer will affect the mobilized resistance in adjacent layers. Thus, the relationship between ϵ_{50} and the computed axial load distribution may be somewhat complex and should not necessarily follow the same pattern with regard to error as the load-settlement response.

5.7 Summary of Sensitivity Analysis

A $t-z$ style analysis was employed to obtain the load-settlement response and axial load distribution of a drilled shaft which is shown in Figure 5-5 and Figure 5-6. It is observed that prediction quality of the response of the drilled shaft is significantly dependent on the assumed material parameters for the soil layers, especially within the range of estimated values for ϵ_{50} . The sensitivity study further exhibited the need for careful selection of the parameter ϵ_{50} when predicting the axial response of drilled shafts. This highlights the need for proper sampling and testing of the soils, including carrying out laboratory tests such as triaxial compression on collected samples.

6 Conclusions and Recommendations

In this research, all available literature on recommended ϵ_{50} values were collected and documented for different soil types and summarized the recommendations to be used in practice (Chapter 2). In addition, benchmarking testing were conducted for proving the accuracy of triaxial test device and the testing method were documented in Chapter 3. In this Chapter, based on the available information regarding the material properties (e.g. soil types, relative density and confining pressure) of VELASC report (Arulmoli 1992), several tests were performed and their results were compared. All Experimental program including the soil types, basic test, testing program, and results and discussion have come in Chapter 4. Additionally, in Chapter 5, the case study of pile axial testing can be seen which investigates the sensitivity of settlement prediction for an axially loaded drilled shaft to ϵ_{50} .

In summary, the influence of several factors such as relative density, confining stress, PI, fines content, friction angle and cohesion on the strain at 50% of maximum deviatoric principle stress, ϵ_{50} , through a series of consolidated undrained triaxial (CU) tests on c- ϕ soil samples were explored.

It was attempted to establish correlations with key characteristics of c- ϕ soils. However, according to the results discussed in Chapter 4, laboratory measurements of ϵ_{50} using triaxial test is the only way to obtain this parameter accurately. Hence, any correlation cannot elicit from these results and running triaxial tests seem to be necessary.

7 References

- Anderson, J. B., Townsend, F. C., Grajales, B. (2003). Case History Evaluation of Laterally Loaded Piles. *J of Geotech. Geoenviron. Eng.*, 129, pp. 187-196.
- Ashour, M., & Helal, A. (2012). Response of Axially Loaded Piles in Sands with and without Seismically Induced Porewater Pressures. *Int. J. of Geomechanics*, doi:10.1061/GM.1943-5622.0000273.
- Ashour, M., Norris, G. M., Elfass, S., & Al-Hamdan, A. Z. (2010). Mobilized side and tip resistances of piles in clay. *Computers and Geotechnics*, 37(7), 858-866.
- Ashour, M., Norris, G., & Pilling, P. (1998). Lateral Loading of a Pile in Layered Soil Using the Strain Wedge Model. *J. of Geotechnical and Geoenvironmental Eng., ASCE*, 124(4), pp. 303-315.
- Ashour, M., & Helal, A. (2012). Response of Axially Loaded Piles in Sands with and without Seismically Induced Porewater Pressures. *Int. J. of Geomechanics*, doi:10.1061/GM.1943-5622.0000273.
- Ashour, M., Norris, G. M., Elfass, S., & Al-Hamdan, A. Z. (2010). Mobilized side and tip resistances of piles in clay. *Computers and Geotechnics*, 37(7), 858-866.
- ASTM D422 (Standard Test Method for Particle-Size Analysis of Soils) (2007)
- ASTM D4253 (Standard Test Method for Maximum Density) (2015)
- ASTM D4254 (Standard Test Method for Minimum Density) (2015)
- ASTM D4767 (Standard Test Method for Consolidation Undrained Triaxial Compression Test) (2011)
- ASTM D854 (Standard Test Method for Specific Gravity) (2014)
- ASTM D4318 (Standard Test Method for Atterberg Limit) (2010)
- Bellana, N. (2009). Shear Wave Velocity as Function of SPT Penetration Resistance and Vertical Effective Stress at California Bridge Sites. M.S. Thesis, University of California, Los Angeles.
- Bishop, A. W., Henkel, D. J., "The measurement of soil properties in the triaxial test", (1970)
- GDS introduction to Triaxial testing, (2013)
- Bowles, J. E. (1988). *Foundation analysis and design*. McGraw-Hill Book Company Limited, England, ISBN: 0-07-006776-7.

Computers & GeoEngineering, Inc. (2011). CGI-DFSAP. Ret. April 7, 2015, from <http://cgi-dfsap.com/>.

Cone Penetration Test Software. (2008, January 1). Retrieved April 12, 2015, from <http://www.novotechsoftware.com/geotechnical-software/cone-penetration-test-software/>

Dickenson, SE (1994). Dynamic Response of Soft and Deep Cohesive Soils during the Loma Prieta Earthquake of October 17, 1989. PhD thesis, Dept. of Civil and Enviro. Eng., University of California, Berkeley, CA.

Dunnavant, T.W., O'Neill, M.W. (1989). Experimental p-y Model for Submerged, Stiff Clay. J of Geotechnical Eng., ELSEVIER, 115(1), pp. 95-114.

Ebrahimian, B., Nazari, A., Yousefnia Pasha, A. (2011). Influence on Lateral Rigidity of Offshore Piles Using Proposed p-y curves. J of Ocean Eng., ELSEVIER, 38, pp. 397-408.

Evans, L.T., & Duncan, G.M. (1982). Simplified analysis of laterally loaded piles. University of California Berkeley, Rept. No. UCB/GT/82-04.

FHWA (Drilled Shafts: Construction Procedures and LRFD Design Methods) (2010)

Geocomp Manual (2013).

Hatanaka, M., & Uchida, A. (1996). A simple method for the determination of Ko-value in sandy soils. Soils and foundations, 36(2), 93-99.

Javadi, A.A., Rezaia, M. (2009). Intelligent Finite Element Method: an Evolutionary Approach to Constitutive Modeling. J of Advanced Engineering Informatics, ELSEVIER, 23, pp. 442-451.

Jeong, S., Kim, Y., Kim, J. (2015). Evaluating ϵ_{50} for Lateral Load-Displacement Behavior of Piles in Clay. J of Ocean Eng., ELSEVIER, 96, pp. 149-160.

K. Alrulmoli, K. K. Muraleetharan, "VELACS verification of liquefaction analysis by centrifuge studies laboratory testing program soil data report". National science foundation (1992).

Kondner, R.L., Zelasko, J.S. (1963). A Hyperbolic Stress-Strain Formulation in Sands. Proceeding of the Second Panamerican Conference on Soil Mechanics and Foundation Eng., 1, pp. 289-324.

Kulhawy, F. H., and Mayne, P. W. (1990). "Manual on estimating soil properties for foundation design." Electric Power Research Institute, Palo Alto, Calif.

Lunne, T., Robertson, P.K., and Powell, J.J.M. (1997). CPT in geotechnical practice. Chapman and Hall, New York, USA.

- Mayne, P.W., 2007. In-situ test calibrations for evaluating soil parameters. *Characterization & Engineering Properties of Natural Soils*, Vol. 3, Taylor & Francis Group, London: 1602-1652.
- Motamed, R., Stanton, K., Nasimifar, M., Pearson, N., and Kluzniak, B. (2015) A Methodology for Axially Loaded Drilled Shaft Performance Predictions Using DFSAP. *IFCEE 2015*: pp. 1791-1805. doi: 10.1061/9780784479087.163
- McClellan, Z.R. (2013). Comparison of Soil Shear Strength Parameters and p-y Curves for Laterally Loaded Piles in Granular Soil. University of Utah, Master Thesis UMI No. 1544611.
- Norris, G.M. (1977). The Drained Shear Strength of Uniform Quartz Sand as Related to Particle Size and Natural Variation in Shape and surface Roughness. PhD thesis, University of California, Berkeley.
- Norris, G. M. (1986). Theoretically Based BEF Laterally Loaded Pile Analysis. *Third Int. Conf. on Numerical Methods in Offshore Piling*, Nantes, France, pp. 361-386.
- Robertson, P. K., & Cabal, K. L. (2010, May). Estimating soil unit weight from CPT. In *2nd International Symposium on Cone Penetration Testing* (pp. 2-40).
- Robertson, P. K. (2009). Interpretation of cone penetration tests—a unified approach. *Canadian Geotechnical Journal*, 46(11), 1337-1355.
- Robertson P.K. (2012). Interpretation of in-situ tests—some insights. *Proceedings, 4th International Conference on Geotechnical and Geophysical Site Characterization (ISC-4)*, R.Q. Coutinho and P.W. Mayne, eds., Pernambuco, Brazil, pp. 22.
- Stanton, K., Motamed, R., Elfass, S., & Ellison, K. (2015) An Evaluation of T-Z Analysis Methods. *Proceedings, The 40th Annual Conference on Deep Foundations*, Oakland, CA, page 27-36.
- Sullivan, W. R., Reese L. C., Fenske. C. W., (1979). Unified Method for Analysis of Laterally Loaded Piles in Clay. *J of Numerical method in offshore piling proceedings of a conference*. Pp. 135-146.
- Zhang, L., Ahmari, S. (2013). Nonlinear Analysis of Laterally Loaded Rigid Piles in Cohesive Soil. *International Journal for Numerical and Analytical Methods in Geomechanics*, 37, pp. 201-220.

Appendix A:

Granite	ϕ (°)	ϕ_{avg} (°)	Black Eagle	ϕ (°)	ϕ_{avg} (°)	Mixed	ϕ (°)	ϕ_{avg} (°)
40 kPa, 40 %	37.4	38.03	40 kPa, 40 %	35.7	35.26	40 kPa, 40 %	30.8,	32.87
80 kPa, 40 %	38.4		80 kPa, 40 %	35.1		80 kPa, 40 %	33.1	
160 kPa, 40 %	38.3		160 kPa, 40 %	35		160 kPa, 40 %	34.7	
40 kPa, 60 %	35.7	36.3	40 kPa, 60 %	34.4	34.83	40 kPa, 60 %	32.5	34.3
80 kPa, 60 %	36.8		80 kPa, 60 %	35		80 kPa, 60 %	35	
160 kPa, 60 %	36.5		160 kPa, 60 %	35.1		160 kPa, 60 %	35.4	
40 kPa, 80 %	38.8	38.36	40 kPa, 80 %	35.3	35.33	40 kPa, 80 %	34.8	35.23
80 kPa, 80 %	38.3		80 kPa, 80 %	35.4		80 kPa, 80 %	35.1	
160 kPa, 80 %	37.8		160 kPa, 80 %	35.3		160 kPa, 80 %	35.8	

Appendix B:

Some Notes for Running Triaxial Test:

1. Check all of the valves,
2. Calibrate Load (Check specimen weight + + download + apply)
3. Raise specimen
4. Calibrate Displacement (Check specimen displacement + download + apply)
5. Set Position and Control valves:
 - Output valve open
 - Supply valve closed
6. Jog cell
7. Calibrate Cell (Cell pressure number + download + apply)
8. Jog cell again
9. Put tube into middle valve
10. Jog sample
11. Calibrate Sample (Sample pressure number + download + apply)
12. Jog sample again
13. Put tube and open the right valve until the specimen seems wet (It may cause several times to fill the Sample FlowTrac II)
14. Start
15. Don't press OK until a message is received.
16. Motor platen up: wait until the motor turns off.
17. Press Ok
18. Unlock piston
19. We are in the initialization phase
20. After 10 minute, we are in saturation phase.
21. Put small tube into the right valve and open it.
22. After pure water flows out from the right tube, close it.